Applied electromagnetic environment cognition to improve a radio communication link

by

Juan AVILÉS CASTILLO

THESIS PRESENTED TO ÉCOLE DE TECHNOLOGIE SUPÉRIEURE
IN PARTIAL FULFILLMENT OF THE REQUIREMENTS
FOR THE DEGREE OF DOCTOR OF PHILOSOPHY
Ph. D.

MONTREAL, MARCH 28, 2017

ÉCOLE DE TECHNOLOGIE SUPÉRIEURE
UNIVERSITÉ DU QUÉBEC

BOARD OF EXAMINERS

THIS THESIS HAS BEEN EVALUATED

BY THE FOLLOWING BOARD OF EXAMINERS:

Mr. Ammar Kouki, Thesis Supervisor
Department of Electrical Engineering at École de technologie supérieure

Mr. Stephane Coulombe, Chair, Board of Examiners
Department of Software and IT Engineering at École de technologie supérieure

Mr. Francois Gagnon, Member of the jury
École de technologie supérieure

Mr. Tayeb A. Denidni, External Evaluator
Institut national de la recherche scientifique

THIS THESIS WAS PRESENTED AND DEFENDED

IN THE PRESENCE OF A BOARD OF EXAMINERS AND THE PUBLIC

ON FEBRUARY 27, 2017

AT ÉCOLE DE TECHNOLOGIE SUPÉRIEURE

ACKNOWLEDGMENT

First of all, my deepest gratitude to my wife and children for their love and great patience. This endeavor would not have been possible without their support.

I wish to express my heartfelt thanks to my supervisor Professor Ammar Kouki for his support, advices and encouragement. My deepest appreciation for his patience, availability and positivism which have added a valuable experience to my professional life.

I am in debt to Professor Sixto Garcia from ESPOL whose encouragement and help made possible my final decision to pursue doctoral studies.

I also would like to thank my colleagues of the LACIME Laboratory, especially the 'Iranian team' Hassan, Hossein, Mustafa, Aref and Aria for his friendship. I will surely miss the little technical discussions within or beyond our areas of study together with the anecdotes and jokes. My appreciation to Norman Gravel for his great logistic support.

Thanks to my colleagues of ESPOL already graduated and still students at ETS who shared their experiences and provided much help.

Finally I would like to acknowledge the decisive financial support from my University Escuela Superior Politecnica del Litoral (ESPOL)

APPLICATION DE LA COGNITION DE L'ENVIRONNEMENT ÉLECTROMAGNÉTIQUE POUR L'AMÉLIORATION D'UN LIEN DE COMMUNICATION RADIO

Juan AVILÉS CASTILLO

RÉSUMÉ

Avec l'adoption continue de dispositifs mobiles, il est prévu que la capacité du réseau cellulaire grandisse à des taux qui ne sont pas compatibles avec les réseaux micro-ondes actuels. Ainsi, l'intérêt donc dans les ondes à bandes millimétriques (30-300 GHz) a augmenté considérablement puisqu'elles offrent la possibilité d'une assignation du spectre plus large par rapport à celle existante actuellement au-dessous le 3 GHz. Spécifiquement, en ce moment l'on considère que la bande de 28-38 GHz possède un grand potentiel pour fournir des services de téléphonie mobile de cinquième génération. Dans ce sens, les mesures *in situ* démontrent qu'il est possible d'établir des liaisons de communications faisables dans un rayon de 200 mètres, même en absence de visibilité directe, en utilisant des antennes directionnelles. Ce scénario est différent de celui utilisé dans les systèmes actuels de téléphonie portable dans lesquels l'application/utilisation des antennes directionnelles normalement s'effectue après avoir complété l'accès au réseau et non pas par l'accès en soi-même. Une estimation de canal en utilisant des méthodes de formation de faisceau hybride a été proposée comme une solution, mais au détriment de l'application de plus d'une chaîne de radiofréquence. D'autre part, les techniques d'estimation à détection compressée qui tirent avantage des caractéristiques éparses des canaux à ondes millimétriques, qui fournissent une représentation précise du profil angulaire de puissance et qui requièrent un petit nombre de mesures révèlent être sensibles au bruit additif. Cette réalité peut affecter principalement des sites qui ne disposent pas d'une ligne de visibilité direct où le niveau du signal peut n'est pas suffisamment élevé.

Dans cet écrit, nous profitons des caractéristiques de propagation spécifiques du site où le système est déployé. Cette connaissance peut être exploitée dans la station de base sous la forme d'une base de données relative à la position de l'utilisateur. L'information sur la localisation d'un utilisateur devient de plus en plus accessible sur les appareils mobiles comme un élément intégré et avec un degré de précision croissant.

Dans la première partie, il est démontré que la sélection préalable des orientations des antennes les plus efficaces pour générer la valeur la plus élevée de puissance pour les utilisateurs situés dans des positions sans visibilité directe, accélère le lien d'accès. Plus précisément, pour la bande de 28 GHz, les données de simulation d'un outil du traçage de rayons appliqué dans les milieux urbains spécifiques indiquent que l'application des valeurs arbitraires des angles est sans bénéfice pour les utilisateurs. Certains angles peuvent être totalement ou partiellement bloqués par des bâtiments proches qui limitent l'éclairage en radiofréquence à une puissance maximale d'une valeur inférieure par rapport à ce qui peut être obtenu avec d'autres. Les simulations montrent qu'on peut obtenir un bénéfice de plus de 2 dB dans un certain nombre de mesures de puissance consécutives, mais cette amélioration

de la performance semble être affectée par la sévérité du type de propagation de corridor urbain existant. En outre, étant donné que les angles discrets de la station de base ou de l'équipement de l'utilisateur sont répétés individuellement ou collectivement dans des nombreuses et différentes localisations géographiques, la répartition en pourcentage des angles qui génèrent une puissance maximale peut également être exploitée pour fournir des améliorations supplémentaires. On développe une méthode de traçage de rayons simplifiée pour déterminer les meilleurs angles ainsi que leur répartition en pourcentage non uniforme. L'impact de la réduction de l'ensemble des angles est déterminé en mesurant l'amélioration du rapport signal/ bruit lorsque les angles de la station de base ainsi que l'équipement de l'utilisateur varient aléatoirement un certain nombre de fois. En outre, une comparaison entre le nombre de commutations de faisceaux d'antenne nécessaire pour établir la liaison d'accès dans une procédure d'alignement de l'antenne spécifique est effectuée. Ces résultats peuvent être utiles dans les systèmes utilisant la formation de faisceau analogique.

Dans la deuxième partie, nous avons développé un algorithme d'alignement d'antenne en profitant de la connaissance des caractéristiques de propagation spécifiques sous la forme d'une base de données liée à la localisation géographique de l'équipement utilisateur. On considère les deux cas dans lesquels la station de base connaît la situation exacte et inexacte de l'utilisateur. Nous profitons de l'observation selon laquelle l'angle de la station de base associée au premier trajet de propagation est répété à des points à l'intérieur d'un cercle de rayon *D* autour de la position indiquée. Le procédé développé peut éclairer de manière appropriée l'utilisateur, même dans le cas d'une information inexacte de la position. La détermination du meilleur angle de BS facilite l'application d'un faisceau étroit d'antenne dans la phase initiale du processus d'alignement, ce qui offre l'avantage d'un plus haut niveau de puissance au démarrage et par conséquent, d'un nombre réduit d'alignement. Les résultats de simulation montrent que l'algorithme proposé possède une performance similaire ou meilleure par rapport à un processus hiérarchique conventionnel modifié, à condition que la situation exacte de l'usager se trouve dans la zone circulaire du rayon *D* contenant des points de la base de données. Par ailleurs, le rayon *D* peut avoir une valeur un peu supérieure à l'erreur maximale du système de positionnement géographique, sans produire une plus grande variation dans la performance. D'un autre côté, on a prouvé qu'il n'est pas nécessaire d'appliquer une base de données de très haute résolution. Les résultats obtenus en appliquant des erreurs maximales de position allant jusqu'à 10 m et de résolution de la base de données allant jusqu'à 4 m, respectivement, indiquent aussi que la distance entre les points de la base de données peut augmenter jusqu'à 2 m sans impact majeur sur les performances. Ces résultats sont maintenus en variant le niveau maximal de puissance reçue à l'équipement utilisateur.

Dans la troisième partie, on développe l'application de la connaissance des caractéristiques spécifiques de la propagation d'un site pour augmenter la capacité de liaison. Étant donné que la base de données peut avoir l'information de toutes les directions de propagation existantes dans une position spécifique de l'utilisateur, nous élargissons l'algorithme développé dans la section précédente en ajoutant une seconde trajectoire sous la condition que la capacité totale soit supérieure à celle qui peut être obtenue avec seulement la première étape. L'inexactitude de la position informée par l'utilisateur force le choix d'un point de référence de la base de

données pour le rapprochement des principaux angles de la seconde trajectoire. Les simulations utilisant le traçage des rayons dans trois zones bien définies montrent que, sous des règles de décision définies, l'augmentation de la capacité supplémentaire qui pourrait être atteint avec l'application de l'algorithme est assez proche du cas idéal où l'utilisateur indique la position exacte. Étant donné qu'une étape supplémentaire est nécessaire pour que la station de base communique les angles de la deuxième trajectoire à l'équipement de l'utilisateur, le procédé d'alignement d'antenne en utilisant une base de données, continue à être plus rapide par rapport à la méthode d'alignement hiérarchique modifiée. En outre, on analyse l'effet de la résolution de la base de données sur les performances de l'algorithme proposé dans des conditions statistiques et variables.

Mots-clés: Base de données, traçage de rayons, antenne directionnelle, alignement de l'antenne, station de base, équipement de l'utilisateur, radiofréquence, localisation de l'utilisateur.

APPLIED ELECTROMAGNETIC ENVIRONMENT COGNITION TO IMPROVE A RADIO COMMUNICATION LINK

Juan AVILÉS CASTILLO

ABSTRACT

With the continuous adoption of mobile devices, the cellular wireless capacity is projected to grow at rates that would not be supported in current microwave networks, therefore, a high interest in millimeter-wave bands (30-300 GHz) has risen since they provide the possibility of a larger spectrum allocation compared to the one below 3 GHz. Specifically, the 28-38 GHz band is currently considered to have a high potential to provide fifth generation cellular services. In this regard, field measurements show that viable links, even in non-line of sight conditions, can be established within a radius of 200 meters but these need to be found with the help of directional antennas. This scheme is different from the one used in current cellular systems in which the application of directional antennas is normally applied after the network access is completed and not for the access itself. Channel estimation implemented with hybrid beamforming methods have been proposed as solutions but at the expense of more than one radio frequency chain. On the other hand, compressed sensing channel estimation techniques which take advantage of the sparse characteristics of the millimeter-wave channels giving an accurate representation of the power angle profile and a very much reduced beamforming overhead turns to be sensitive to additive noise. This latter effect can produce an impact mostly in non-line of sight locations where the signal power may not be high enough.

In this work, we take advantage of the site-specific propagation characteristics in which the system is deployed. This knowledge can be exploited at the base station side in the form of a database linked to the position of the user equipment. The location information is becoming more accessible in cellular equipment as a built-in feature with an increasing degree of accuracy.

In the first part, it is shown that a prior selection of the most effective base station antenna directions to deliver the highest possible power value to users located in non-line of sight positions can speed up an access link. Specifically for the 28 GHz band, simulation data from a ray tracing tool applied in specific urban environments indicate that the utilization of arbitrary base station angles in a cell search procedure is not of maximum benefit for the users. Some of the angles are largely or partially blocked by nearby buildings restricting the radio frequency illumination to a maximum power of a lower value compared to what can be obtained from others. A power level benefit higher than 2 dB can be obtained in a defined number of consecutive power measurements, however this performance improvement appears to be conditioned by the severity of the existing street canyon propagation. Moreover, given that the same base station or user equipment discrete angles are repeated individually or together at many different geographical positions, their percentage distribution for maximum power delivery can also be exploited for further improvement. A simplified ray tracing procedure is developed to identify the best base station angles together

with their non-uniform percentage distribution. The application impact (two scenarios) of this reduced set of angles is determined by contrasting the improvement in the signal to noise ratio when both the base station and user equipment change their main beam orientations in a random fashion a certain number of trials. Additionally, a comparison of the number of antenna beam switches needed for an access link in a particular antenna alignment procedure is performed. These results may be helpful especially for those systems using analog beamforming.

In the second part, we developed an antenna alignment algorithm exploiting specific propagation knowledge in the form of a database linked to the geographical position of the user equipment. Both cases in which the base station knows the exact and inexact location of the user are considered. We take advantage of the observation that the base station angle associated to the first propagation path serving the user repeat exactly or approximately in the database points located within a circle of radius D around the reported position. This result allows to illuminate appropriately the user even for the case of an inexact position information. The determination of the best BS angle facilitates the application of a narrow beamwidth antenna in the initial stage of the antenna alignment process providing the advantage of an increased starting illumination power and consequently of a reduced total number of alignment steps. Through ray tracing simulations it is shown that the proposed algorithm has similar or better performance relative to a modified classical hierarchical procedure as long as the exact geographical position is located inside a circular area of database points. Moreover the radius D of the circular area can be set to a value a little larger than the maximum error of the positioning system without much variation on the performance. On the other hand, there is no need of a very high resolution database. Simulation results applying maximum position errors up to 10 m and database resolutions up to 4 m, respectively, indicate that the distance between the database points can be increased up to 2m without much impact. These outcomes are sustained when the maximum power level received at the user equipment varies.

In the third part, we expand the application of a site-specific propagation characteristics knowledge to increase a link capacity. Given that a database can have information of all propagation paths associated to a specific position of the user, we extend the algorithm developed in the previous part to take advantage of a second path as long as the total capacity link is larger than what can be obtained with just the first path. The inaccuracy in the position reported forces the selection of a reference point in the database to approximate the main angles of the second path. Ray tracing simulations in three well defined areas show that for the decision rules adopted, the additional capacity gain accomplished with the algorithm is fairly close to the ideal case where the exact user position is known. Given that only one additional step is needed for the base station to communicate the angle information of the second path to the user, a database dependent alignment process remains faster relative to a comparable modified classical hierarchical method. Additionally, we examine the effect of the database resolution on the performance of the proposed algorithm for static and variable conditions.

Keywords: Database, Ray tracing, Directional antenna, Antenna alignment, Base station, User equipment, Radio frequency, User position.

TABLE OF CONTENTS

Page

INTRODUCTION 1

CHAPTER 1 BACKGROUND 13
1.1 Propagation characteristics of mmW band (outdoor links) 13
1.2 Compressive sensing in channel estimation in mmW 14
1.3 Classical hierarchical alignment procedure 15
1.4 Hybrid beamforming 16
1.5 Ray Tracing 17
1.5.1 Wireless Insite 17
1.6 Genetic algorithm 18
1.7 Global Positioning System (GPS) and Assisted GPS (A-GPS) 19

CHAPTER 2 EXPLOITING SITE-SPECIFIC PROPAGATION CHARACTERISTICS IN DIRECTIONAL SEARCH AT 28 GHz 21
2.1 Introduction 21
2.2 System model and simulation methodology 24
2.2.1 System model 24
2.2.2 Simulation methodology 32
2.3 Approximate identification of the angle range 34
2.3.1 Angle identification assessment 39
2.4 Performance impact 44
2.4.1 Maximum received SNR using the complete and best sets of BS angles 45
2.4.2 Maximum received SNR using a limited number of BS angles 48
2.4.3 Maximum received SNR in a mobile user using a limited number of BS angles 52
2.4.4 Number of switches in a beam training 53
2.5 Conclusions 54

CHAPTER 3 POSITION-AIDED MILLIMETER WAVE BEAM TRAINING UNDER NLOS CONDITION 55
3.1 Introduction 55
3.2 System model and simulation methodology 58
3.2.1 System model 58
3.2.2 Simulation methodology 59
3.3 Proposed Hierarchical Method 60
3.3.1 Number of steps 73
3.4 Algorithm performance 74
3.4.1 Static case 74
3.4.2 Random variation of the maximum received power 77
3.5 Conclusions 80

CHAPTER 4 TAKING ADVANTAGE OF A SECOND PROPAGATION PATH AT 28 GHz UNDER NLOS CONDITIONS 83
4.1 Introduction 83
4.2 System model and simulation methodology 85
4.2.1 System model 85
4.2.2 Simulation methodology 86
4.3 Proposed method 86
4.4 Algorithm performance 94
4.4.1 Static case 94
4.4.2 Random variation of the maximum received power 98
4.5 Conclusions 100

CONCLUSION 101

APPENDIX I DISTRIBUTION FUNCTION OF MAXIMUM POWER IN *L* READINGS 105

APPENDIX II SPATIAL FILTERING ON PROPAGATION DATA 113

APPENDIX III BS ANGLE IDENTIFICATION 115

APPENDIX IV ORDERED (ASCENDING) $\tilde{A}_i$ VALUES PER EACH UE IN SERVICE AREAS 119

APPENDIX V SNR COMPARISON 121

APPENDIX VI DATABASE GENERATION 125

APPENDIX VII MODIFIED CLASSICAL HIERARCHICAL PROCEDURE SIMULATION 129

APPENDIX VIII LINK WITH TWO PROPAGATION PATHS 131

BIBLIOGRAPHY 137

LIST OF TABLES

Page

Table 2.1 Percentage of combinations where $F_{\hat{Z}_1}(\hat{z}) - F_{\hat{Z}_2}(\hat{z}) \geq 0$ 30

Table 2.2 Linear routes and grid of points 37

Table 2.3 Percentage of positions of the user where $\Delta F_{\hat{Z}}(\hat{z}) \geq 0$ in service areas 1 and 2 48

Table 3.1 $D^{(maxprob)} \geq e_p$ and difference in $p_{rBestBSang}$ for $e_p \leq e_{pmax}$ 69

Table 3.2 Comparison of the number of antenna alignment steps per 180° (UE) angle span 73

Table 3.3 *D* value for the first maximum '*tspd*' 80

Table 4.1 Additional link capacity - second beam, different/same BS angle. Different DB_{res} and D ($>e_{pmax}$) 97

LIST OF FIGURES

Page

Figure 0.1 Objectives and methodology stages 8

Figure 2.1 Cellular System 25

Figure 2.2 Illustration of 1-D maximum RF coverage for different BS angles 25

Figure 2.3 UE antenna pattern and the multipath component arriving at $\theta_{UEalign}$ 26

Figure 2.4 UE antenna gain $g_u(\theta^{\Delta})$ versus the angle difference $\theta^{\Delta} = \theta_{UEalign} - \theta_{UE}$ 26

Figure 2.5 Cumulative Distribution of Z_i and $\hat{Z} = \max[Z_1 \quad Z_2 \ldots \quad Z_L]$, L=3, N=8 28

Figure 2.6 Study area 33

Figure 2.7 Simulation setups 1 and 2 36

Figure 2.8 Percentage of UEs per BS angle reaching maximum power (setup 1,3) 37

Figure 2.9 Percentage of UEs per BS angle reaching max. power (setup 2, 4) 38

Figure 2.10 Percentage of UE positions per UE angle (max. rcvd. power) in setups 1,2 39

Figure 2.11 Specific Cumulative Distribution Functions F_{BS49}, F_{BS76}, F_{UEsc1}, F_{UEsc2} 39

Figure 2.12 Setup 3 and 4 (Tx1/Tx2 center left/bottom) 40

Figure 2.13 Precision difference: 49 (setup 1) versus 50 (setup 3) and 76 (setup 2) versus 79 (setup 4) 41

Figure 2.14 Percentage of UE positions per BS angle (max. SNR) in setup 3 42

Figure 2.15 Percentage of UE positions per BS angle (received power < thres) 43

Figure 2.16 SNR at UE positions (500) 44

Figure 2.17 UE MaxSNR in 50 (25) measurements. 121 versus 49 BS angles (setup 3) 46

Figure 2.18 UE maxSNR in 50 (25) measurements 121 versus 76 BS angles (setup 4) 47

Figure 2.19 Sum of power difference (dB) versus k-BS angle groups (setup 3) 50

Figure 2.20 Number of blockings and power difference sum (dB) versus k-BS angle groups.....51

Figure 2.21 SNR in setups 3 and 4. Twenty five BS equally-spaced versus 25 selected angles (equal probability) 51

Figure 2.22 SNR statistics for a UE mobile (30 Km/h) in setup 3.....52

Figure 2.23 UE beam switches until power ≥ -85 dBm (thres) in setup 3 54

Figure 3.1 Simplified cellular system.....58

Figure 3.2 BS with a database. UE has a random initial angle 59

Figure 3.3 BS applies directly a high antenna gain.....60

Figure 3.4 DB reference curve and UE power reads.....62

Figure 3.5 Algorithm 3.1 versus modified hierarchical. BS knows the exact UE position.....63

Figure 3.6 SNR of the closest point for different DB resolutions.....65

Figure 3.7 Circular area of DB points (radius D) around the reported inexact UE position 66

Figure 3.8 Best BS & UE angles in $\hat{a}_1$ (1st row) and $\hat{a}_2$ (2nd row) for DB_{res}=0.5m. UEs are represented as black dots 67

Figure 3.9 Angle pairs (first power lobe) of all DB points and UE (exact e inexact positions) in $å_{DB}$ ($\hat{a}_1$). 67

Figure 3.10 Probability of BS angle repetition versus D in $å_{DB}$ ($\hat{a}_1$) for the conditions $ep' \in [e_p, e_p + \Delta e_p]$ and $e_p \leq e_{pmax.}$ DB_{res} = 0.5 m 68

Figure 3.11 SNR obtained ($\hat{a}_1$) from the application of one or the best of two or three BS angles inside $å_{DB}$ (selection based on repetition or power differences) 72

Figure 3.12 Performance of algorithm 3.2 ($\hat{a}_1$). DB_{res}=0.5m, D=e_{pmax}=10m (e_{pmax}=2m,6m,10m, green curves) 74

Figure 3.13 Performance of algorithm 3.2 ($\hat{a}_2$). DB_{res}=0.5m, D= e_{pmax} =10m (e_{pmax}=2m,6m,10m, green curves) 75

Figure 3.14 Performance of algorithm 3.2 ($\hat{a}_1$, $\hat{a}_2$). D=e_{pmax}=10m, DB_{res}= 1m, 2m, 3m, 4m. 76

Figure 3.15 SNR comparison ($\hat{a}_1$). Power distribution variation at UE, D=e_{pmax}=10m. $d_{DBr} \leq D$, DB_{res}=1 and 4m 77

Figure 3.16 SNR comparison ($\hat{a}_2$). Power distribution variation at UE, D=e_{pmax}=10m, $d_{DBr} \leq D$, DB_{res}=1m,2m,3m,4m 78

Figure 3.17 Relative sum of power difference versus D for $\hat{a}_1$, $\hat{a}_2$. DB_{res}=2m 79

Figure 3.18 Relative sum of power difference versus D for $\hat{a}_1$, $\hat{a}_2$. DB_{res}=1.5m 80

Figure 4.1 Cellular system.....85

Figure 4.2 Propagation power lobes at a specific location.....87

Figure 4.3 Database points used by the proposed algorithm.....89

Figure 4.4 Statistics of $\Delta d = dist(X_{DBcr2}\text{-}X_{EP}) \text{-} dist(X_{BDcr1}\text{-}X_{EP})$ in $\hat{a}_1$ and $\hat{a}_2$ 90

Figure 4.5 ($\hat{a}_1$) Capacity vs percentage of DB points in ordered set F. DB_{res}=0.5m, D=10m, e_{pmax}=8m 90

Figure 4.6 Values of of SNR_1 and SNR_2 that satisfy $C_{1*}+C_{2c} \geq C_1$ (waterfilling) 93

Figure 4.7 BS-UE angle combinations for all DB points in $\mathring{a}_{DB}$ ($\hat{a}_1$) 94

Figure 4.8 ($\hat{a}_1$) Performance of algorithm 4.1. PercBDPoints=20%, DB_{res}=2m, D=10m, e_{pmax}=8m 95

Figure 4.9 ($\hat{a}_2$) Performance of algorithm 4.1. PercBDPoints =20%, DB_{res}=2m, e_{pmax}=8m, D=10m 95

Figure 4.10 ($\hat{a}_3$) Performance of algorithm 4.1. PercBDPoints =5%, DB_{res}=2m (1.5m, 0.5m), D=10m, e_{pmax} =8m.....96

Figure 4.11 ($\hat{a}_1$) Performance of algorithm 4.1. PercBDPoints =20%, DB_{res}=0.5m,1.5m,2.0m,4.0m. D=10m, e_{pmax} =8m 97

Figure 4.12 ($\hat{a}_1$) Performance of algorithm 4.1. PercBDPoints=20%, DB_{res}=2m, D=10m, e_{pmax}=8m, E_r=8m.....98

Figure 4.13 ($\hat{a}_2$) Performance of algorithm 4.1. PercBDPoints=20%, DB_{res}=2m, D=10m, e_{pmax}=8m, E_r=8m.....99

Figure 4.14 ($\hat{a}_3$) Performance of algorithm 4.1. PercBDPoints=5%, DB_{res}=2m, D=10m, e_{pmax}=8m, E_r=8m.....99

LIST OF ALGORITHMS

Page

Algorithm 3.1 BS and UE beam alignment. BS knows the exact position of the user and has a DB with propagation information of that location.....61

Algorithm 3.2 BS and UE beam alignment. BS knows an inexact position of the user and has a DB with resolution DB_{res} of d meters 71

Algorithm 4.1 Capacity increase using a second propagation path.....91

LIST OF ABREVIATIONS

A-GPS	Assisted GPS
AoA	Angle of Arrival
AoD	Angle of Departure
BS	Base Station
CDF	Cumulative Distribution Function
CIR	Channel Impulse Response
CS	Compressive Sensing
CSI	Channel State Information
DB	Database
G_T	Maximum antenna gain transmitter
GA	Genetic Algorithm
GHz	Gigahertz
GPS	Global Positioning System
LOS	Line of Sight
MHz	Megahertz
MIMO	Multiple Input Multiple Output
mmW	Millimeter Wave
MPC	Multipath component
NLOS	Non-Line of Sight
NF	Noise figure
PAP	Power Angle Profile
PDF	Probability Density Function
RIP	Restricted Isometry Property
RMS	Root Mean Square
RMSE	Root Mean Square Error
RT	Ray Tracing
RF	Radio Frequency
Rx	Receiver

SNR	Signal to Noise Ratio
TDD	Time Division Duplex
ToA	Time of arrival
thres	threshold level
Tx	Transmitter
UE	User Equipment
ULA	Uniform Linear Array
URA	Uniform Rectangular Array
WAAS	Wide Area Augmentation System
WLAN	Wireless Local Access
WPAN	Wireless Personal Access
5G	Fifth Generation
1D	One-dimensional
3D	Tri-dimensional

LIST OF SYMBOLS AND UNITS OF MEASUREMENTS

$\hat{a}_1$	Database area 1
$å_{DB}$	Circular area of database points
$\mathcal{A}$	Set of angle values
$\tilde{A}_j$	Maximum power value at a UE position associated to a BS angle
BW	Signal beamwidth
$C(N,K)$	Combinations of K elements from Ns
D	Radius of a circular area of database points
DB_{res}	Database resolution
e_p	Position error
e_{pmax}	Maximum error of the positioning system
$f_z(z)$	Probability Density Function of the random variable z
$F_z(z)$	Cumulative Distribution Function of the random variable z
g_u	Antenna gain user (receiver)
h_{tx}	Height of antenna (transmitter)
h_{rx}	Height of antenna (receiver)
P_n	Noise power level
P_{ref}	Reference power level
$\boldsymbol{\lambda}$	Wavelength
θ_{iBS}	Base station azimuth angle i
$\emptyset_{kBS}$	Base station elevation angle k
θ_{jUE}	User Equipment azimuth angle j

$\emptyset_{lUE}$	User Equipment elevation angle l
θ_{BS}^{b}	Best BS angle
θ_{UEinit}	Random initial UE angle
θ_{UERUE}	UE angle relative to the user's reference
$\theta_{DBmaxPOw}$	UE angle for maximum power registered in the database
θ^{Δ}	angle difference
T	Period of time
$P_{i,\mathrm{j}}$	Partial maximum avg. power at UE$_i$ for any $\theta_{UE} \in [0^o : 5^o : 360^o]$ and θ_{jBS}
$\mathrm{þ}_{iN}$	Maximum average power at UE$_i$ illuminated by the best of all N-BS angles
$\mathrm{þ}_{ik}$	Maximum average power at UE$_i$ illuminated by best of a set of K-BS angles
$p_{\tilde{A}_j}$	Probability of $\tilde{A}_j$ value (max. power level at a UE position associated to θ_{BSi})
$p_{\theta_{iBS}}$	Probability of the base station angle θ_i
$\gtrsim$	Slightly larger than
U~	Uniform Distribution

INTRODUCTION

The evolution of wireless communications systems requires new technologies and methods to support better quality, new services and applications. The ever increasing need for speed (Cisco Visual Networking Index, 2016), better coverage and reduced intra-inter cell interference are the drivers of a constant improvement. Due to the capacity saturation of current microwave-band cellular systems, the millimeter waves (30-300 GHz) have risen as a viable alternative due to its potential high bandwidth capability, nevertheless they introduce special characteristics and challenges. Their almost 'optical' type of propagation predominates, that is, the reflections are more specular and the diffraction smaller; along with an increased scattering effect in rough surfaces because of their smaller wavelength. The larger free space path loss imposes the application of directional antennas both at the base station and user equipment not only for the data transmission stage but for the system access itself. Such fact together with a significant possibility of link intermittency become key differences relative to microwave systems.

The 28 GHz band for cellular system applications have attracted a high research interest, in which the channel estimation for a full MIMO connection and the initial network access play an important role. Some studies have considered (as an alternative to the versatility that can be obtained from the costly digital beamforming) the use of a hybrid beamforming scheme combined with adaptive compressed sensing to estimate the channel but with the application of more than one RF chain at both BS and UE sides. Other research efforts have proposed solutions using analog beamforming which, although limited due to its inherent 'one look' capability, also offer advantages because they apply only one RF front with reduced cost, power consumption and suitability for integration in the UE. These latter solutions force the UE to steer its antenna beam pattern in well-defined or arbitrary directions in order to catch the largest signal power emitted by the base station. Such procedure produce an impact in the period of time needed for the antenna alignment (link establishment without channel estimation) depending if this was accomplished in a hierarchical, sequential or random fashion.

The standard compressed sensing techniques (applied in systems with one RF front at Tx and Rx), which have the potential to provide close to real power and angle values of the main paths using a reduced number of iterations, appear to be more sensitive to noise. This latter fact can generate an operational difficulty especially at Non-Line-Of-Sight (NLOS) locations where the power level may not be of sufficient value to sustain the link.

Given the probable intermittent-like connection which imposes a fast link (re)establishment, context-based information techniques (position, site-specific characteristics) are emerging as alternatives (or complementary) in mmW bands. Currently, such techniques are facilitated by the more readily availability of location information, field measurement and ray tracing tools. The information can be exchanged using a lower-frequency band in which the mmW system is overlaid.

Motivation

Normally, a radio frequency (RF) coverage prediction of a specific site is done before the start of an operation for best base station (BS) positioning or for the deployment of a new base station site in an already deployed cellular operation. This RF prediction is accomplished using geographical databases (DBs) related to the topography, building geometry and distribution, clutter (terrain characteristics) and the location of neighbor BSs along with specialized software (large scale propagation model). The basic goal for this task has been the provision of sufficient average power and minimum inter-cell interference in the service area. One interesting idea that surfaced was that given the propagation prediction data are an important source of information, those can also be exploited in the operation of the base station in mmW bands because of their particular characteristics. The physical relationship between the operational parameters of a directional antenna (which facilitates viable links) and the site-specific propagation characteristics provided a research motivation on the methods that could be developed to exploit such propagation cognition to improve a communication link, specifically for NLOS location. The predicted information (path gains, main angles,…) can be used advantageously not only for a faster antenna alignment but for

other applications such as random network access, interference mitigation, prediction of the next best BS angle for a mobile user, application of a second link to the same user whether to increase the total link capacity or to cope with intermittent connections (link reliability).

Problem overview

The implementation of cellular networks in mmW bands is challenging. Some of the main difficulties that would appear in a communication link at 28 GHz are the increased propagation path loss and its vulnerability to shadowing which may result in outages and an intermittent-like connection (Rangan et al., 2014). The large path loss imposes the application of directional antennas even for the system access itself. A lack of sufficient power level prevents the UE to 'hear' the BS and consequently the provision of an appropriate feedback to BS, especially at NLOS locations. Additionally, given that the RF illumination using some BS angles may be partially (or totally) blocked for certain NLOS positions, the application of arbitrary or equally-spaced BS angles may increase the overhead in a system access procedure or in a channel estimation. Proposed algorithms normally apply iteratively the entire set of possible angles in order to find the one that optimizes some cost function. If the possible BS angles were pre-selected based on their effectiveness for RF coverage in the service area, such optimization would be more efficient because of an increased average power at the UE.

On the other hand, new techniques have emerged as solutions for mmW bands that are based on environment or context information. Among such proposals were two search algorithms introduced for cell search (Capone et al., 2015). Those algorithms used a starting beamwidth and azimuth angle related to the position of the UE (assumed to be acquired through a separate control plane operating at microwave frequency in legacy infrastructure) for the case of BS and UE equipped with a directional and omnidirectional antenna, respectively. Another proposal was the mmW beam training with receive beamforming that prioritized certain directions determined from the propagation geometry and long term statistics (Kim et al., 2014). Such solutions considered only omnidirectional antennas for the UEs that limit their

direct application in the 28 GHz band. The inclusion of a directional antenna at the UE poses the inconvenience of the lack of knowledge of its arbitrary orientation. Moreover, the techniques focused on the first main propagation path without an attempt to exploit an additional propagation path (e.g. the second) that could increase the total link capacity.

The research work should provide answers on how to exploit the site-specific propagation characteristics to improve:

- A random access procedure and quantify such improvement;
- An antenna alignment procedure (one beam). How many alignment steps can be saved?
- Increase the total capacity of a link. Although a full MIMO connection is always desirable, there are many cases in which a very large fraction of the total power is carried using just the first two main paths (the contribution of other paths to the total link capacity may be really small). Since a mmW connection may be of intermittent-like characteristic (the link can be lost easily and needs a frequent reconnection), it becomes interesting to investigate how much can be gained (in terms of link connection speed) by seeking only few propagation paths.

The application of propagation cognition at NLOS positions present the following main challenges:

- The best BS-UE angle combination for the first main propagation path extracted from a database (DB) cannot be applied directly just as a function the position of the user, even if that information was exact. The user equipment can experience an unexpected rotation both in azimuth and elevation (e.g. due to a movement of the user hand) whose random magnitude cannot be recorded for future use. This arbitrary rotation contributes with 'initial' angles ($\theta_{UEinit}, \emptyset_{UEinit}$) that changes the best UE angle saved in the DB and whose direct application may reduce greatly the received power. The DB information of other paths can neither be fully exploited unless the angles ($\theta_{UEinit}, \emptyset_{UEinit}$) are known at BS;
- The application of an inexact position of the user has the potential to generate a large received power penalty at the UE when it is used to extract the best BS angle from a DB;

- An external event may cause a variation of the power received at the UE location that cannot be predicted from the saved information in the DB;
- The application of a DB at BS must provide some advantage with respect to a well-designed hierarchical antenna alignment method (one RF front per side), which does not require any prior information for its operation.

Objectives

The general goal of this research work is to contribute with methods that exploit a prior knowledge of the propagation characteristics of a specific site to improve a communication link in an mmW band applicable for outdoors. Particularly, the research effort is concentrated in the 28 GHz band considered to have a great potential for fifth generation cellular services. The chosen environment corresponds to an urban microcellular[1] type where the base station is installed at low heights and for NLOS locations only.

A first objective is the development of a method that identifies the set of best BS and UE angles for maximum received power at any receiver position within a service area and quantify its benefit.

Given that the DB is position dependent, a second objective is to develop a method to exploit the propagation information to reduce the number of steps in an antenna alignment procedure applicable for NLOS locations. The developed method must provide results for the case of an inexact position reported by the user.

The development of a method to exploit a second propagation path to increase a link capacity for users at NLOS locations is considered as a third objective considering that a DB can have information of all the main propagation paths. Such objective is expected to be pursued even

1 Micro, pico and femtocells are the type of current urban cell deployments given that exists an increasing need to rely on smaller cells to get additional system capacity and improve radio frequency coverage. A low base station height helps to provide higher RF isolation among neighbor cells.

for cases in which there is an inexact knowledge of the position of the user. A previous evaluation of the second path viability may become necessary because there are some locations where there is a large path loss difference the first two paths.

Additional objectives are:

- Establish a relationship between the maximum positioning system error and the number of DB points needed;
- Investigate the effect of the DB resolution on the application of the propagation cognition;
- Investigate the effect of the variation of the received power at the position of the user.

Methodology

The current research work is focused on how to apply propagation cognition to improve a communication link (figure 0.1).

The research work required the development of a Matlab-Ray Tracing tool interface, for the following purposes:

- Automate the generation and saving of propagation data from a large a large number of links. Such task consisted primarily of an automatic angle variation of the transmitter and receiver directional antennas;
- Data filtering of the multipath components;
- Generation of tables with the maximum power levels per BS angle and user.

In the first part, it is generated propagation data for the case of transmitter and receivers equipped with directional and isotropic antennas, respectively. Positions of UEs located along linear routes and grids that cover two independent NLOS areas are considered. Specifically, the linear and grid of receivers were deployed for scenario 1, and only a grid of

receivers for scenario 2. The best BS and UE angles for maximum received power associated to the first propagation path were determined by a data scanning procedure. Such data filtering was accomplished by applying a narrow beamwidth antenna (array) to the multipath components existing in the channel formed between the transmitter and each one of the receivers.

To evaluate the exactness of the identified set of best angles in each service area, a new set of best angles was obtained (by simulation) in the same scenarios but with the transmitter and receivers equipped with directional (horn) antennas. The received power at UE was recorded for each combination of the 121 BS and 72 UE angles. The combination that generated the maximum power for each one of the positions considered was recorded as an element of the best set. A comparison of the maximum power received in a defined number of BS and UE random antenna switches applying both angle groups provided a measure of the exactness of the identified set of best angles.

Another performance comparison of the reduced set of best BS angles versus the complete set in each scenario was accomplished to quantify its performance benefit. Similarly, the maximum power read by the UE in a defined number of random switches of the transmitter and receiver antenna directions (angles) was used as a decision parameter. A separate performance comparison was accomplished using an equal number of angles. For this latter task, the best 25 angles from the identified set were selected using a Genetic Algorithm (GA) and contrasted their performance against 25 angles equally-spaced that covered the angle span of each service area.

In the second stage, we addressed the problem of the RF illumination of a user equipment based on a reported exact/inexact position and using only one beam at both the BS and UE.

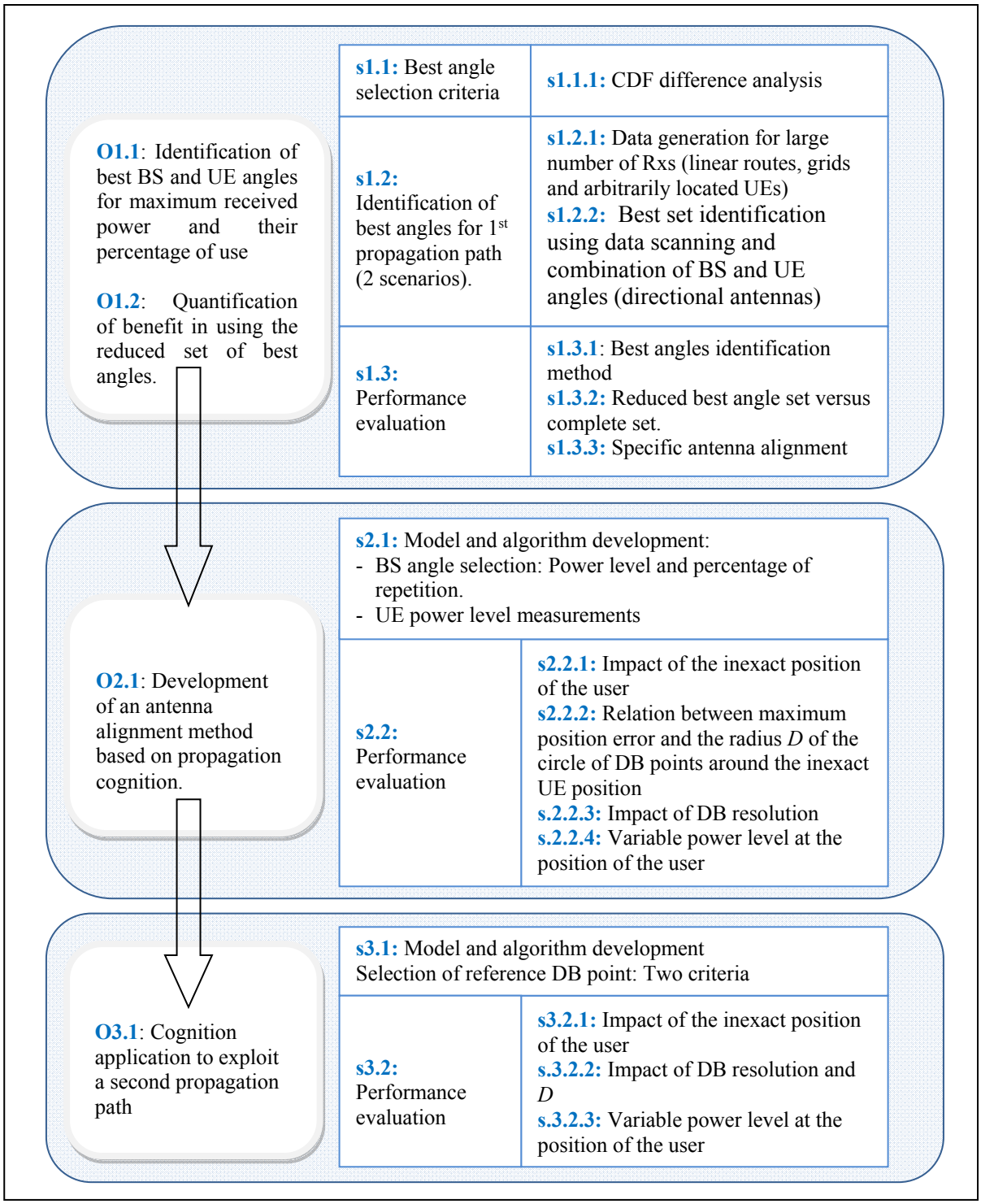

Figure 0.1 Objectives and methodology stages

Although it may seem that the knowledge of an exact position makes the antenna alignment a trivial task since the best BS angle can be applied directly from the DB information, in reality it is still necessary to take a sequence of power measurements to determine the best UE angle because it may exist an arbitrary 'initial' rotation in the user equipment that cannot be predicted from the DB information.

For the special case of an exact position information reported by the user, it is applied a simple algorithm that selects the best BS and UE angles for maximum received power. The effect of different DB resolutions are considered.

The problem of an inexact user position is tackled by selecting a subset from the total group of BS angles best serving all DB points located around the reported position within a circular area of radius *D*. The subset is chosen based on the criteria of the sum of maximum power differences and the percentage of repetition of the angles. The UE selects the BS angle from this reduced set and the best UE angle after a sequence of consecutive power level measurements. The trade-off between a variable *D* and the maximum positioning system error is analyzed for static and variable power-angle distributions. An initial DB resolution of 0.5 m is used to generate the lower resolutions of 1m, 1.5m, …, 4m. These new DBs allowed to analyze the effect of a lower resolution on the performance of the proposed algorithm. A modified classical hierarchical alignment procedure is used as a benchmark.

An extension of the previous algorithm is developed in the third stage in order to exploit a second propagation path for link capacity improvement. A key step in the proposed algorithm is the selection of a reference point among those located within a circle (radius *D*) of DB points that satisfy defined conditions (set *F*). The conditions include that of using the same (or close) BS angle for the first path determined from the application of the algorithm developed in chapter 3. Some of those DB points also have the same or close main angles of the second path associated to the UE but with a different degree of visibility in terms of power levels. Two criteria were applied. The first corresponded to the selection of the DB point receiving the maximum power whereas the second to the selection of that which

belongs to a top fraction of an ordered set (power based) and it is located statistically closer to the geographical center of the DB points in set *F*.

Contributions and Novelty of the Thesis

To the best of the author knowledge, this study is the first work that exploits the site specific information associated with the user position at millimeter band for outdoor cellular links. Governed by the objectives and methodology presented, the research work accomplished the following contributions:

- Ray tracing method to identify the best BS and UE angles for maximum received power at the user position. The resulting set has a lower number of elements (cardinality) compared to the full set of BS angles for which its repetition generates a larger received average power in a defined number of random power sample readings at the UE location. The application of the percentage of use (based on the RF coverage of many Rx positions) of each of the best angles has the potential to further increase the received average power. This application is most beneficial in a random access scheme especially for systems using one RF front;

- Algorithm that exploits the propagation characteristics of a specific site linked to an exact/inexact position reported by the user equipment to the BS. The algorithm takes advantage of the fact that the best BS angle that serves a user is repeated in its geographic vicinity. By considering the DB points located within a circular area of radius *D* a little larger than the maximum positioning system error, the algorithm is able to select a small group of BS angles that best illuminate the UE. The user equipment select both the BS angle from this group and its best UE angle after a sequence of power measurements;

- Extension of the previous algorithm to exploit a second propagation path. The total capacity of the two-beam communication link is increased even for the case of an inexact reported position. Defined rules are applied to evaluate the viability of the second path.

The algorithm selects a reference DB point (located within a circle of radius *D* around the reported position) based on the criteria of maximum power delivery and percentage of angle repetition. The algorithm uses the power distribution profile of the DB reference point to approximate the best main angles of the second path.

Publications

The list of publications associated with the research work is the following:

Journal Published

Aviles, Juan and Ammar kouki. 2016. 'Exploiting site-specific propagation characteristics in directional search at 28 GHz'. *IEEE Access*, vol. 4, p. 3894-3906.

Aviles, Juan and Ammar Kouki. 2016. "Position-aided mm-wave beam training under the NLOS condition'. *IEEE Access.* vol. 4 p. 8703-8714.

Journals submitted

Aviles, Juan and Ammar Kouki. 2106. 'Taking advantage of a second propagation path at 28 GHz under NLOS condition'. *Physical Communication* (Elsevier). October 2016

Thesis outline

This thesis is organized into four chapters and 8 appendices.

Chapter 1 summarizes the literature review related to the addressed problems.

Chapter 2 introduces a practical ray tracing method to identify the set of the best BS and UE angles along with their percentage of use within the service area. A defined set of linear and grid of receiver points were selected in two different scenarios in which the transmitter and receivers were equipped with directional and isotropic antennas, respectively. An assessment of the proposed method is accomplished by comparing the performance of the set of angles

selected against the best angles obtained using directional antennas at both Tx and Rxs. A quantification of the benefit reached in applying the set of best angles and their usage percentage is presented for a random access application in a system using one RF front at BS and UE.

Chapter 3 studies the advantage of using propagation cognition in the form of a database linked to the position of the user equipment. Both cases of exact and inexact positions of the user are considered. It is proposed an algorithm that determines the best BS and UE angles from the database points located around the inexact position reported by the user. The impact of different database resolutions is simulated for static and variable propagation conditions. A relationship between the radius *D* of the circle containing the database points around the reported location and the maximum error of the positioning system is established through simulations. A modified classical hierarchical antenna alignment method was used as a benchmark for comparison purposes. Two different areas of high and relatively small signal to noise ratios (SNR) were selected for the simulations.

Chapter 4 presents an algorithm extension developed in chapter 3 that takes advantage of a second propagation path in order to increase the total link capacity. Results are shown for static and variable power levels at the user position. The additional capacity benefit is analyzed as a function of the DB resolution and the radius *D*. The benchmark is the same as that applied in the previous chapter.

The appendices includes complementary information to the work developed in the chapters.

CHAPTER 1

BACKGROUND

1.1 Propagation characteristics of mmW band (outdoor links)

The field measurement campaign performed in New York City and the University of Texas at Austin Campus in order to characterize the outdoor propagation of mmW band signals (28 and 38 GHz) in urban environments brought the following conclusions:

- Modern building materials are good reflectors which facilitate not only outdoor Non-Line-Of-Sight (NLOS) links but Radio Frequency (RF) power contention within buildings (Zhao et al., 2013);
- There is a large number of distinguishable propagation paths at any receiver position in both Line-of-Sight (LOS)/NLOS environments with excess delay spreads (20 dB) up to 753.5 ns and 1,388.4 ns, respectively, allowing feasible links in cell sizes of around 200 m with the help of high gain steerable antennas. The NLOS path loss exponent (PLE) determined was 5.76 with a shadow fading (SF) of 9.02 dB. These values decreased to 4.58 and 8.83 dB, respectively, when only the strongest NLOS links were considered (Azar et al., 2013);
- The power levels for small scale fading do not change significantly from the mean power level at a fixed AoA and there is an average of 2.5 signal lobes, each with an average total and RMS angle spread of 40.3^{o} and 7.8^{o}, respectively (Samimi et al., 2013);
- At 38 GHz, urban canyons entail beam steering over a small range of angles at the transmitter site (Rappaport, 2012);
- Elevated 38 GHz transmitters installed at building heights between the second and eighth floor and using beam steering may need up to ±30^{o} off boresight in azimuth to cover nearly all possible NLOS links within the service area and for cases where the LOS direction is blocked, there is a reflection, scattered or diffraction path that permits the UE to receive sufficient power (Rappaport, 2013);

- Even for heavy rainfall of 25 mm/hour, the rain attenuation reaches only 1.4 dB/200m at 28 GHz and 1.6 dB/200m at 38 GHz although it may have larger values for short period of times (Zhao, et al., 2006);
- Millimeter wave channels are typically characterized by a few dominant paths. The propagation is accurately predicted by ray tracing with a small number of rays (Hur et al., 2015);
- Urban canyon topologies may result in a frequent lack of LOS connectivity and severe shadowing (Rangan et al., 2014).

1.2 Compressive sensing in channel estimation in mmW

Due to the characteristics of the mmW signals, the multipath components are normally concentrated in few main propagation paths. This sparsity property facilitates the combined application of analog or hybrid beamforming and compressive sensing (CS) to estimate the channel parameters AoDs, AoAs and path complex gain (Berraki et al, 2014, Alkhateeb et al., 2015). CS theory indicates that a sparse signal in a certain transform domain can be recovered with fewer measurements compared to traditional methods. For this effect, the sampling (measurements) process must be incoherent relative to the transform used to represent the sparse signal (Berger et al., 2010). The coherence between the sensing basis $\mathbf{\Phi}$ and the signal representation basis $\mathbf{\Psi}$ measures the correlation between any two elements in these sets. The smaller the coherence, the lower the number of measurements needed (e.g. random matrices present a large incoherence relative to any fixed basis). Assume $\mathbf{y} \in C^{\mathrm{n}}$ can be represented with an arbitrary basis $\{\Psi_k\}_{k=1}^{\mathrm{n}}$ and the coefficients x_k so that $\mathbf{y}=\mathbf{\Psi x}$. The vector $\mathbf{x}$ has s elements different from zero (s-sparse). The acquisition of the signal from m<n measurements can be written as $\mathbf{z} = \mathbf{\Phi}^H\mathbf{y}+\mathbf{v} = \mathbf{\Phi}^H\mathbf{\Psi x}+\mathbf{v} = \mathbf{Ax}+\mathbf{v}$, where $\mathbf{v}$ is a noise vector. The solution requires that $\mathbf{A}$ satisfies the Restricted Isometry Property (RIP), that is, there exists a δ_s such that $(1-\delta_s)\|\mathbf{x}\|_2^2 \leq \|\mathbf{Ax}\|_2^2 \leq (1+\delta_s)\|\mathbf{x}\|_2^2$ (Candès et al., 2008). It can be shown that for m≥(Cs)log(n/s) measurements, the probability that $\delta_s \geq \delta$ decreases exponentially with m and δ (Berger et al., 2010). C is specified for the various types of

matrices. There exists a large group of random matrix classes that satisfy the RIP property such as those with identical and independent (i.i.d.) Gaussian or Bernoulli entries.

The application of a classical compressive sensing with analog beamforming for a channel estimation demonstrates its usefulness in the AoD and AoA accuracy reached and especially the lower number of iterations than that of the classical hierarchical alignment method, however it is affected in cases of low SNR (Berraki et al, 2014). Such condition may appear when the transmitter emits beacons by applying random phases to the elements of its antenna array in order to comply with the RIP property; which in turn diminishes the beamforming gain. Moreover, given that it is important to have the possibility to determine new propagation paths that arise due to a sudden environment change or movement of the UE, the antenna of the UE needs to be mainly omnidirectional. As a result, the receiver directivity gain is also unavailable during the channel sounding stage compared to the data communication part (Ramasamy et al., 2012). The alternatives to circumvent these difficulties for LOS links are the use of a narrowband signal (e.g. 1 MHz instead of 1GHz which gives 30 dB gain) and a transmitter power increase, nevertheless, these gains may not be sufficient at NLOS positions due to a larger path loss.

1.3 Classical hierarchical alignment procedure

A classical hierarchical beamforming method for antenna alignment purposes uses one antenna main lobe both at BS and UE with a variable beamwidth starting with a low gain in the first level that covers a large space and ending with a high gain (small beamwidth) applied for an angle refinement in a much more restricted angular space. At the end of each level the UE feeds back the best beam identification that permits the BS to direct the illumination in certain specific sector using a new group of antenna patterns with higher gains. This scheme requires much less iterations compared to the exhaustive beam search in which all possible beam directions (fixed beamwidth) both at the BS and UE are tried in order to discover the best beam combination for a maximum received power at the UE position. Hierarchical beamforming techniques applicable at millimeter frequencies have

been researched and adopted in the standards IEEE 803.15c for WPAN and IEEE 802.11ad for WLAN which are intended for indoor applications in the 60 GHz band for a maximum range up to 10m (IEEE 802.15.3c/802.11ad Specifications). These techniques do not extend directly for outdoors due to the much larger distances involved (Hur et al., 2013; Ramasamy et al., 2012) and consequently an increased path loss which poses challenges especially in the first stages of the alignment procedure where the antenna presents a wider beamwidth, that is a lower gain.

A variation of the hierarchical method applicable for outdoor pico cells for backhauling and access purposes at 60 GHz has been proposed as a beam alignment technique using adaptive subspace sampling and hierarchical beam codebooks (Hur et al., 2013). The classical alignment scheme applies just one beam both at the BS and UE and concentrates primarily to find the best angles that maximize the received power instead of finding all the dominant path gains and angles (channel estimation).

1.4 Hybrid beamforming

A hybrid beamforming has been devised as an alternative method to overcome the large path loss in mmW bands avoiding the costly digital beamforming which requires one RF chain per antenna element and a complete channel state information (CSI) knowledge for its operation. CSI is problematic to get in mmW bands (e.g. 28 GHz) due to the large number of antennas both at BS and UE and the low SNR existent before beamforming. Hybrid beamforming is configured as a combination of a baseband digital precoder followed by analog precoder implemented with RF phase shifters. The combination of this configuration with an adaptive algorithm allows to estimate the mmW channel using for example a hierarchical multi-resolution codebook (El Ayach et al. 2012; Alkhateeb et al., 2014). The final number of RF fronts needed depends on the design of the codebook. The discovery of the main propagation paths can be exploited during the data transmission stage.

It is to be noted that the use of hybrid beamforming may allow to get a close spectral efficiency achieved with digital beamforming, nevertheless this cannot increase in terms of

the number of data streams due to the limited scattering of the mmW channel (Kwon et al., 2014).

1.5 Ray Tracing

Ray Tracing (RT) is a very well-known technique that has the ability to simulate site-specific multipath propagation and the time-space dispersion characteristics of the Tx-Rx channel (Hur et al., 2015, Molisch, et al., 2016). Its high computation time demand becomes easier to overcome with the current computing capabilities. RT is based on the Geometrical Theory of Propagation. The effect of diffraction (edges, vertex) is considered separately through the Geometrical Theory of Diffraction (GTD). Besides the reflection, transmission and diffraction components, modern RT engines incorporates diffuse scattering to include the effect of a larger roughness of the walls and the surface irregularities which are accentuated due to the small wavelength. The larger directivity of the RF illumination obtained with mm-wave frequencies facilitates a high level of accuracy in the RT predictions (Degli-Esposti et al., 2014).

RT requires a detailed description of the geometrical and electromagnetic properties of every object (buildings, vegetation,…) in the simulated service area together with the antenna radiation patterns applied. Its algorithm can be separated in the visibility algorithm and the field computation procedure. The first creates a database of the objects and their visibility relations are used to trace the ray paths. In the second part, the path reflection, transmission and diffraction losses are computed together with the diffuse scattering effect (Degli-Esposti et al., 2014). Commercial software packages for mmW propagation prediction in urban environments provide different output and analysis options (Međedović et al., 2012).

1.5.1 Wireless Insite

Wireless InSite (http://www.remcom.com/wireless-insite) is a friendly and efficient software application designed to predict propagation characteristics with high accuracy in complex

environments (indoor, outdoor) in the range 50MHz-100GHz. The calculations are accomplished by ray launching, that is, by emitting rays from the transmit location according to the antenna radiation pattern. These rays interact with the surroundings in the form of reflections from building surfaces, diffractions (edges, vertex) and transmission through objects until they reach the receiver or their power strength goes below a certain defined level. The main input corresponds to a full 3D digital map (prepared using an editor facility in the software package or imported from an external source) that details the building distribution, streets layout and eventually trees or any other physical object affecting the propagation along with their electromagnetic characteristics (i.e. permittivity, conductivity). The result of the simulation is a series a text tables providing information of the different multipath components connecting the transmitter with the receiver. The information includes DoA, AoA, ToA, received power, path loss, CIR, delay spread, electric/magnetic signal magnitude and phase, power delay profile, doppler shift, carrier-to-interferer ratio, identification of the propagation paths. The accuracy of the calculations is determined by the degree of exactness of the digital map and electric characteristics of the material relative to reality.

1.6 Genetic algorithm

The GA is an optimization and search procedure based on genetics principles and natural selection where the solutions are represented as chromosomes. It allows a population of individuals to evolve to a maximum fitness state under well-defined selection rules (Zalzala and Fleming, 1997). The process that generate new solutions is accomplished through the repeated application of three genetic operators: selection, mating or crossover, and mutation. The best chromosomes are selected to become parents in the next iteration. Among the selection methods are the pairing from top to bottom, random pairing, weighted random pairing (roulette wheel weighting), tournament Selection (Haupt, 2013).

The mating is creation of one or more offspring from the parents selected in the pairing process. The genetic characteristics are limited to the current population. A crossover point is

randomly selected between the first and last bits of the combining chromosomes so the offspring inherit genes from the two parents. Since the mating may select some type of individuals more often than others so that the new solutions may become similar after several generations, the mutation mechanism comes into play to inject diversity into the population. The mutation can introduce traits not existent in the original population and keeps the GA from converging too fast.

Among the advantages that GA provide are: optimization with continuous or discrete variables, does not require derivative information, work with a large number of variables and optimizes variables with extremely complex cost surfaces (Haupt, 2013).

1.7 Global Positioning System (GPS) and Assisted GPS (A-GPS)

The Global Positioning System (USA) is a space-based navigation system (24 satellites) that provides location, speed and time information to a user anywhere on the earth under any weather condition. There are other systems available or under development for the same purpose like the Russian Global Navigation Satellite System (GLONASS), the European Union Galileo, Indian Regional Navigation Satellite System, BeiDou Navigation Satellite System (China) and the Japanese Quasi-Zenith Satellite System.

A GPS receiver must be locked to at least to 3 satellites to calculate a 2-D position (latitude and longitude) and track movement. Four or more satellites allows the receiver to determine the 3-D position, that is, the latitude, longitude and altitude. The GPS unit can also calculate the speed, bearing, trip distance and more. Current commercial GPS receivers can have an average accuracy equal or less than 15 meters which can be lowered to 3 meters with a Wide Area Augmentation System (WAAS). Among the factors that can affect the GPS accuracy are the signal multipath, number of satellites visible and geometry, intentional degradation of the satellite signal (Selective Availability-SA). As of May 2000, SA was turned off so that only Precise Positioning Service (PPS) was provided which significantly increased the accuracy of the civilian GPS receivers (http://www8.garmin.com/aboutGPS/).

An average position error is reported periodically (GPS, SPS, Performance Analysis Report, Federal Aviation Administration). The 95% (99%) of predicted horizontal and vertical GPS positioning error corresponding to the period of January 01-March 30, 2015 was of 3.097m (7.4m) and 5.044m (11.4m) respectively. The data was collected for every second at 28 selected WAAS locations where there was 100% availability at all sites.

A-GPS operates differently than the typical handheld GPS receiver. Many of the functions of a full GPS receiver are executed at a remote server which provides satellite orbit, clock information, initial position and time estimate, satellite selection, range and position computation. This information permits the UE to get a fast position lock-on since it does not need to decode the GPS messages for each satellite or perform an extensive search for visible satellites when this built-in feature is applied. A-GPS uses remote server data to enhance quality and precision when there exists poor satellite signal conditions. In urban areas satellite signals may present multipath propagation that impairs the GPS system to provide better accuracy or a rapid position determination. An assisted GPS system can address these problems by using external data.

Unobstructed ten 20-minute field measurements (every 5 seconds-240 measurements) using a 3G iPhone indicate that A-GPS locations are less accurate than those obtained from regular GPS units. Data shows an A-GPS horizontal position error with a median of 9 m and RMSE of 7.7m (Zandbergen et al., 2009).

CHAPTER 2

EXPLOITING SITE-SPECIFIC PROPAGATION CHARACTERISTICS IN DIRECTIONAL SEARCH AT 28 GHz

2.1 Introduction

With the increasing adoption of mobile devices (e.g. smartphones), cellular wireless capacity is projected to grow at a rate that would not be supported in today's networks (Cisco Visual Networking Index, 2016). Therefore, there has been increasing interest in cellular systems based on the so-called millimeter-wave -mmW- bands (30-300GHz) because such systems provide the possibility of a larger spectrum allocation than that obtained for cellular systems below 3GHz (Khan, 2011). Specifically, the 28-38 GHz band is currently considered to have a strong potential to provide 5th Generation cellular services. In this regard, measurements and simulations have been performed in order to characterize outdoor propagation of mmW signals (Zhao, 2012; Azar et al., 2013; Samimi et al., 2013; Rappaport 2012 and 2103, Hur et al., 2014). Due to the large propagation path loss, the potential communication links that can be establish between the Base station (BS) and User Equipment (UE) need to be "found" through the application of high gain directional antennas at both sides of the link before the payload data transfer takes place. Since the small wavelength related to this frequency band facilitates packing many antenna elements, the required antenna gain can be accomplished through the help of beamforming techniques. However, new procedures must be designed in order to take advantage of these techniques given that their application is different than those used in cellular systems operating at microwave frequencies where the beamforming normally takes effect after the user gets an access connection (Desai et al., 2104) and not for the access itself. The same situation would appear in a random access where it is difficult to take advantage of the beamforming gain due to an insufficient knowledge of the best beam combination (Jeong et al., 2015), especially for NLOS environments. Digital beamforming would offer much more flexibility for a faster BS-UE link set up in directional cell search

methods where the base station transmits periodically a synchronization signal[2] in random directions (Barati et al. 2014), nevertheless the number of required RF front ends with analog to digital converters becomes costly and it would not be practical for the UE. On the other hand, analog beamforming, while limited to match the characteristics of digital beamforming mostly due to its inherent 'one look direction' offers advantages since it uses a single RF chain with reduced cost, complexity and power consumption as well as suitability for integration in the UE. Despite this shortcoming, which poses significant challenges in the BS-UE initial connection, interest on analog beamforming used alone, or in combination with digital precoding in a hybrid solution, is increasing. In (Eliasi et al., 2014), considering that an accurate mmW channel estimation for beamforming purposes is challenging and the channel measurements may be accomplished with analog beamforming, a novel method to estimate the receiver side covariance is introduced based on a sequence of UE power measurements taken from different directions whereas the BS beam pattern is kept fixed. In (Alkhateeb et al., 2014), an adaptive algorithm is developed that estimates an mmW channel based on a novel hierarchical multi-resolution codebook. Using the estimated channel data the paper additionally proposes a new hybrid analog-digital precoding algorithm that approaches the performance of the digital solution. In (Kim and Molisch, 2014), it is proposed two types of adaptive beam training protocols (Indoor-60GHz) with receive beamforming. For the fixed modulation scheme, an interactive beam training stops the angle search when a local maximum is found that has sufficient power to support the selected modulation. Furthermore, simulations suggest that a search prioritization of certain directions determined from operational long term statistics speeds up the link configuration over a traditional exhaustive search.

Much of the research effort for directional search in mmW bands is largely directed to seek the most suitable propagation paths or equivalently the best antenna beam directions that maximizes the power received by the UE because the larger the power, the more efficient a cell discovery or a beam training procedure becomes. Nevertheless, this task is complicated

---

[2] The UE measures the power received from different BS angles in L (=50, each every 5ms) consecutive 100 μs time slots.

due to the presence of blocking, that is, the probability that the mmw signal is completely blocked (Akdeniz et al. 2013). RF illumination using some BS-UE beam directions may be so blocked by nearby buildings that its application could be considered an inefficient use of power. This inefficient use generates a potential lack of appropriate power level received at an NLOS position even at short distances from BS that prevents a guaranteed feedback from the UE. In contrast, there is a high probability (urban environments) that the best antenna orientations are only in the direction of the streets (street canyon propagation), which does not favor the general use of a complete set of equally spaced BS angles for transmission of the synchronization signals.

One line of research that has not been fully explored is based on the concept of utilizing the knowledge of the propagation characteristic of the service area. This information may be coordinated from a legacy microwave cellular infrastructure on which the mmW system is overlaid (Khan and Pi, 2011; Desai et al., 2014). A separation between control and user planes in this type of compounded networks may facilitate the use of information related to a specific service area or the position of the user for cell search (Capone et al., 2105). Cognition of the site-specific propagation characteristics can be exploited in the initial stage of the NLOS BS-UE connection procedure in the 28-38 GHz band, particularly for systems using analog beamforming.

Because the propagation information is site specific, we first propose a simplified ray-tracing (RT) procedure to identify the most effective BS and UE angles in terms of the maximum received power at any position of the user. Second, the application of the reduced set of identified BS angles is demonstrated to have the potential to increase the average signal-to-noise ratio (SNR) in a defined number of power measurements compared to that obtained using arbitrary angles. Moreover, given that the same best BS and UE discrete angles may be repeated individually or together at many different UE geographical positions, it is also shown that their percentage distribution at the NLOS positions can also be exploited for further improvement. The performance benefit using this reduced set of angles is determined in two scenarios with different street canyon propagation characteristics. For this task, it is

contrasted the improvement in the SNR when both the BS and UE change their main beam orientations randomly and from the difference in the number of angles switches used in a specific beam alignment method.

Potential advantages can be expected for such cases where the BS transmits simultaneously in various directions using different pilot carrier frequencies (Desai et al, 2014), broadcasts synchronization signals periodically using a random switching of the beamforming vector angles (Barati et al. 2104; Jeong et al., 2015), or uses the UE position and/or its associated context-based information for beamforming (Capone et al., 2015).

The remainder of the chapter is organized as follows. Section 2.2 describes the system model and simulation methodology. A RT method for an approximate identification of best angle ranges for BS RF illumination is proposed in section 2.3. Section 2.4 presents applications of the selected angles. Finally, the concluding remarks are provided in section 4.5.

2.2 System model and simulation methodology

2.2.1 System model

Consider one time division duplex (TDD) cellular system sector (figure 2.1) of dimensions 60ºx200 m located in a specific urban environment where both BS and UE are equipped with one RF chain and directional antennas. The UE is located at a NLOS position. The BS illuminates (downlink) the service area whereas the UE measures the received power (using discrete angles from defined sets), both switching their antenna beams L times in a random fashion within a time period T. At the end of each period, the UE determines the maximum received power.

To get insight on the benefit of applying the selected BS angles for RF illumination in an access procedure, it is first considered a simplified one-dimensional (1-D) scheme in which the UE receives only one multipath component with an angle of arrival (AoA) $\theta_{UEalign}$.

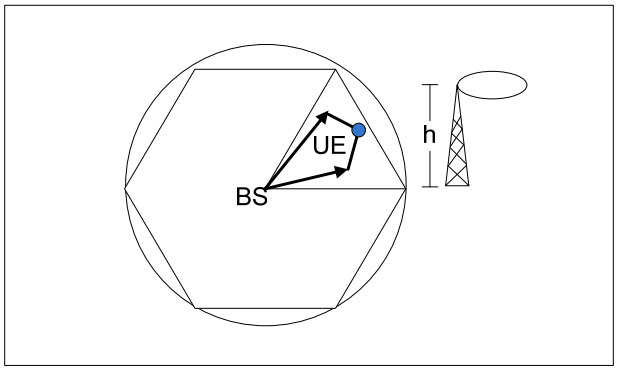

Figure 2.1 Cellular System

Given that each BS angle θ_{iBS} renders a different RF spatial coverage, the UE reads a power a maximum power level $\tilde{A}_i$ (figure 2.2) when its antenna's main beam is aligned with respect to $\theta_{UEalign}$ (Figure 2.3). For any UE angle, the received power is affected by the gain of the antenna. We assume the BS uses θ_{iBS} with $p_{\theta_{iBS}}$ =Prob(θ_{iBS}), and for each θ_{iBS}, it is associated a maximum power level $\tilde{A}_i$ where $p_{\tilde{A}_i}$=Prob($\tilde{A}_i$)= $p_{\theta_{iBS}}$ (i=1,2,3,…..,N) and $\tilde{A}_1 < \tilde{A}_2 < \ldots . < \tilde{A}_N$.

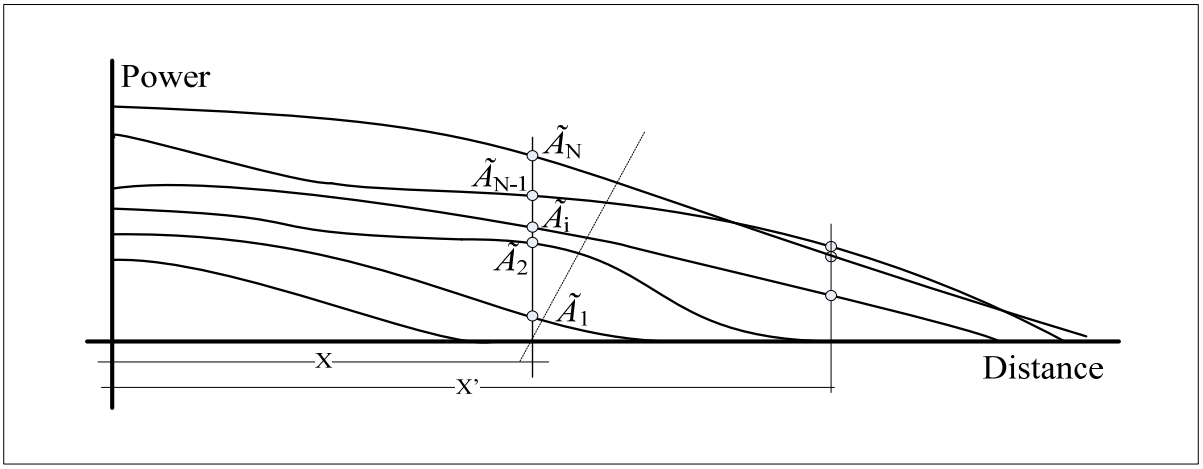

Figure 2.2 Illustration of 1-D maximum RF coverage for different BS angles

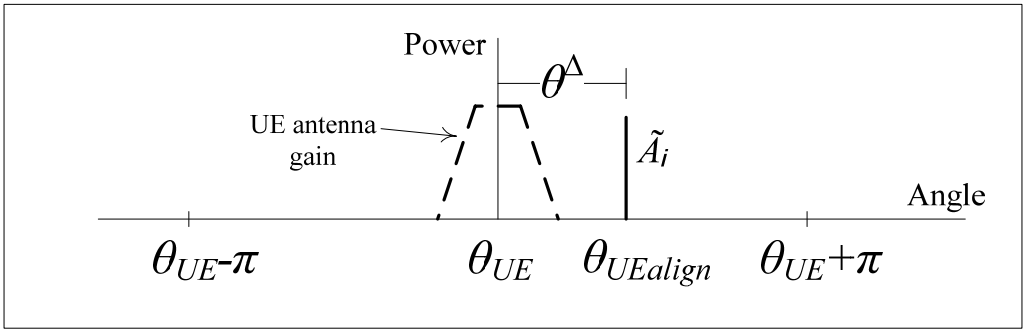

Figure 2.3 UE antenna pattern and the multipath component arriving at $\theta_{UEalign}$

For any UE angle, the received power is $Z=\tilde{A}\ g_u(\theta^{\Delta})$, where g_u is the gain of the UE antenna assumed to have the pattern in Figure 2.4 and represented by the equation 2.1 (Akoum et al., 2012). $\theta^{\Delta} = (\theta_{UEalign} - \theta_{UE})$ is the difference in the UE azimuth angles between the arriving multipath component with orientation $\theta_{UEalign}$ and the UE antenna direction θ_{UE}. The values of θ^{Δ} follow a uniform distribution, i.e., $\theta^{\Delta} \sim$ U(-π,π].

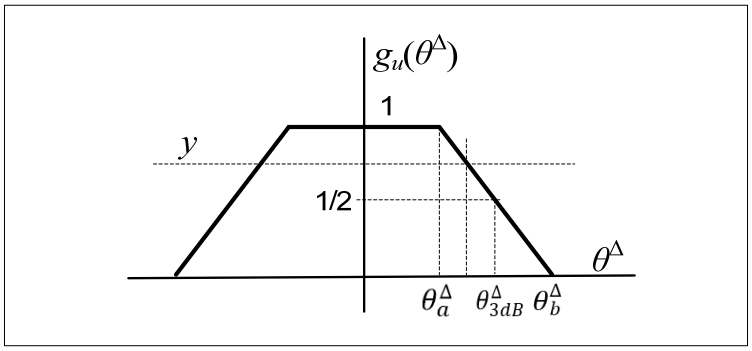

Figure 2.4 UE antenna gain $g_u(\theta^{\Delta})$ versus the angle difference $\theta^{\Delta} = \theta_{UEalign} - \theta_{UE}$

$$y = g_u(\theta^{\Delta}) = \left\{ \begin{matrix} 1 & |\theta^{\Delta}| \le \theta_a^{\Delta} \\ \left| 1 - \frac{|\theta^{\Delta}| - \theta_a^{\Delta}}{2(\theta_{3dB}^{\Delta} - \theta_a^{\Delta})} \right| & \theta_a^{\Delta} < |\theta^{\Delta}| \le \theta_b^{\Delta} \\ 0 & \theta_b^{\Delta} < |\theta^{\Delta}| < \pi \end{matrix} \right\};\ \theta_{3dB}^{\Delta} = \frac{\theta_a^{\Delta} + \theta_b^{\Delta}}{2} \quad (2.1)$$

The Cumulative Distribution Function (CDF) of Z in the range $\tilde{A}_{j-1} \leqslant z < \tilde{A}_j$; j=1,2,…,N, for any antenna orientation can be calculated (Papoulis, 2002) as follows (Appendix I):

$$F_Z(z) = \left(1 - \frac{\theta_b^{\Delta}}{\pi}\right) + \left(\frac{\theta_b^{\Delta}}{\pi}\right) \sum_{i=1}^{j-1} p_{\tilde{A}_i} + \left(\frac{\theta_b^{\Delta} - \theta_a^{\Delta}}{\pi}\right) z \left[\sum_{i=j}^{N} \frac{p_{\tilde{A}_i}}{\tilde{A}_i}\right] \tag{2.2}$$

and the CDF of g_u corresponds to (Appendix I):

$$F_{g_u}(y) = \begin{Bmatrix} 1 & y \geq 1 \\ 1 + \frac{1}{\pi}\left[2y\left(\theta_{3dB}^{\Delta} - \theta_a^{\Delta}\right) - \left(2\theta_{3dB}^{\Delta} - \theta_a^{\Delta}\right)\right] & 0 \leq y < 1 \\ 0 & y < 0 \end{Bmatrix} \tag{2.3}$$

After L measurements Z_i (considered as independent random variables), the maximum UE power read and its CDF can be written as (Papoulis, 2002):

$$\hat{\mathrm{Z}} = \max[Z_1 \quad Z_2 \ldots \ldots \quad Z_L] \tag{2.4}$$

$$F_{\hat{\mathrm{Z}}}(\hat{\mathrm{z}}) = F_{Z_1}(\hat{\mathrm{z}}) F_{Z_2}(\hat{\mathrm{z}}) \ldots F_{Z_i}(\hat{\mathrm{z}}) \ldots F_{Z_L}(\hat{\mathrm{z}}) \tag{2.5}$$

$$\begin{aligned} F_{\hat{\mathrm{Z}}}(\hat{\mathrm{z}}) = & \left\{\left(1 - \frac{\theta_b^{\Delta}}{\pi}\right) + \left(\frac{\theta_b^{\Delta}}{\pi}\right) \sum_{i_1=1}^{j-1} p_{\tilde{A}_i} + \left(\frac{\theta_b^{\Delta} - \theta_a^{\Delta}}{\pi}\right) \hat{\mathrm{z}} \left[\sum_{i_1=j}^{N} \frac{p_{\tilde{A}_i}}{\tilde{A}_i}\right]\right\} \cdot \\ & \cdot \left\{\left(1 - \frac{\theta_b^{\Delta}}{\pi}\right) + \left(\frac{\theta_b^{\Delta}}{\pi}\right) \sum_{i_2=1}^{j-1} p_{\tilde{A}_i} + \left(\frac{\theta_b^{\Delta} - \theta_a^{\Delta}}{\pi}\right) \hat{\mathrm{z}} \left[\sum_{i_2=j}^{N} \frac{p_{\tilde{A}_i}}{\tilde{A}_i}\right]\right\} \ldots \ldots \ldots \\ & \ldots \ldots \ldots \left\{\left(1 - \frac{\theta_b^{\Delta}}{\pi}\right) + \left(\frac{\theta_b^{\Delta}}{\pi}\right) \sum_{i_L=1}^{j-1} p_{\tilde{A}_i} + \left(\frac{\theta_b^{\Delta} - \theta_a^{\Delta}}{\pi}\right) \hat{\mathrm{z}} \left[\sum_{i_L=j}^{N} \frac{p_{\tilde{A}_i}}{\tilde{A}_i}\right]\right\} \end{aligned} \tag{2.6}$$

Figure 2.5 shows plots of three individual $F_{Z_i}(\hat{\mathrm{z}})$ for the particular cases of a) arbitrary $\tilde{A}_i$*'s* and $p_{\theta_{iBS}} = p_{\tilde{A}_i} = P_i$ values ($\tilde{A}_{\mathrm{ia}}$, $\mathrm{P_{ia}}$ -black o) considered as a reference; b) same P_i values but increased $\tilde{A}_i$ values ($\tilde{A}_{\mathrm{ib}}$, $\mathrm{P_{ia}}$ - black square) and c[3]) same $\tilde{A}_i$ values but with an increased probability for the higher values of $\tilde{A}_i$ ($\tilde{A}_{\mathrm{ia}}$, $\mathrm{P_{ib}}$ - black Δ). We assumed θ_{3dB}^{Δ}=6.5°, θ_a^{Δ}=3°; θ_b^{Δ}=10°, L=3, N=8 for the simulation. For an arbitrary level *arlv*, F_{Z_l}(*arlv*) calculated with the

3 Note that these variations help increase the total power $\check{\mathrm{Z}} = \sum_{i=1}^{L} z_i$ (read by the UE in L time slots), which in turn improves the cell detection when it is applied in a Generalized Likelihood Radio test for cell search in systems using analog beamforming (Barati et al., 2014).

parameters of case 'b' is lower than that of case 'a' because the third term of (2.2) decreases with larger $\tilde{A}_i$ values. Similarly, $F_{Z_l}(arlv)$ evaluated with the parameters of 'c' is lower than that of case 'a' because the decrease in value of the second term in (2.2) is greater than the increase of the third term. Such results are enhanced for $\hat{Z} = \max(Z_1, Z_2, \ldots, Z_N)$ with $F_{\hat{Z}}(\hat{z}) = \prod_{i=1}^{L} F_{Z_i}$ in L UE power readings. The red and magenta curves in figure 2.5 show that $F_{\hat{Z}}(\hat{z}) \leq F_{Z_l}(\hat{z})$ and $F_{\hat{Z}}(\hat{z})$ calculated with the parameters of case 'c' is lower than that of case 'a'. A decreased $F_{\hat{Z}}(\hat{z})$ implies a better system performance.

In order to validate equations (2.2) and (2.6), we applied a brute force procedure (green dotted curve in figure 2.5) in which we determined the values of $F_{\hat{Z}}(\hat{z})$, that is, we generated θ^{Δ} and $\tilde{A}_i$ according to a uniform distribution and the probabilities of case 'a' respectively, calculated the antenna gain g_u using (2.1) and the power level as $Z_l = \tilde{A}_i\, g_u$. This process was repeated L=3 times in each of 35,000 iterations.

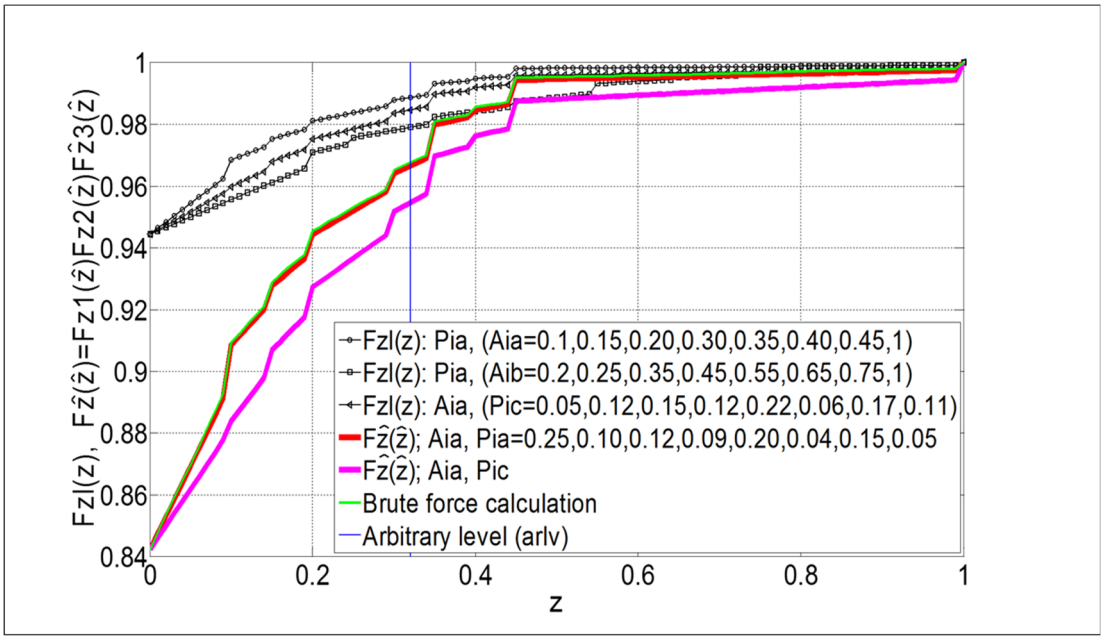

Figure 2.5 Cumulative Distribution of $\hat{Z}_i$ and $\hat{Z} = \max[Z_1 \quad Z_2 \ldots\ldots \quad Z_L]$, L=3, N=8

Given L and N $\tilde{A}_i$ values (or equivalently N θ_{iBS} angles), we can calculate $F_{\hat{Z}}(\hat{z})$=$F_{\hat{Z}_2}(\hat{z})$ for

any combination $C(N,n_o)=\binom{N}{n_o}=\frac{N!}{n_o!\,(N-n_o)!}$ of n_o $\tilde{A}_i$ values with $p_{\tilde{A}_i}$=0 and the remaining (N-n_o) $\tilde{A}_i$ values with $p_{\tilde{A}_i}$=1/(N-n_o), and $F_{\hat{Z}_1}(\hat{z})$ with $p_{\tilde{A}_i}$= 1/N assigned to all N $\tilde{A}_i$ values. Using (2.2) and (2.5), it is easy to show mathematically that $F_{\hat{Z}_2}(\hat{z})$ decreases relative to $F_{\hat{Z}_1}(\hat{z})$ if the zero probability was applied to the n_o lowest values of $\tilde{A}_i$. Moreover, the application of zero probability to the (n_o+1) lowest values of $\tilde{A}_i$ and equally increasing the probability (1/(N-n_o-1)) to the remaining values, decreases $F_{\hat{Z}_2}(\hat{z})$ even more. For other cases in the set of $C(N,n_o)$ combinations, we used a simulation to assess them. Note that the application of $p_{\theta_{iBS}}$=$p_{\tilde{A}_i}$=0 to a particular BS angle (discarded) results in a null contribution of its corresponding power level $\tilde{A}_i$ to $F_{Z_l}(z)$ in (2.2) because that angle is not used and that for any $C(N,n_o)$ in which $F_{\hat{Z}_2}(\hat{z})\leq F_{\hat{Z}_1}(\hat{z})$, the UE has an increased probability to receive a higher power level in L power measurements using a reduced set of (N-n_o) BS angles compared to that using the full set of N BS angles.

Table 2.1 shows the statistics of $\Delta F_{\hat{Z}}(\hat{z}) = F_{\hat{Z}_1}(\hat{z})-F_{\hat{Z}_2}(\hat{z})\geq 0$, obtained by using the general parameters θ_{3dB}^{Δ}=6.5°, θ_a^{Δ}=3°, θ_b^{Δ}=10°, N=20, L=50 and a set $\mathcal{A}$ of realistic received power values[4] (normalized to 100 and sorted in ascending order). $F_{\hat{Z}_1}(\hat{z})$ was calculated using (2.4) and $p_{\theta_{iBS}}$=1/20 (i=1,2,…,20) whereas $F_{\hat{Z}_2}(\hat{z})$ was evaluated similarly for $C(N,n_o)$ combinations of the (N-n_o) $\tilde{A}_i$ values with $p_{\tilde{A}_i}$=1/(N-n_o) and (n_o) $\tilde{A}_i$ values with $p_{\tilde{A}_i}$=0. Four different cases (n_o=5,7,9,11; $C(N,n_o)$=15,504, 77,520, 167,960, 167,960) were analyzed. Particularly, Table 2.1 shows groups of combinations where k specific $\tilde{A}_i$ values were assigned with a $p_{\tilde{A}_i}\neq 0$. $\hat{z}$ was allowed to take values in [0:0.01:100]. For any combination, the statistics of $\Delta F_{\hat{Z}}(\hat{z}) \geq 0$ were increased only in the event of a condition compliance in at least 99.5% of its 10,001 values.

---

[4] $\mathcal{A}$ = {[1.63305e-5, 2.00909e-5, 2.22331e-5, 2.96483e-5, 4.13048e-5, 5.17607e-5, 6.26614e-5, 1.24451e-4, 1.85353e-4, 5.82103e-4, 6.88652e-5, 1.28233e-3, 3.98107e-3, 6.83912e-3, 1.47571e-2, 3.23594e-2, 7.88860e-2, 1.74985e-1, 5.66239e-1, 1.00000]*100}

Table 2.1 Percentage of combinations in which $F_{\hat{Z}_1}(\hat{z}) - F_{\hat{Z}_2}(\hat{z}) \geq 0$

C(N,n_o) where ($p_{\tilde{A}_{i1}}, .., p_{\tilde{A}_{ik}}$)≠0 and there are n_o values of $p_{\tilde{A}_i}$=0 in the remaining (N-k) $\tilde{A}_i$ values	$F_{\hat{Z}_1}(\hat{z}) - F_{\hat{Z}_2}(\hat{z}) \geq 0$			
	n_o=5	**n_o=7**	**n_o=9**	**n_o=11**
$(p_{\tilde{A}_{20}})$≠0	43.0	43.4	40.5	53.6
$(p_{\tilde{A}_{19}}, p_{\tilde{A}_{20}})$≠0	58.4	68.7	76.9	86.3
$(p_{\tilde{A}_1}, p_{\tilde{A}_2}, p_{\tilde{A}_{19}}, p_{\tilde{A}_{20}})$≠0	52.1	58.9	66.8	77.1
$(p_{\tilde{A}_1}, p_{\tilde{A}_2}, p_{\tilde{A}_{15}}, p_{\tilde{A}_{19}}, p_{\tilde{A}_{20}})$≠0	59.3	66.2	81.5	84.6
$(p_{\tilde{A}_1}, p_{\tilde{A}_2}, p_{\tilde{A}_5}, p_{\tilde{A}_{19}}, p_{\tilde{A}_{20}})$≠0	48.5	52.7	59.8	69.7

Table 2.1 indicates that there is an opportunity to decrease $F_{\hat{Z}_2}(\hat{z})$ in more than 50% of the combinations for those cases where the BS angles associated to the largest $\tilde{A}_i$ values are not discarded (if $p_{\tilde{A}_{20}}$=0, $\Delta F_{\hat{Z}}(\hat{z})$<0 for any $C(N, n_o)$). For a given n_o, the percentages increase as a greater number of the highest $\tilde{A}_i$ are considered (e.g., rows 1 vs. 2). Those combinations are not the only possibilities. There are cases where $F_{\hat{Z}_2}(\hat{z})$ decreases (>50%) if the BS angles linked to the maximum and minimum power values were taken into account (e.g., row 3). The typical large difference between the minimum and maximum $\tilde{A}_i$ values (>40dB) facilitates these results. Similarly, Table 2.1 shows that there are cases in which the percentages of $\Delta F_{\hat{Z}}(\hat{z})\geq 0$ increase with n_o as higher $\tilde{A}_i$ values are considered (e.g., rows 4 vs. 5). Note that each row in Table 2.1 has a different maximum number of combinations (e.g., 48,620 for row 2; 11,440 for row 3). The percentage for each case is calculated using the fraction of those combinations in which $\Delta F_{\hat{Z}}(\hat{z})\geq 0$ (e.g., 37,372 for row 2 and n_o=9 (76.9%)).

Given that there is a high probability value of blocking in urban environments, it is not difficult to find a group of n_o angles that do not help the BS deliver the maximum possible power level at any position compared to others within the service area. Equations (2.2) and (2.5) reveal that not using, or equivalently applying zero probability to the elements of this group and equally increasing the probability (1/(N-n_o)) to the remaining BS angles can improve the system performance. Specifically, if any of the (N-n_o) BS angles was associated

with the maximum possible received power level at an arbitrary position, that maximum level (i.e. an equivalent to $\tilde{A}_{20}$) would be included in (2.2). Because some of the other (N- n_o -1) angles also facilitate the delivery of the highest power levels at the position considered, the combined effect of the application of the best angles and the avoidance of those that do not help the BS deliver a maximum power level can generate the condition $\Delta F_{\hat{Z}}(\hat{z})\geq 0$ for many locations of the service area.

The exclusion of n_o BS angles has a different impact at each position of the user because these angles are not associated exclusively with the lowest power levels everywhere. Considering that the $\tilde{A}_i$ values can be sorted in ascending order, two different geographical positions may have individual ordered sets of N values of $\tilde{A}_i$ linked to different distributions of N BS angles (e.g., $\{\tilde{A}_1,.,\tilde{A}_{12},.,\tilde{A}_{20}\}$ in position 1 corresponds to $\{\theta_{4BS},.,\theta_{10BS},.\theta_{12BS}\}$ whereas $\{\tilde{A}'_1,.,\tilde{A}'_{12},\ldots,\tilde{A}'_{20}\}$ in position 2 corresponds to $\{\theta_{17BS},.,\theta_{1BS},.\theta_{2BS}\}$). Given that the discarded angles eliminates the contribution of different n_o ($\tilde{A}_i$) values in each ordered set, their impact on $\Delta F_{\hat{Z}}(\hat{z})$ varies. The outcome can be negative if most of the eliminated $\tilde{A}_i$ values were the highest, but this possibility is greatly diminished by identifying the best BS angles in the service area.

A special case is the scenario in which there are two sets of well-separated positions of the user and where the best angles of one group become the worst angles of the other group. Under such scheme, the (n_o) discarded BS angles are mostly linked to the intermediate $\tilde{A}_i$ values at each position. Row 3 in Table 2.1 shows that even for this scenario, there is a large percentage of combinations for which $\Delta F_{\hat{Z}}(\hat{z}) \geq 0$. The elimination of 35% (n_o=7) of BS angles can be realistic in NLOS environments. A severe street canyon propagation may exclude a greater number of angles.

The probabilities of the best BS angles $p_{\theta_{iBS}}$ can also be varied according to their effectiveness in RF illumination (estimated as the percentage of UE positions that receives the maximum power per BS angle) for a potential further increase in performance. The application of a lower probability for certain BS angles does not necessarily mean an increase

of power blocking because the UE can be served by other BS angles. This effect can be exemplified for the UE located at X' in figure 2.2 where BS angle '*N-1*' allows to deliver the maximum power possible but this position is also covered with BS angle '*N*' with a lower but close power value.

The 1-D scheme considered highlights the advantage of identifying the best BS antenna angles. This information can be approximated off-line using RT as will be explained in the following section.

2.2.2 Simulation methodology

An accurate 3D commercial ray tracing tool (Wireless Insite) is applied to simulate the wireless channel established between a fixed transmitter BS and UE receivers whether in arbitrary locations, well-defined grid of geographical points or along specific routes, all under NLOS conditions (Appendix VI).

The UE received power is predicted for different combinations of BS-UE antenna directions. The BS power was set to 30 dBm, the center frequency to 28 GHz. A reference threshold (thres) power level of -85 dBm is considered assuming a signal bandwidth of 1 GHz, thermal noise Power Spectral Density of -174 dBm/Hz, 7 dB UE Rx Noise Figure (NF) and RF coverage for a minimum rate R of 100 Mbps. We apply (Abouelseoud et al., 2013; Barati et al., 2014):

$$P_{ref} = (\text{SNR})\, P_n \tag{2.7}$$

$$P_n = -174 + 10\log_{10}(BW) + NF \tag{2.8}$$

$$R = \beta \Delta W \log_2(1 + SNR) \tag{2.9}$$

where $\beta = (0.5)(0.8)$ for half-TDD constraints and 20% control overhead.

The BS-UE antennas used, all with vertical polarization were an ideal sector antenna, and 10^{o} (3-dB beamwidth) pyramidal horn antennas with a 24 dB gain (Balanis, 2005). The BS horn antenna changes its orientation in different angle ranges depending on the scenario. Both BS

and UE have only one RF chain. The BS antenna height was set up to 8[5] m while the UE antenna height was fixed at 1.5 m. A 5º angle step in the range [0º, 360º) for the UE antenna orientation was chosen as a compromise between resolution and computation time. The horn antenna can be replaced with a Uniform linear/Rectangular antenna array (ULA/URA) for the beam switching (Van Trees, 2002). General setting for the 3D RT simulation tool were 6 reflections, 1 diffraction and 0.1º ray spacing. The area under study corresponded to a small city area in Rosslyn, Virginia, USA (figure 2.6), where the exterior buildings walls are assumed made of brick.

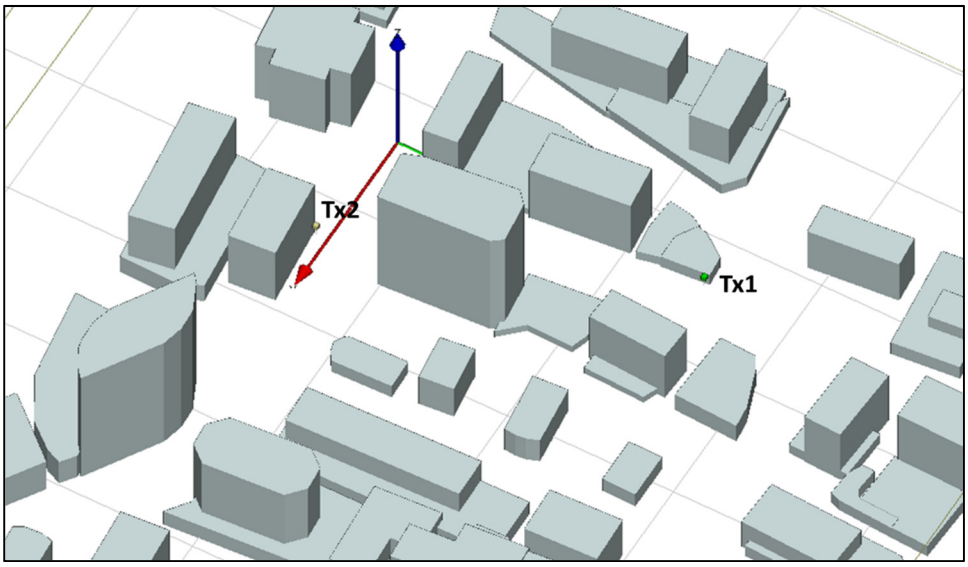

Figure 2.6 Study area

The simulations are divided in two parts. The first corresponds to the identification and evaluation of the best BS angles and the second part to the performance impact in the application of the identified angles. The simulations were carried out in two different scenarios for comparison purposes. The difference between the scenarios resides in the

[5] A low BS antenna height (h=8m) avoids a large vertical AoD variation of the multipath components. Average variations of -1.96º (8m), -3.09º (12m), -4.13º (16m) were registered from RT simulation using 500 NLOS positioned arbitrarily where the BS and UE were equipped with horn antennas of 60º and 10º, respectively. The UE received power difference for h=8m versus h=16m was up to around 9dB with a tendency to decrease for lower SNRs.

BS(Tx)-UE(Rx) geographical positions and antenna types applied. The antenna type used in each scenario is identified as a setup 1, 2, ... In scenario 1, the BS-Tx1 (center left in figure 2.6) was positioned in front of three buildings of heights 14 m, 38 m and 6 m located across the street at a distance of approximately 48 m, whereas Tx2 (center down in figure 2.6) in scenario 2 was located in front of a building with a height of 80 m. The positions of the UE considered along the streets are behind the buildings, and thus, NLOS propagation conditions exist.

2.3 Approximate identification of the angle range

The task of identifying the best BS-UE angles is accomplished assuming static or very slow movers (i.e nomadic users or pedestrians traveling at speeds below 1.54 km/h) which permits to apply the simplification that all UE power measurements for different BS/UE angle combination are taken at the same UE position or within a distance of $10\boldsymbol{\lambda}$ where the UE experiences little fading (Samimi et al., 2013). Instead of determining all the multipath components in the link BS-UE, we focused only on the first main propagation path associated with the largest received power so the number of possible BS-UE beam orientations best illuminating all UE positions was greatly reduced. This strategy was considered reasonable because field data show that an average of 2.5 power lobes exist in urban environments (Samimi et al., 2013), and our RT simulations accomplished in an entire service area with 500 arbitrary NLOS positions suggest there was an approximate power difference of 10 dB between the first and second path, such that the first clearly became the most important one (Appendix VIII).

A general RT procedure that can be applied for this task consists in the prediction of the link propagation characteristics for each possible NLOS UE position and for all angle combinations of the BS-UE directional antennas. The angles take values both in azimuth and elevation within a certain range using small steps. The best BS-UE angles combination corresponds to:

$$\text{Best}\left[\theta_{jBS}, \emptyset_{kBS}, \theta_{lUE}, \emptyset_{qUE}\right] = \max_{\substack{\theta_{BSmin} \le \theta_{jBS} \le \theta_{BSmax} \\ \emptyset_{BSmin} \le \emptyset_{kBS} \le \emptyset_{BSmax} \\ 0 \le \theta_{lUE} < 2\pi \\ \emptyset_{UEmin} \le \emptyset_{qUE} \le \emptyset_{UEmax} \\ \Delta\theta_{BS}, \Delta\emptyset_{BS}, \Delta\theta_{UE}, \Delta\emptyset_{UE} \neq 0 \\ \theta_{(j+1)BS} = \theta_{jBS} + \Delta\theta_{BS};\ \theta_{(l+1)UE} = \theta_{lUE} + \Delta\theta_{UE} \\ \emptyset_{(k+1)BS} = \emptyset_{kBS} + \Delta\emptyset_{BS};\ \emptyset_{(q+1)UE} = \emptyset_{qBS} + \Delta\emptyset_{BS} \\ i = 1,2,3,\ldots,M}} \left(P_{rUE_i}\right) \qquad (2.10)$$

Clearly, this method becomes impractical due to the huge amount of computing time demanded.

An alternative method, which requires much less time and that is suitable for BS antennas installed at low heights (multipath components with small vertical angle variation) is proposed instead as the following two-step process:

- Predict propagation characteristics for a large number of NLOS points in the area of interest using a sector antenna (i.e. an ideal directional antenna 120ºx20º or 150ºx20º) for the BS and an isotropic antenna for the UE. The UE positions can be chosen to form part of sets of linear routes conveniently located or a 2D-grid that covers the NLOS service area;
- For each UE position, scan the propagation data results applying a narrow beamwidth antenna in small angle steps. The total power per scanned angle is calculated as the sum of the individual multipath component powers 'seen' by the scanning antenna. The BS and UE antenna orientation angles where the maximum UE received power occurs (first path) correspond to the angles sought.

Although the UE received power is diminished due to the combination of both particular antenna gains in the first step, the application of these types of antennas reduces greatly the computation time and renders close results in the identification of the best angles compared to a RT outcome using very directional antennas at BS and UE (i.e. narrow beamwidth horns or ULA/URAs). Appendix II provides an example of this approximation.

The use of a large number of UE positions in the form of linear routes and 2D grids, which are easy to implement in a modern RT tool, helps identify the largest quantity of best BS-UE

angle directions. Moreover, since it is not unusual to find that the same BS angle can be used for the best RF coverage of many different UE positions, especially for canyon propagation in urban environments, a non-uniform percentage of RF illumination per BS-UE discrete angle is expected in the application of the proposed method. The identification of the best angles was accomplished using a 150º directional antenna for the BS and an isotropic antenna for the UE in the two service areas. In service area 1 the Tx and Rx are positioned as indicated in Figure 2.7 (setup 1) where each UE is part of 21 linear routes (19 parallel to the X,Y axis, 2 sloped) . For the majority of points, a separation of 0.1m along the routes was chosen to record the BS angle variation for close UE positions.

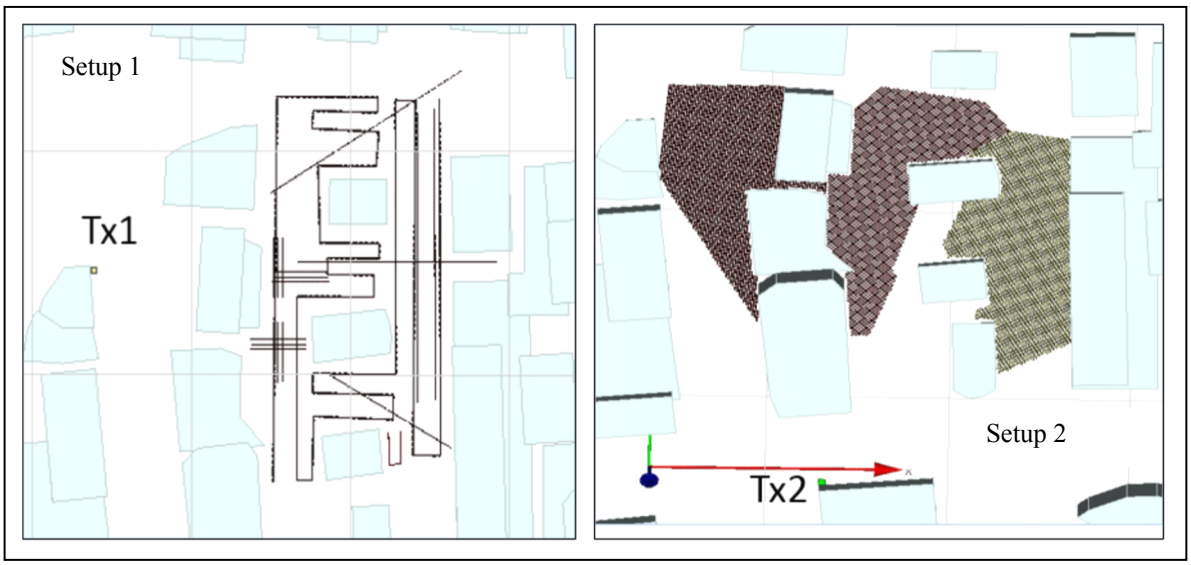

Figure 2.7 Simulation setups 1 and 2

The distance between some of the routes was set up around 5 m. For the service area 2 (Figure 2.7), the positions of the Tx and Rx (setup 2) are such each UE (1 m separation) belongs to one of three 2D-grids whose union covers the whole NLOS area. The details of the routes and grids of points applied are shown in Table 2.1. Alternatively, a grid of points (setup 5) and linear routes could also be used to approximate the best BS angles in the service areas 1 and 2, respectively. The grid of receivers applied in scenario 1 (setup 5) and the identified angles are shown in Appendix III.

Table 2.2 Linear routes and grid of points

Setup 1 **BSTx 150° DirectAnt.** **UERx Isotr. Ant.** **Data scanTx: set [-60°:1°:60°]** **Data scanRx: set [0°:1°:359°]**	**Setup 2** **BSTx 150° DirectAnt.** **UERx Isotr. Ant.** **Data scan: set [30°:1°:150°]** **Data scanRx: set [0°:1°:359°]**
21 Linear Routes: 12 routes (0.1m): 251 pts each 7 routes (0.1m): 1201, 1202, 1009, 659, 903, 501, 325) = 8,812 pts 1 route (0.75m): 1,532 pts 1 route (0.5m): 121pts Total 10,465 pts	Total Grid = Union of three smaller grids Grid 1 (1m): 3,808pts Grid 2 (1m): 3,987pts Grid 3 (1m): 3,559pts Total 11,354pts

RT output data from both setups 1 and 2 were scanned using a 32-ULA (1^o angle step) exploiting the fact that its 3.2^o 3dB-beamwidth (Van Tress, 2002) facilitates indication of the BS-UE angle combination of the first propagation path.

Figures 2.8 and 2.9 show in red color the angles and the percentage of UE positions where each BS angle delivers the maximum power compared to the rest.

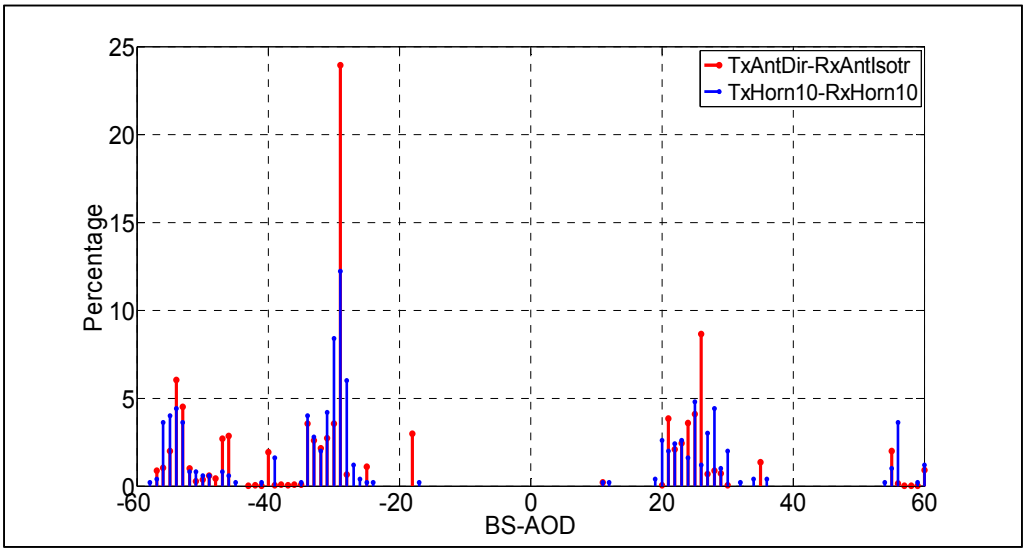

Figure 2.8 Percentage of UEs per BS angle reaching maximum power (setup 1,3)

The set $\mathcal{A}$ ={ -57º to -46º, -43º to -28º, -25º, -18º, 11º, 20º to 30º, 35º, 55º to 60º} and set $\mathcal{F}$ ={30º to 36º, 40º to 56º, 58º to 64º, 67º to 75º, 85º to 89º, 103º, 104º, 115º to 143º} with card($\mathcal{A}$)=49 and card($\mathcal{F}$)=76 were identified for setup 1 and 2 respectively. In Figure 2.8 we notice that the angle ranges ([-17º, 10º], [12º,19º],…., [36º, 53º]) and other smaller segments are not used in any circumstance. BS angles -55º, -28º and 25º are the most used. On the other hand, figure 2.9 shows a smaller number of angle voids and a relatively larger BS angle distribution related to a lower building blockage 'seen' by Tx2 in service area 2 compared to the case of figure 2.8. The percentage values are detailed in Appendix III.

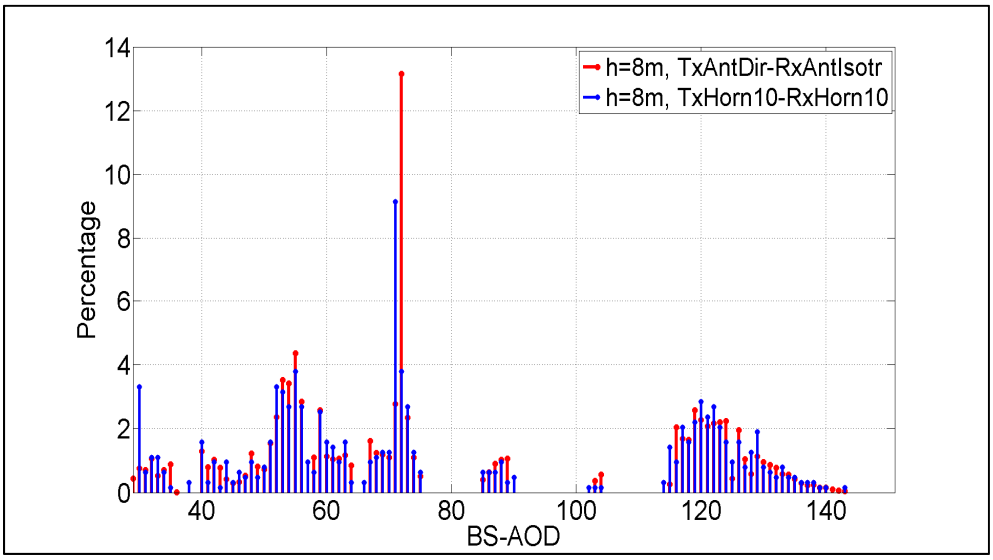

Figure 2.9 Percentage of UEs per BS angle reaching max. power (setup 2, 4)

Figure 2.10 shows the percentage of UE positions reaching the highest maximum power per UE angle for both setups. Since these percentages are not equal, we generate for future use four CDFs F_{BS49}, F_{BS76}, F_{UEsc1}, and F_{UEsc2} assuming that the percentage of UE positions is equivalent to the probability of each angle to generate a maximum power delivery. The first two CDF*s* correspond to the 49 and 76 BS angles whereas the last two to the best UE angles (Figure 2.11). Clearly the distributions of the best BS and UE angles are not uniform.

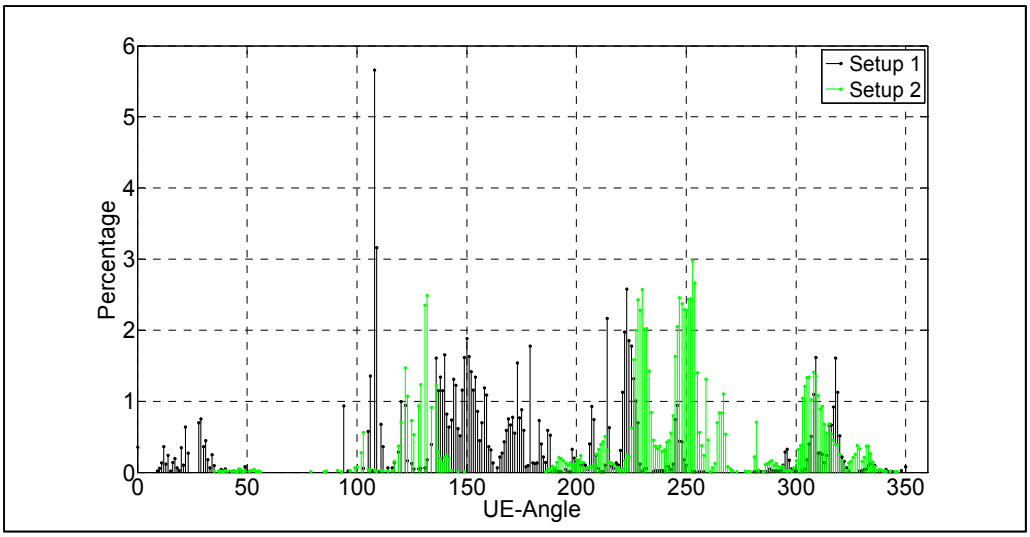

Figure 2.10 Percentage of UE positions per UE angle (max. rcvd. power) in setups 1,2

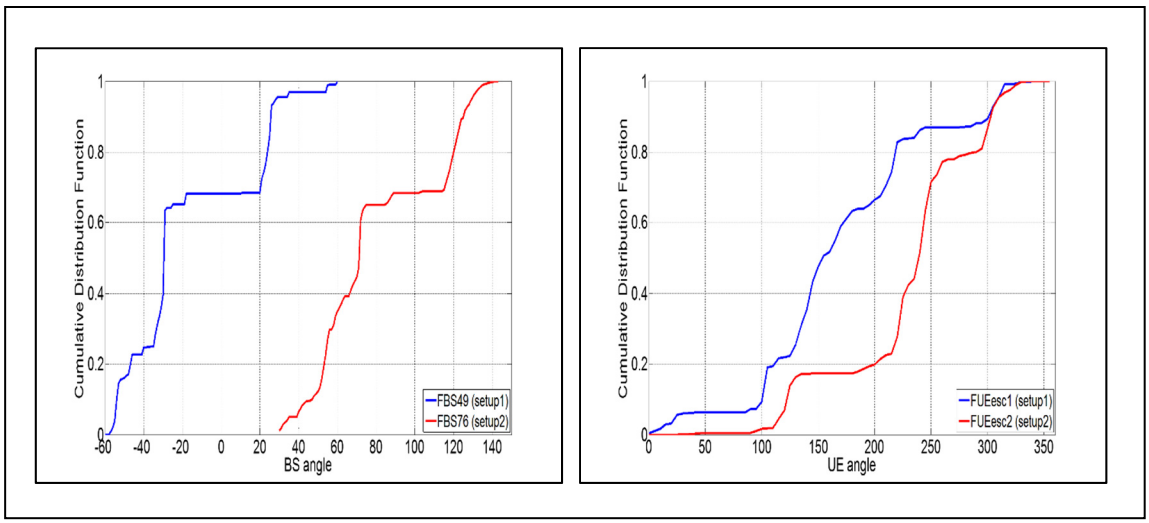

Figure 2.11 Specific Cumulative Distribution Functions F_{BS49}, F_{BS76}, F_{UEsc1}, F_{UEsc2}

2.3.1 Angle identification assessment

In order to evaluate the proposed method, we contrast its results against a RT outcome using the same setup in each service area but with the BS and UE now both equipped with 10º (3-dB beamwidth) horn antennas. Setup 3 in service area 1 consists of a Tx1 (center left) that

illuminates 500 arbitrary positions (red color-figure 2.12) whereas setup 4 in service area 2 consists of a Tx2 (center bottom) servicing 634 positions uniformly separated by 4m (black color-figure 2.12).

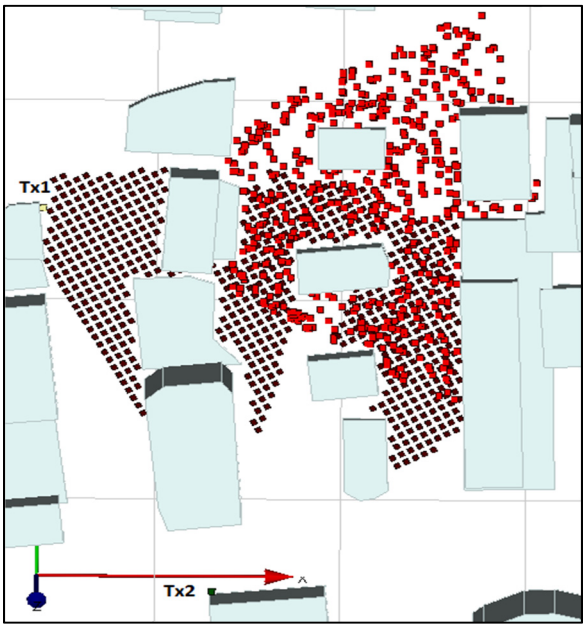

Figure 2.12 Setup 3 and 4 (Tx1/Tx2 center left/bottom)

The positions considered are NLOS. Sets $\mathcal{C}$ ([-60º:1º:60º]) and $\mathcal{G}$ ([30º:1º:150º]) of 121 angles each were used to illuminate all positions in the different areas respectively. A set $\mathcal{Q}$ ([0º:5º:355º]) of 72 angles was applied for the UE antenna beam switching. The best BS-UE angle association is obtained by comparing the UE received power for all combinations of the BS and UE angles. A total of 50[6] (set $\mathcal{B}$) BS angles for setup 3 and 79[7] (set $\mathcal{F}$) for setup 4 were identified as the best ones. Figures 2.8 and 2.9 show in blue color the percentage of positions reaching the maximum received power per BS angle in these two setups.

---

6 -58º to -49º,-47º to -45º,-41º, -39º,-35º to -24º, -17º, 11º, 12º, 19º to 30º, 32º, 34º, 36º, 54º to 56º, 59º to 60º

7 30º to 35º, 38º, 40º to 64º, 66º to 75º, 85º to 90º, 102º to 104º, 114º to 140º, 143º

An angle identification comparison shows differences but these have a rather small impact on performance. For service area 1, set *A* includes 11 angles that do not belong to set *B* and does not contain 12 angles that do belong to *B*. These dissimilarities occurred in 7.01% and 4.2% of the UE positions in setup 1 and 3, respectively. For service area 2, set *F* shows 3 angles that do not appear in set *E* and it does not include 6 angles that do appear in set *E*. For that area, the differences appeared in 0.17% and 2.52% of the UE positions in setups 2 and 4.

The maximum power received by any UE (500 or 634) in a number of random switches of the BS-UE antenna beam directions is used to measure the largest error generated in applying set *A* (*F*) versus set *B* (*E*). In each iteration, a different UE is picked randomly and the BS-UE angles are varied randomly 50 times. The maximum received power was recorded (20,000 iterations). The largest performance difference was less than 0.70 dB (0.5 dB in the fiftieth percentile) in the case of *A* vs *B* (setups 1,3) and less than 0.40 dB (0.2 dB in the fiftieth percentile) for *F* vs *E* (setups 2,4). Figure 2.13 shows the performance in each case. The small errors were anticipated given that the angle sets basically occupy the same range. The angles were selected based on power delivery only.

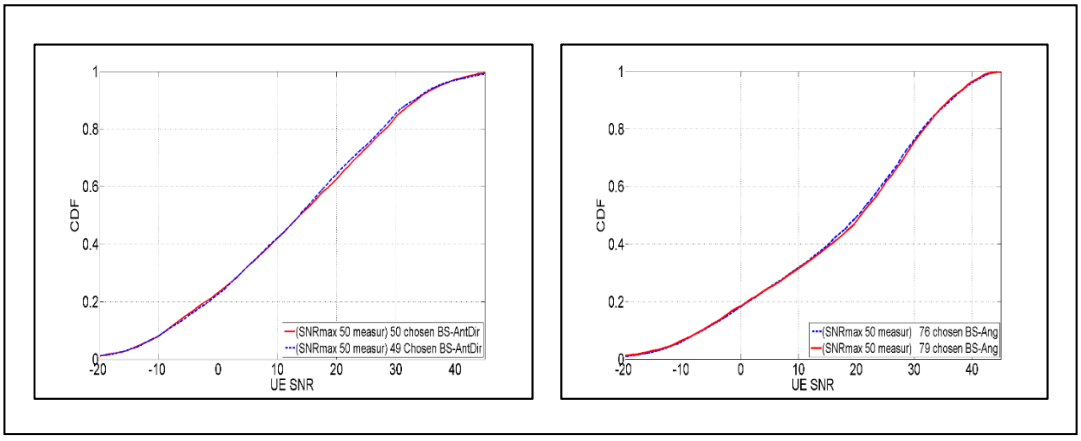

Figure 2.13 Precision difference: 49 (setup 1) versus 50 (setup 3) and 76 (setup 2) versus 79 (setup 4)

Increasing the number of linear routes (i.e. decreasing the route separation) in setup 1 improves the accuracy. There is no need to use very close points. Actually the application of

a grid of receivers is better to cover uniformly the area of study. In general we expect that the UE positions affected by angle errors and the received power error be less than 5% and 0.70 dB respectively. The results observed indicate that the proposed method may constitute in a first approximation for the prior identification of the best discrete BS angles that can be applied to improve a directional search procedure or to reduce the extension of a propagation database.

A closer look to the RF coverage achieved with different subsets of BS angles in setup 3 gives a clear differentiation of their efficacy. Figure 2.14 shows the simulation results for maximum UE power delivery applying four different set of chosen BS angles. For the case of the BS antenna beam orientations $\theta_{BS} \in \{-55^o, -45^o, .. 0^o, ...,45^o, 55^o\}$=[-55º:10º:55º], the angles -5º, 5º and 45º statistically provide the worst possibilities for the UE to 'hear' the BS signal compared to other angles like -35º, -25º (red color). While BS angles -55º, -25º and 25º render best RF illumination in 18.4%, 27.4%, 28% of the total UE positions, the angles -5º, 5º and 45º do not concede such possibility.

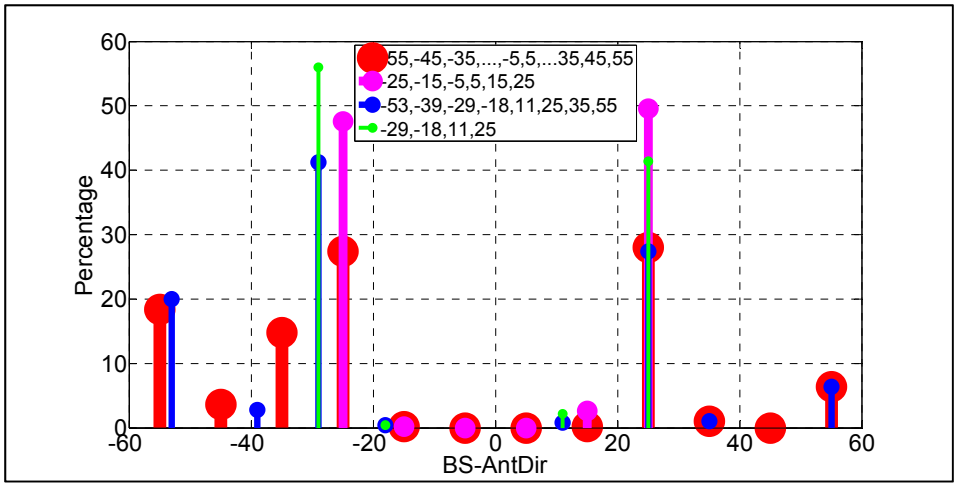

Figure 2.14 Percentage of UE positions per BS angle (max. SNR) in setup 3

Note that zero percentage in maximum power delivery simply means that the rest of the angles allow the BS to provide higher power levels at a UE position compared to those obtained using the angles -5º, 5º, 45º at the same position. Likewise, the value of 1%

obtained with the BS angle of 35º represents the percentage of UE positions with maximum power levels that cannot be reached using any other angle in the set [-55º:10º:55º]. The angles -25º, 25º correspond approximately (Figure 2.12) to the direction of the streets adjacent to the buildings located in front of Tx1 indicating that the NLOS UE positions receive power in the form of street canyon propagation.

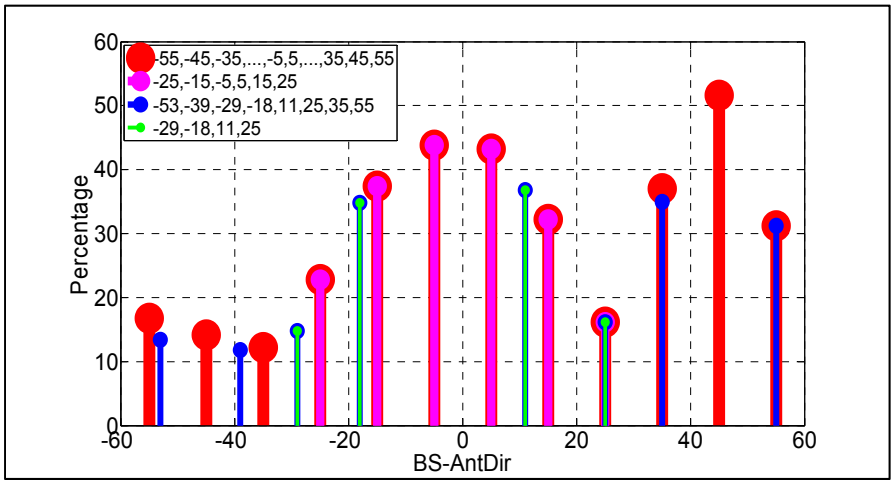

Figure 2.15 Percentage of UE positions per BS angle (received power < thres)

Figure 2.15 (red lines) shows the percentages of UE Rx positions not reaching a power value equal to or higher than a threshold level (-85 dBm) for each specific BS angle. These values are highest for angles -5º, 5º and 45º. The RF coverage of the different BS angles makes it difficult to be certain that a UE can 'hear' the BS for any specific angle even if the BS-UE antenna main beams are oriented in the correct direction.

Figures 2.14 and 2.15 also show that although the UE positions are restricted to an area of ±30º x 200 m, some of the best BS angles are outside this scan range. 18.4% and 6.4% correspond to angles -55º and 55º respectively, that is, in the directions of a neighbor sector within the same cell. If the BS beam orientations were restricted to ±30º (magenta color), the percentages for which a maximum UE power delivery occurs increase notably in the directions ±25º (from a 28%-27.4% to 49.6%-47.6% respectively) with a negative impact in the total number of UEs that cannot get power above the threshold because this value

increases from 1.6% (8 UE) to 5.4% (27 UEs). Nevertheless, even for this last scenario, the angles -5º and 5º remain the most inefficient for RF coverage.

As anticipated, although many UE positions may not reach a certain minimum power level for a particular BS beam direction, the same position can be covered by the base station using a different angle. Figure 2.16 shows the statistics obtained in setup 3 using five different groups of angles.

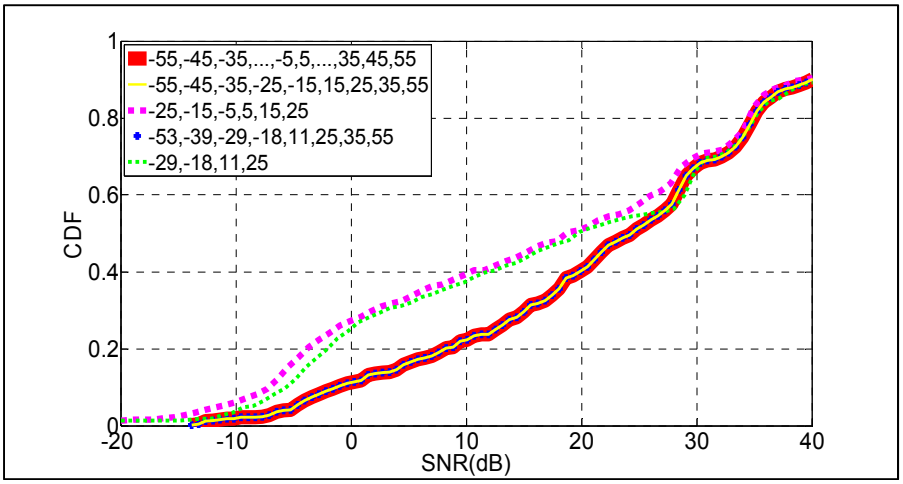

Figure 2.16 SNR at UE positions (500)

The statistics basically do not change when the number of equally spaced angles is reduced from 12 (red) to 9 (yellow curve), that is, not using the angles -5º, 5º, 45º since these latter do not contribute to the highest power levels. Figure 2.16 also shows that there is basically no difference in performance between the set of equally spaced (red) and the chosen (blue) angles although there are 4 angles less (12 versus 8). Note that some of the maximum power values obtained for BS discrete angles restricted in the range ±30º (magenta and green curves) can take lower levels compared with what can be obtained using others outside this range.

2.4 Performance impact

To quantify the performance benefit of using a reduced set of best BS angles (49 and 76 for

service areas 1 and 2, respectively), we applied such set in a system that changes the BS and UE angles randomly L times over a period T in order to determine the best link angles (θ_{BS}, θ_{UE}). It is considered the following cases:

2.4.1 Maximum received SNR using the complete and best sets of BS angles

A comparison of the maximum SNR received using the identified best BS angles with respect to the complete group of 121 angles in setups 3 and 4, is shown in Figures 2.17 and 2.18, respectively. In both figures, 'the maximum possible SNR' is plotted in green color which represent the highest SNR value obtained after considering all possible combinations of BS (121) and UE (72) discrete angles.

In figure 2.17, shows two groups (L=25,50) of three plots (blue/magenta/black) representing the maximum received SNR under the following conditions: a) BS used angles from set $\mathcal{C}$ ([-60º:1º:60º]) with equal probability; b) BS used angles from set $\mathcal{A}$ (best 49) with equal probability and c) BS used angles from set $\mathcal{A}$ with different probability values according to the distribution function F_{BS49}. In all three cases, the UE changed the beam directions from set $\mathcal{Q}$ ([0º:5º:355º]), with equal probability. The simulations indicated that the SNR obtained for case b is on average 3.03 dB (fiftieth percentile) larger than the values obtained for case a. This is due to the fact that the 49 angles are the ones that contribute with the 'highest' levels of power at the UE positions and are generated with a larger probability (1/49 versus 1/121). In other words, assigning a zero probability to the 72(=121-49) BS angles in the set '$\mathcal{C}$ - $\mathcal{A}$' and an increased equal probability to the rest generates a performance improvement. This outcome was already analyzed in section 2.2.1. Furthermore, assigning different probabilities to the elements of set $\mathcal{A}$ based on CDF F_{BS49} renders an additional benefit of 2.1 dB (fiftieth percentile), yielding an overall average gain of 5.13 dB. The performance gain based on F_{BS49} starts to add-up at a SNR of 2.3dB.

Figure 2.17 also shows (red dash-dot line) that a potential increase of 4 dB (fiftieth percentile) is possible in the hypothetical circumstance in which the UE, assuming it has the

same spatial reference of the BS, varies its antenna beam direction randomly according with a CDF F_{UEsc1} passed by the BS and previously obtained off-line from RT data. Figure 2.17 includes the ideal case of a UE capable of estimating the angle of arrival of the main propagation path for each power measurement (solid blue/dash-dot magenta curves) and reporting to BS the maximum power received after L readings (i.e digital beamforming). We only used L=20 because the plots basically coincide with 'the maximum possible SNR' curves for larger values of L, revealing a very small opportunity for improvement. Nevertheless, even for this ideal case there is a potential gain when the L decreases. As expected, the figure also indicates (green curve) that the maximum power obtained by applying set $\mathcal{A}$ (best 49) was the same as for set $\mathcal{C}$ (full 121 angles) and that a reduced number of UE readings (L=25) per period resulted in a lower received power.

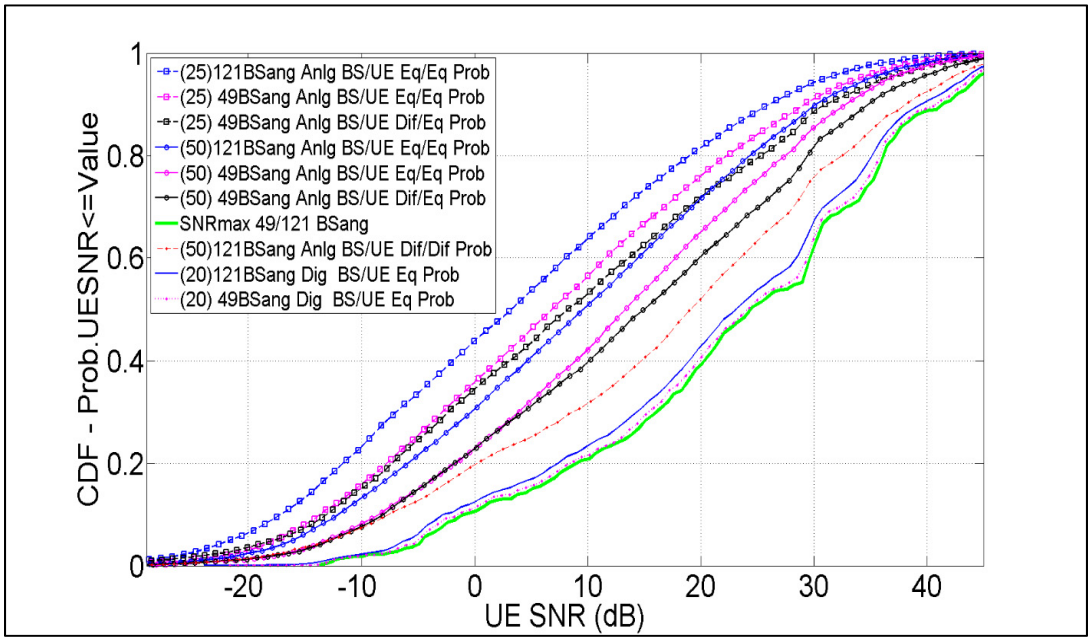

Figure 2.17 UE MaxSNR in 50 (25) measurements. 121 versus 49 BS angles (setup 3)

Figure 2.18 shows equivalent plots presented in figure 2.17 but for setup 4. The overall SNR gain, including the BS angle variation based on CDF F_{BS76} (figure 2.11), reaches 2.65 (1.85+0.8) dB in the 50th percentile, which is lower than that obtained from setup 3. This result suggests that the performance improvement gain has a relation to the canyon

propagation severity which is higher in service area 1 (figure 2.12).

Similarly, if the UE had the same spatial reference as the BS, the use of random beam orientations generated from F_{UEsc2} would represent an additional gain of approximately 7 dB which becomes interesting in terms of potential performance improvement based on site-specific propagation knowledge. A smaller number of best BS angles for RF illumination led to a higher performance gain because their more frequent application (49 for service area 1 versus 76 for service area 2) in a defined time period generates larger average power levels at UE positions.

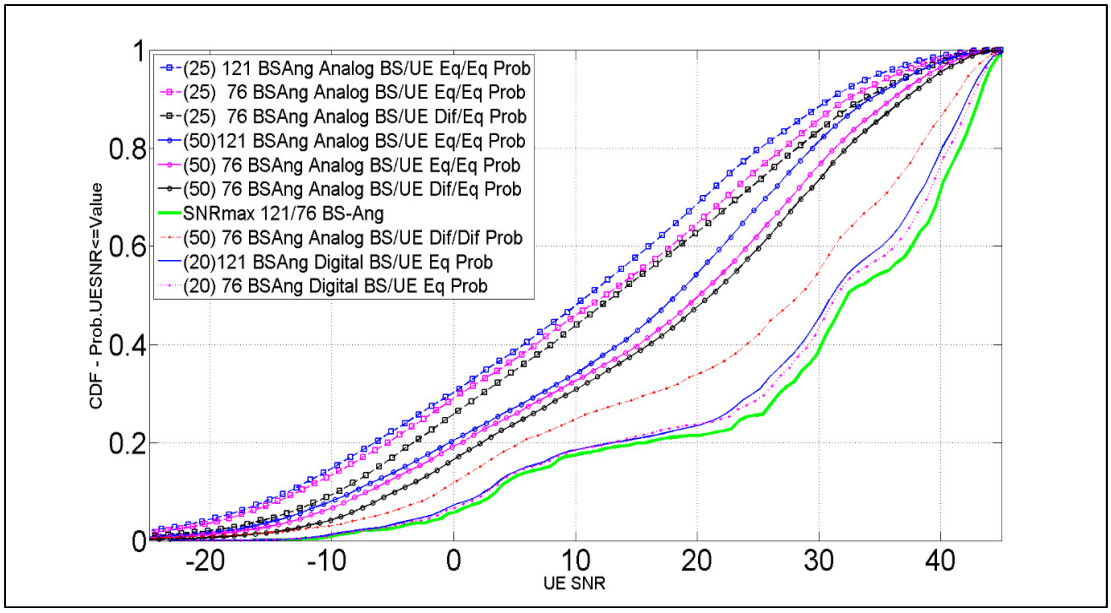

Figure 2.18 UE maxSNR in 50 (25) measurements 121 versus 76 BS angles (setup 4)

An evaluation of $\Delta F_{\hat{z}}(\hat{z}) = F_{\hat{z}_1}(\hat{z})$-$F_{\hat{z}_2}(\hat{z})$ using (2.2) and (2.5) for all positions of the user in the two service areas provides an alternative vision of the RT results. Each position has a different set of $\tilde{A}_i$ values (i=1,2,..,121) linked to a different distribution of the 121 angles (e.g., position 1 has $\{\tilde{A}_1, \tilde{A}_2, \dots, \tilde{A}_{121}\}$ associated to $\{\theta_{1BS}, \theta_{2BS}, .., \theta_{121BS}\}$, whereas position 2 has $\{\tilde{A}'_1, \tilde{A}'_2, .., \tilde{A}'_{121}\}$ related to $\{\theta_{5BS}, .., \theta_{121BS}, \dots, \theta_{10BS}\}$). The application of the reduced set of best angles means discarding different $\tilde{A}_i$ values at different locations.

In general, we applied θ_{3dB}^{Δ}=10°, θ_{a}^{Δ}=5°, θ_{b}^{Δ}=15°, L=50 and N=121. Specifically $F_{\hat{\mathrm{Z}}_2}(\hat{\mathrm{z}})$ was calculated with the probability values of 1/49 and 1/76 in service areas 1 and 2, respectively, whereas $F_{\hat{\mathrm{Z}}_1}(\hat{\mathrm{z}})$ with the value of 1/121 for all 121 $\tilde{A}_i$ values in both service areas. For each UE position, we calculated 10,001 values of $\Delta F_{\hat{\mathrm{Z}}}(\hat{\mathrm{z}})$ due to the large difference between the minimum and maximum $\tilde{A}_i$ values (>40dB).

The percentage of user positions where $\Delta F_{\hat{\mathrm{Z}}}(\hat{\mathrm{z}}) \geq 0$ provides an estimation of the efficacy of the proposed method to improve the performance. Assuming that a positive result means that at least 99.5% of the 10,001 values of $\Delta F_{\hat{\mathrm{Z}}}(\hat{\mathrm{z}})$ are greater than or equal to zero at any location, then Table 3 indicates that the proposed method provides an opportunity of improvement in 82.8% and 64.7% of the UE positions in the service areas 1 and 2, respectively.

Table 2.3 Percentage of positions of the user where $\Delta F_{\hat{\mathrm{Z}}}(\hat{\mathrm{z}}) \geq 0$ in service areas 1 and 2

	$\Delta F_{\hat{\mathrm{Z}}}(\hat{\mathrm{z}}) \geq 0$ (all 10,001 values) or $\Delta F_{\hat{\mathrm{Z}}}(\hat{\mathrm{z}}) < 0$ in less than (X)% of the 10,001 values				
	X=0.0	**X=0.25**	**X=0.5**	**X=1.0**	**X=2.0**
500 UEs 49 BS angles	66.4%	81.0%	82.8%	83.0%	91.0%
634 UEs 76 BS angles	28.4%	57.3%	64.7%	70.2%	75.1%

Clearly, the opportunity of improvement is greater in service area 1 where there are a smaller number of best BS angles. Appendix IV shows a visualization of the ordered set of A_i values for all positions of the UE in service areas 1 and 2.

2.4.2 Maximum received SNR using a limited number of BS angles

A performance comparison of a group of equally-spaced angles with larger separation relative to the same number of chosen directions shows a higher gain. For this task, we contrasted 25 BS angles from the sets ([-60º:5º:60º], [30º:5º:150º])) to angles chosen from

the previously identified sets $\mathcal{A}$ and $\mathcal{F}$. Two different approaches were followed.

i) Selection of the 25 BS angles with the largest percentage values (figures 2.8 and 2.9) by sorting in descending order the percentages of UE positions per BS angle obtained from the application of the proposed method in setups 1 and 2.

ii) Selection of the best 25 angles by applying the following search objective on data obtained from simulations in setups 3 and 4:

$$e_T = \min\left[\sum_{i=1}^{M} |\text{þ}_{iN} - \text{þ}_{ik}|_{\text{all } \binom{N}{k} \text{ of BS angles}}\right] \tag{2.11}$$

where: $\text{þ}_{iN} = \max\left[P_{i,\text{j}}\right]_{j=1,2,\ldots,N}$

$\text{þ}_{ik} = \max\left[P_{i,\text{j}}\right]_{j=1,2,\ldots,k}$; $k \leq N$

$[\theta_{1BS}, \theta_{2BS}, .., \theta_{kBS}] \in \left\{\binom{N}{k} \text{ of } [\theta_{1BS}, \theta_{2BS}, .., \theta_{NBS}]\right\}$; $\theta_{iBS} \neq \theta_{kBS}$

$P_{i,j}$ represents the partial maximum average power at a UE with position i (UEi) considering all the power values measured when the UE antenna beam is rotated 360º in 5º steps for a particular BS discrete angle θ_{jBS}. þ_{iN} and þ_{ik} correspond to the 'maximum possible power' at UEi considering all N and k BS-angles, respectively. e_T must be evaluated for all combinations of k out of N discrete BS angles for all M positions.

Since $C(N,K) = \binom{N}{k}$ generates a very large number of combinations (i.e. $C(76,25) \approx 7.8367 \times 10^{19}$), it is difficult to evaluate the objective function using an exhaustive search. Instead, we rather resort on a modified Binary GA (with fixed N gene-chromosome) for the determination of the best combination of BS angles (Haupt, 2004). As expected, Figure 2.19 shows that the sum of power differences (2.11) decreases as the number (k) of best BS angles increases. For k>42, this value becomes very small indicating that a large part of the 121 angles in setup 3 do not contribute to a maximum power.

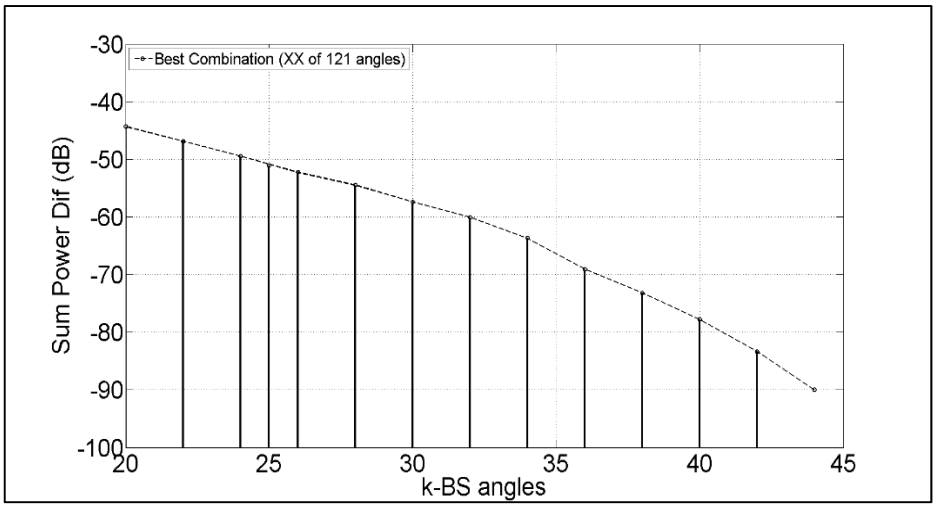

Figure 2.19 Sum of power difference (dB) versus k-BS angle groups (setup 3)

Since the selection of sets $\mathcal{A}$ and $\mathcal{F}$ was accomplished based on a maximum power criteria, the search of the best 25 angles[8] from these sets must be obtained using the same criteria. Basically there is no gain in that selection if we incorporated a second objective function such as 'minimize the total number of blockings (maximum received power lower than a threshold)':

$$\min\left[\sum_{i=1}^{M}\sum_{j=1}^{k}(b_{ij})_{\text{all } C(N,k)\text{of BS angles}}\right] \tag{2.12}$$

where: $b_{ij}=\begin{Bmatrix}1 & \text{if } P_{i,j}<\text{thres}\\ 0 & \text{otherwise}\end{Bmatrix}$; $[\theta_{1\text{BS}},..,\theta_{kBS}]\in\left\{\binom{N}{k}\text{ of }(\theta_{1\text{BS}},..,\theta_{NBS})\right\}$; $\theta_{iBS}\neq\theta_{kBS}$

The small gain can be seen in figure 2.20 for setup 3 (the vertical lines indicate the number of blockings). For the two-objective optimization, one of the Pareto optimal solutions was picked for each group of k (=10,11,12,..25,…) angles.

---

8 Best 25 angles from set $\mathcal{A}$: {-56º, -55º, -53º, -48º, -39º, -34º, -32º, -31º, -30º, -29º, -28º, -25º,-18º, 20º, 21º, 22º, 23º, 24º, 25º, 26º, 27º, 28º, 30º, 35º, 56º}

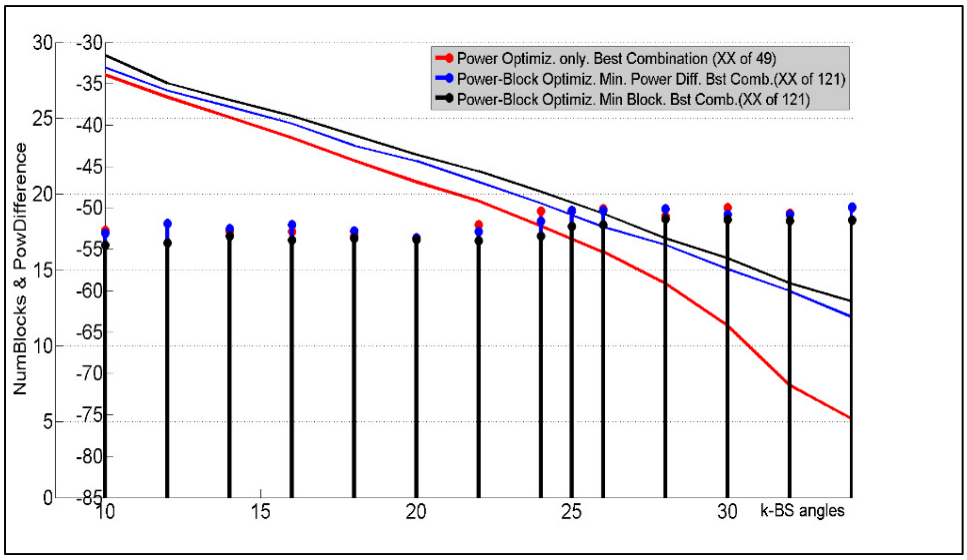

Figure 2.20 Number of blockings and power difference sum (dB) versus k-BS angle groups

Figure 2.21 shows the simulation of the maximum SNR at the UE in L=50 measurements assuming an equal probability for the BS and UE angle switching (10,000 iterations).

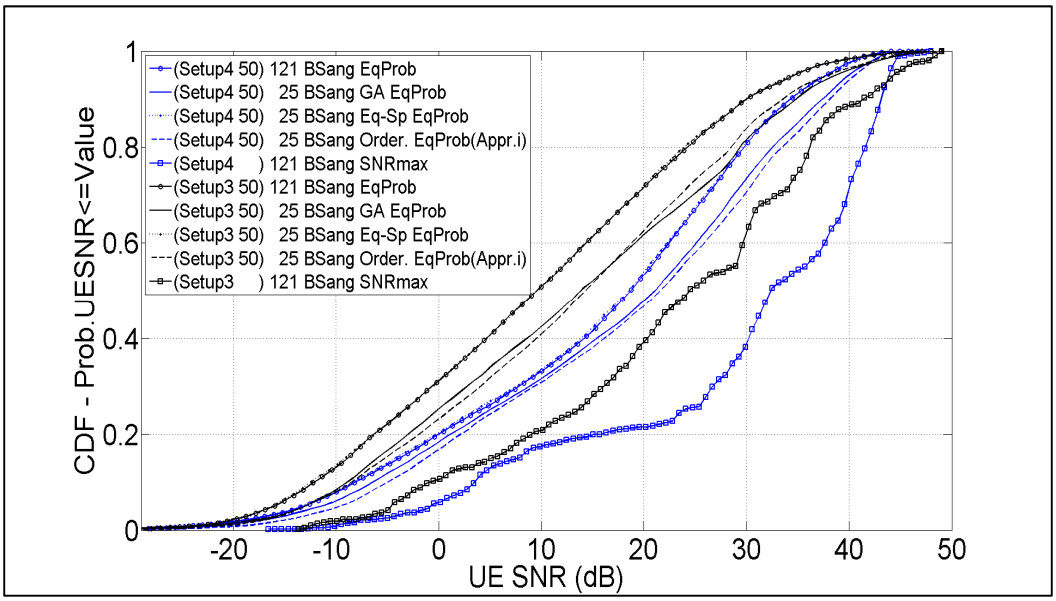

Figure 2.21 SNR in setups 3 and 4. Twenty five BS equally-spaced versus 25 selected angles (equal probability)

The angles selected applying approaches ii showed better performances (solid black and blue lines) of approximately 4.40 dB and 2.80 dB on average compared to the 25 equally spaced angles (black and blue dotted lines) for setups 3 and 4, respectively. These results reiterated the lower gain for service area 2. The application of the first approach (i) (black and blue dashed lines) is computationally simpler and produces results within 1.7 dB compared to those obtained with approach (ii).

2.4.3 Maximum received SNR in a mobile user using a limited number of BS angles

Figure 2.22 shows a comparison of the 25 best BS antenna orientations chosen from set A in setup 3 versus 25 equally spaced angles [-60º:5º:60º] for the case of a UE moving at 30 km/h. Both BS and UE switched their beams randomly with equal probability. Ten linear routes, each of 50 points separated 4.1667 cm (total distance = 2.08m), were applied such that the UE measured the received power at a displaced position at each new BS angle switch time. The selected routes were placed to be well separated and were oriented in different direction inside service area 1.

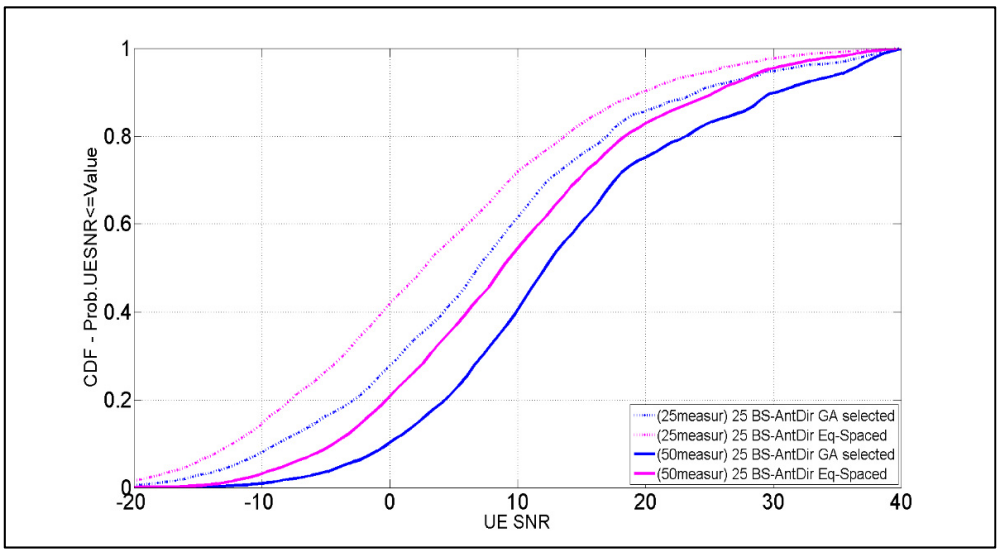

Figure 2.22 SNR statistics for a UE mobile (30 Km/h) in setup 3

Under this scenario a performance gain of 3.3 dB (fiftieth percentile) was obtained. This lower gain (than the static case) appears to be compatible with the method of determining the maximum power in 50 different positions along each route and averaged over many iterations. Figure 2.2 shows that the *L* power samples for a moving UE are obtained from the intersections with a tilted line instead of a vertical one. The power sample values depended on the spatial power distribution generated using each discrete BS, the UE beam orientation, the speed and direction of movement of the user.

2.4.4 Number of switches in a beam training

A particular initial beam training procedure where the BS repeats the same BS angle for a number of UE main beam shifts benefits from the knowledge of the most effective BS angles. It is assumed that the UE takes an initial arbitrary beam direction (azimuth). Our simulation in setup 3 (Figure 2.23) shows that the average number of sequential beam shifts (5^{o}) needed until the UE received a power level equal or larger than a reference threshold (-85 dBm) decreased when a selected set of BS angles was used. It was assumed that the UE had an initial arbitrary beam direction.

Specifically, the comparison of the full set of 121 BS angles versus the 49 BS (best) angles indicates that the number of UE beam switches decreased from 46 to 32 (50^{th} percentile) when the BS changed the beam directions, whether sequentially or randomly (uniform distribution). The percentage (per BS angle) of UE positions that could not connect in 72 beam switches (360°) decreased from 38% to 27%. Three additional beam shifts were saved if the 49 BS angles changed values according to the coverage distribution function F_{BS49} (red line). Figures 2.21 and 2.23 show that the performance of the 25 equally-spaced BS angles was approximately the same as that of the full set of 121 angles.

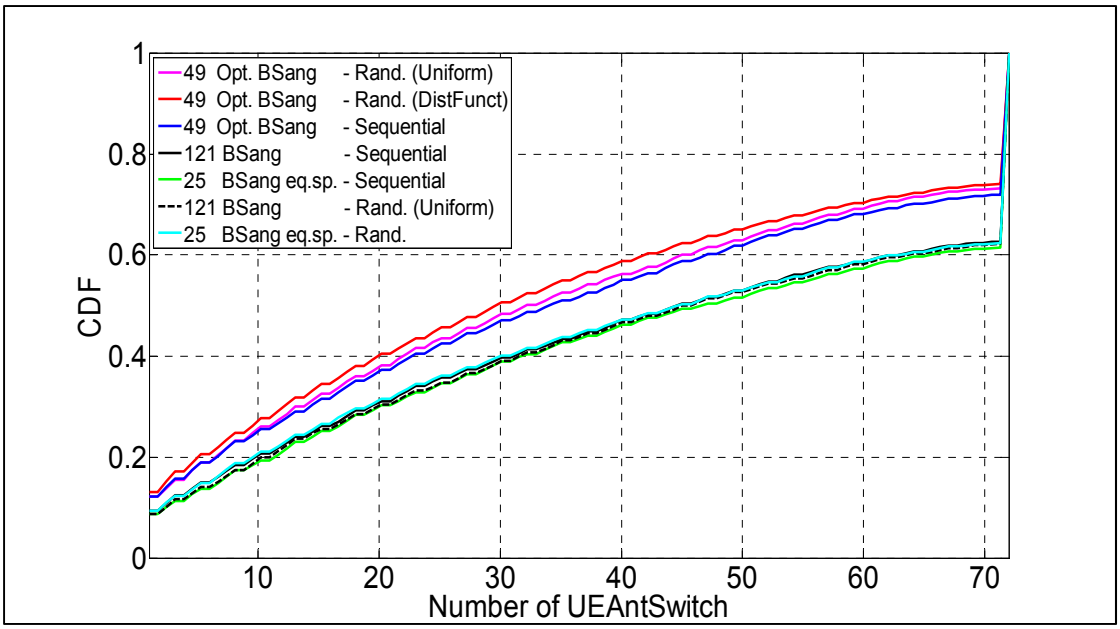

Figure 2.23 UE beam switches until power ≥ -85 dBm (thres) in setup 3

2.5 Conclusions

Results from RT simulations in the 28 GHz band suggests that a priori information regarding the efficacy of some discrete BS angles to deliver the maximum power possible at NLOS locations within a service area can be exploited in a directional cell search or in the initial part of a beam training procedure, particularly for those cases where the BS and UE apply analog beamforming. A performance gain of more than 2 dB was obtained when both the BS and UE change their antenna orientations randomly, but this result may depend on the street canyon propagation severity and the probability of the angle use. The percentage of UE positions per BS angle where the maximum received power is reached may also be applied to improve the performance further. The approximate identification of the best BS angles can be accomplished using a simple RT procedure.

CHAPTER 3

POSITION-AIDED MILLIMETER WAVE BEAM TRAINING UNDER NLOS CONDITION

3.1 Introduction

Field measurement data under NLOS conditions at 28 GHz indicate the existence of many propagation path alternatives in a BS-UE communication link, but these links need to be "discovered" using a combination of directional antennas both at the Base Station (BS) and User Equipment (UE). Although the small wavelength allows to pack many antenna elements and combine their radiation patterns with beamforming techniques to cope with the large propagation path losses, the discovery process is complicated especially in systems that use one RF front per side due to its 'one look' limitation. A direct application of this scheme constitutes the classical hierarchical antenna alignment method (IEEE 802.15.3c Specification, Part 15.3, 2009; Perahia et al., 2010) in which an initial coarse search procedure that covers a large space is followed by a refined search using smaller beamwidth antennas. Such antenna alignment method, normally used in the 60 GHz band, must be redesigned at 28 GHz because the application of low-gain antennas (i.e. omnidirectional), whether in transmit or receive beamforming mode, limits the possibility to obtain UE feedback from a distant UE even with narrowband signals. This effect could generate a mismatch between the discoverable versus the actual supportable RF coverage (Li Q et al., 2013).

Many alternatives have already been proposed. The standard compressed channel sensing techniques that leverage the sparsity property of mmWave channels that can provide an accurate representation of the Power Angle Profile (PAP) and a very much reduced beamforming overhead (Alkhateeb et al., 2015) are sensitive to additive noise (Berraki et al., 2014). Such result may have an impact in NLOS locations where the Signal to Noise ratio (SNR) is not high enough (Ramasamy, 2012). In contrast, as a substitute of the versatility that can be obtained from the costly digital beamforming, recent research work consider the

use of the so-called hybrid beamforming scheme combined with adaptive compressed sensing to estimate the channel but with the application of more than one RF chain at both BS and UE sides (El Ayach et al., 2013; Alkhateeb et al., 2014).

One approach not yet fully explored utilizes the site-specific propagation characteristics knowledge in the form of a database (DB) linked to the position of the UE (Sand et al., 2009). Nowadays, the location information is becoming more readily available as a built-in feature (i.e. GPS or network positioning system) with an increasing degree of accuracy. In fact, some researchers share the vision that context and location information can address some of the key challenges in 5G networks (Taranto et al., 2014). The application of a database has the potential to allow for a faster connection in terms of the number of steps and an initial larger antenna gain for the benefit of the antenna alignment.

Previous studies in this direction include:

- A proposal to exploit the geographical position of an UE (assumed to be acquired through a separate control plane operating at microwave frequency in legacy infrastructure) to improve a cell search procedure. For the case of BS/UE equipped with a directional/omnidirectional antenna, respectively, two search algorithms are introduced that use a starting beamwidth and azimuth angle related to the position of the UE. The initial version of an Enhanced Discovery Procedure (Capone et al., Jan. 2015) is improved using a learning approach (Capone et al., Aug. 2105) which takes advantage of past successful connections saved in a fingerprint map;
- A study that indicates that analog beamforming can still be a viable choice when context information regarding the mmWave base stations is available at the mobile station (Abbas et al., May 2016);
- A 3D RT model is applied as a propagation-prediction engine to evaluate the performance of three cases of beamforming in an indoor communication system formed by a Tx-Rx equipped with directional/omnidirectional antennas, respectively. The RT itself is proposed as a real-time prediction tool to assist future beamforming techniques considering that progresses in environment digitalization, distributed computing, sensing

and localization techniques will facilitate the use of deterministic propagation models (Degli-Esposti et al., 2014).

In this work, we study the application of specific propagation knowledge at 28 GHz band in the form of a DB associated with the geographical position of the UE. 3D RT simulations on a simplified communication system in two different areas inside an urban environment were performed for both cases where the BS knew the exact and inexact location of the user. We propose an algorithm that capitalizes the observation that the BS angles linked to the first propagation path repeat exactly or approximately at other close geographical points around an arbitrary UE position and the result of our previous work in section 2.3 in which the best discrete BS angles were identified for the entire service area. Using an antenna alignment scheme similar to a classical hierarchical method, the proposed algorithm gets the UE appropriately illuminated even for the case of an inaccurate location information. The algorithm facilitates the application of a narrow beamwidth antenna at BS in the initial stage of the antenna alignment procedure providing the advantage of an increased starting illumination power and of a reduced total number of steps. RT simulations showed that the proposed algorithm had a better or similar performance (in terms of received power) than that of a modified classical hierarchical procedure as along as the exact position of the user is within a circular area containing the group of neighbor database points considered. Additionally, we examined the effect of the DB resolution, maximum position error and the radius of the circular area of DB points both for static and moderate variable conditions.

We use the following notation: $\boldsymbol{A}$ is a matrix, $\|\boldsymbol{A}\|_p$ is the p-norm of $\boldsymbol{A}$, $\boldsymbol{a} = \boldsymbol{A}(:,i)$ is a vector, $[\theta_1{:}\Delta\theta{:}\ \theta_2]$ is the set of values $(\theta_1,\ \theta_1+\Delta\theta\ ,\ \theta_1+2\Delta\theta,\ldots,\ \theta_2)$, unique(.) is a computation operator that eliminates the repetition of an element in a defined group of angles.

The remainder of the chapter is organized as follows. Section 3.2 describes the system model and simulation methodology. A description of proposed algorithm is treated in Section 3.3 whereas in Section 3.4 we consider the performance of the algorithm under various conditions. Finally, concluding remarks are highlighted in section 3.5.

3.2 System model and simulation methodology

3.2.1 System model

Consider one sector TDD cellular system (figures 3.1 & 3.2) of dimensions 60ºx200 m located in a specific urban environment where the predominant RF propagation corresponds to a street canyon type. The system is composed of a BS-Tx and UE located at NLOS positions within the service area. Both BS and UE are equipped with horn antennas. The BS knows the geographical position of the UE with a certain error (e_p=dist(*ExctPos-ErrPos*)) relative to its exact location. The position information is assumed to be reported periodically by the UE to the BS through the help of a separate control layer working on a lower microwave band in which the mmW system is overlaid.

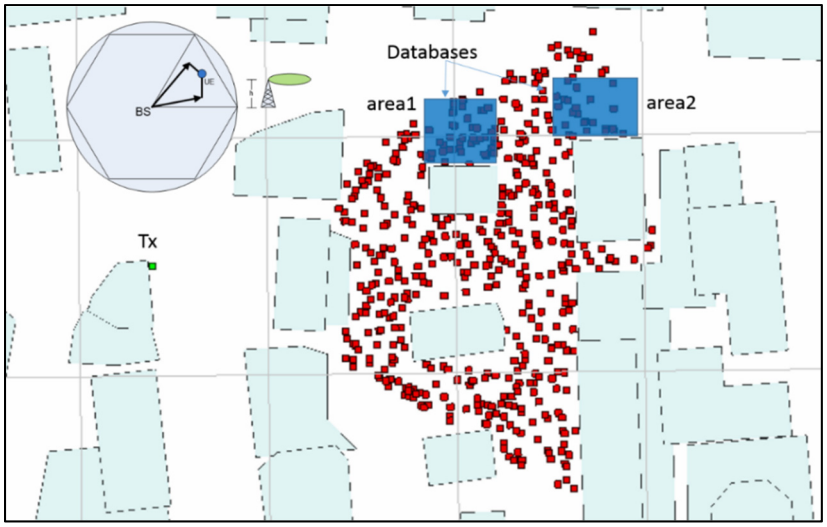

Figure 3.1 Simplified cellular system

The BS has a DB with propagation information of 2,652 and 2,944 points uniformly distributed in two areas $\hat{a}_1$ (25mx25m) and $\hat{a}_2$ (23mx32m), respectively (blue squares in figure 3.2). The DB points are separated 0.5 m (database resolution DB_{res}). Particularly, the DB information includes the power level received at each point for every combination of the BS and UE angles, assumed to vary in azimuth only. $\hat{a}_1$ corresponds to an area of higher SNR values than that of $\hat{a}_2$.

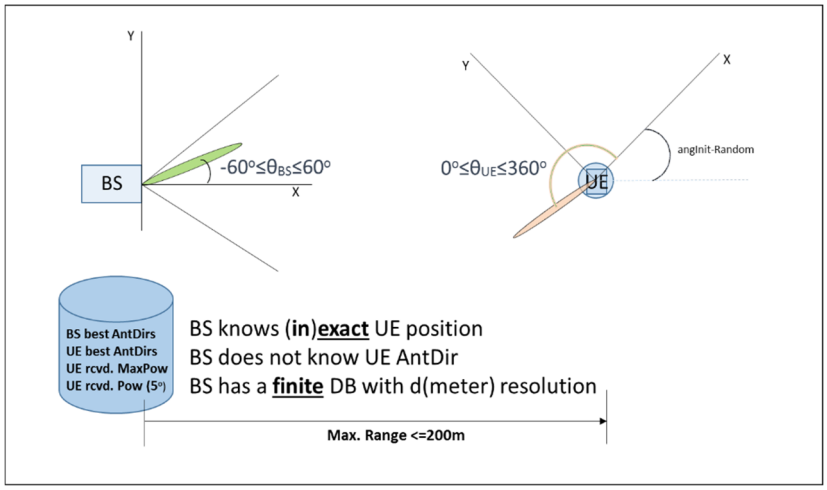

Figure 3.2 BS with a database. UE has a random initial angle

There are 44 and 100 arbitrary positions within the limits of $\hat{a}_1$ and $\hat{a}_2$, respectively, where the UE can be located. It is also assumed that the UE angle has an initial random value θ_{UEinit} (kept constant for the entire block of measurements) in the range [0°:5°:355°] from which it starts to measure the power levels in consecutive fixed angle steps. θ_{UEinit} can be considered as a physical random rotation (azimuth) of the user equipment. At the end of the measuring block, the UE feedbacks the best BS beam angle.

3.2.2 Simulation methodology

An accurate 3D commercial RT tool (Wireless Insite) is applied to simulate the wireless channel between a fixed BS-Tx and a UE located arbitrarily (Appendix VI). A combination of (3dB-beamwidth) 10° and 30° horn antennas together with a narrow bandwidth signal of 1 MHz were considered in order to make sure that a fair comparison between the proposed procedure and a modified classical hierarchical method (Appendix V). All antennas have vertical polarization (Balanis, C., 2005). Phased arrays (Van Trees, 2002) can replace the horn antennas. Propagation data (average received power, ToA, AoD, AoA and the power levels associated to individual MPC) were generated for each DB point and position of the UE. The distance of 0.5m between contiguous DB points facilitates the simulations with lower resolutions (i.e. 1m, 1.5m, 2m,…, etc). The BS discrete angle considered were: best 49 angles

(set $\mathcal{A}$) identified in section 2.3, [-55º:10º:55º], [-57.5º:5º:57.5º] used with a 10º BS horn antenna and [-45º:30º:45º] with a 30º horn antenna. The UE discrete angles [0º:5º:355º] were applied with both 10º and 30º horn antennas whereas the angles [2.5º:5º:357.5º] were applied with the 10º horn antennas only. A 5º angle step was chosen as a compromise between resolution and computation time. The BS and UE antenna heights were set up to 8 m and 1.5 m, respectively. General settings for the tool (full 3D) were 6 reflections, 1 diffraction, 0.1º ray spacing and uniform material for all the building walls. The area under study corresponded to a small city in Rosslyn, Virginia, USA (figure 3.1), where the exterior buildings walls were assumed made of brick. The Tx was installed in front of three buildings of heights 14 m, 38 m (center) and 6 m located across the street at a distance of 48 m approximately. The UE and DB points are located along the streets, primarily behind the two taller buildings (14, 38 m height) so NLOS propagation conditions exist at all positions.

3.3 Proposed Hierarchical Method

In order to improve an initial BS-UE connection in the 28 GHz band using only one RF front for both BS and UE, we propose an alternative version of a hierarchical alignment method that exploits knowledge of the approximate position of the user and the propagation characteristics of neighbor locations. In such procedure, the BS initially selects a small set of angles to illuminate the intended UE directly with a high gain antenna (figure 3.3).

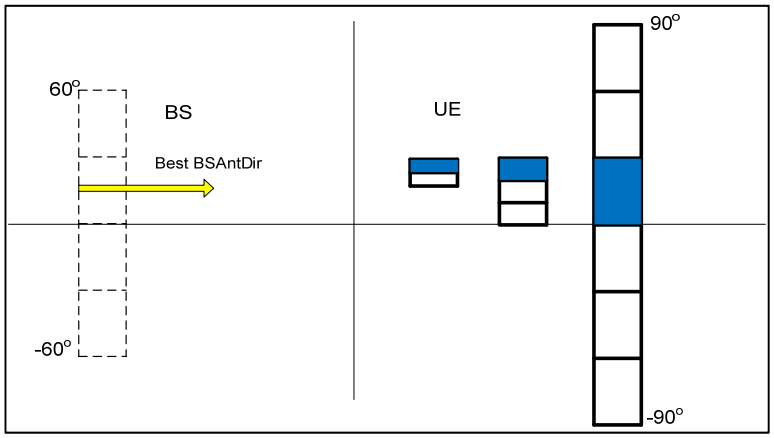

Figure 3.3 BS applies directly a high antenna gain

The UE seeks the highest received power level by steering its antenna (for each BS angle) using an initial beamwidth and a defined angle step. After the complete set of measurements, the UE feedbacks the best BS angle, changes its antenna to one with a higher gain and finds the maximum power applying a refined search within a small angle span. This method has the advantages of faster alignment of the BS-UE main beams and a higher starting received power level. For comparison purposes, we contrast the proposed method against a modified classical hierarchical procedure (Appendix VII) which starts the alignment process with 30º antennas in both BS and UE and ends both with 10º antennas.

Case 1: BS knows the exact UE position X_{EP} and has database information for that position.

The BS (equipped with a 10º horn antenna) illuminates the UE with the best BS angle extracted from the DB, whereas the UE initially samples the received power in equal angle steps using a 30º horn antenna and then switches to a narrower one (10º). The best UE angle cannot be applied directly from the DB information because of the random initial value of θ_{UEinit}, which is unknown to the BS. The total initial and final BS-UE antenna gains are 39.5 (24.5+15) dB and 49 dB, respectively. The proposed algorithm is the following:

Algorithm 3.1 BS and UE beam alignment. BS knows the exact position of the user and has a DB with propagation information of that location

1	The BS (10º horn antenna) applies the best θ_{BS}^{b} obtained from the DB based on the geographical position of the UE;
2	The UE (30º horn antenna) reads the power level at $\theta_{UERUE} = \frac{(n-1)\pi}{6}$; $n = 1,2,\ldots,12$ relative to θ_{UEinit}. The data set is saved as $\boldsymbol{v}(1{:}12,1)$;
3	UE generates $\boldsymbol{v}_{ext} = [\boldsymbol{v}_i(7{:}12,1); \boldsymbol{v}_i(1{:}12,1); \boldsymbol{v}_i(1{:}6,1)]$;
4	The UE applies interpolation and curve fitting to $\boldsymbol{v}_{ext}$, and determines: $[\boldsymbol{v}''_{ext}]_{720x1}$, $[\mathbf{v}'_{ext}]_{360x1} = \boldsymbol{v}''_{ext}\,(181{:}540,1)$ and $\theta_{UEmaxPowRUE}^{1^o} = \underset{pow}{\operatorname{argmax}}(\mathbf{v}'_{ext})$;
5	UE decreases the beamwidth of its antenna (to 10º) and finds its final best angle θ_{UERUE}^{u} by applying a refinement stage of power measurements at $\theta_{UEmaxPowRUE}^{5^o} + (\pm 5^o, \pm 10^o)$.

The power values $\boldsymbol{v}(1{:}12,1)$ in the range $[\theta_{UEinit}+0^o{:}30^o{:}\theta_{UEinit}+330^o]$ are arranged as an extended vector $\boldsymbol{v}_{ext}$ in order to follow correctly the 'circular' characteristic of the PAP around the limits $\theta_{UEinit}+0^o$ and $\theta_{UEinit}+330^o$. The 24 extended vector elements correspond to power values in 720 degrees. The interpolation and curve fitting procedure applied to $\boldsymbol{v}_{ext}$ becomes necessary to improve the angle resolution of $\theta_{UEmaxPowRUE}$ from 30º to 1º. This procedure avoids the inconvenience that the highest power sample value does not always coincide with the maximum possible generating a potential angle (UE) determination error in the range of [-15º:5º:15º]. Figure 3.4 shows the power lobes (also referred as 'clusters'), the PAP using θ_{BS}=-57º of a reference DB point and the sample powers read by the UE using a 30º beamwidth antenna.

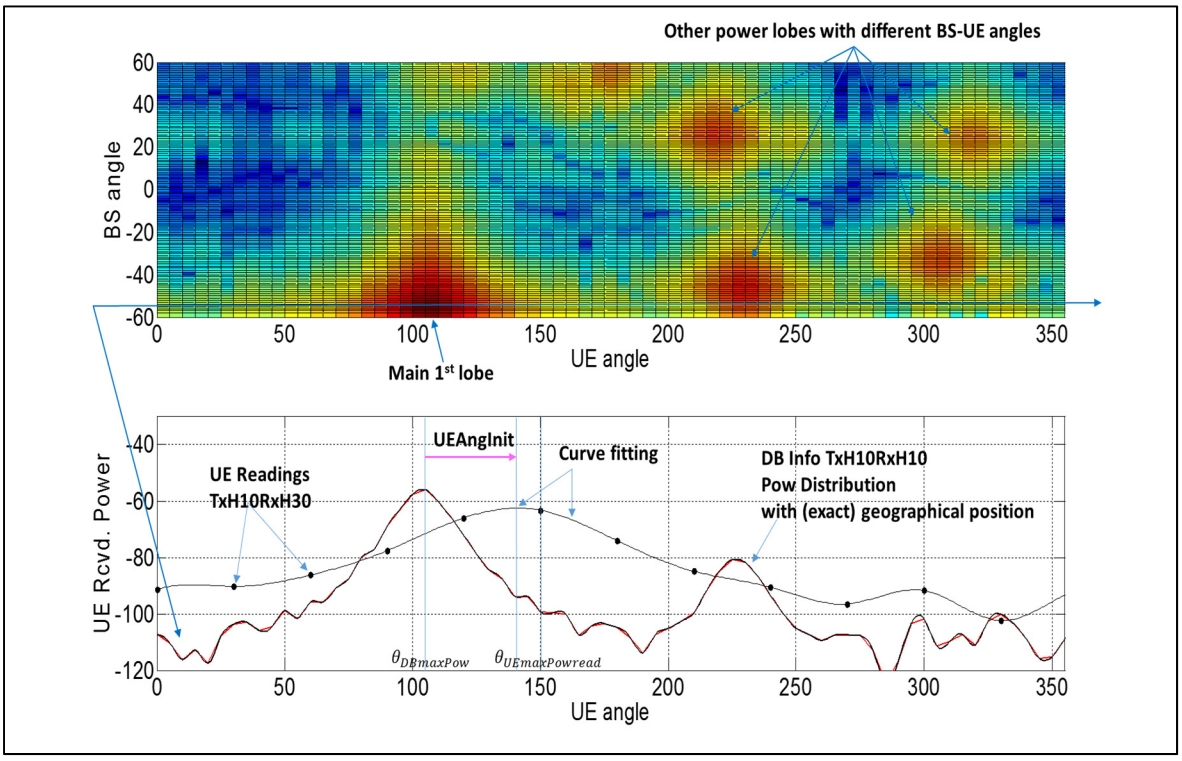

Figure 3.4 DB reference curve and UE power reads

Note that $\theta^{1^o}_{UEmaxPowRUE} \in [0^o{:}1^o{:}360^o)$ is mapped to $\theta^{5^o}_{UEmaxPowRUE} \in [0^o{:}5^o{:}360^o)$ in the refinement stage of power measurements.

The interpolation method may fail to provide a close estimate of $\theta_{UEmaxPowRUE}$ when there are two power lobes very close to each other, producing a PAP much wider. Such scenario does not appear frequently.

Figure 3.5 shows that performance of the algorithm 3.1 for the ideal case 1 (red curve for area 1 ($\hat{a}_1$) and blue curve for area 2 ($\hat{a}_2$)). Algorithm 3.1 outperforms the modified classical hierarchical method (black curve) in both areas. The power difference received at UE is mainly due to a higher power obtained by applying the best angles at the BS (extracted from the DB), in contrast to just using approximate ones in the modified classical hierarchical method. The starting antenna gain difference of 9.5 dB (39.5dB-30dB) is important for achieving a better initial RF coverage in the alignment process. The maximum power difference reaches 3 dB in $\hat{a}_1$ and $\hat{a}_2$, but in general is much smaller in $\hat{a}_1$. For reference purposes, the dashed black line represents the power obtained in the application of the modified hierarchical method in $\hat{a}_1$ using a 5º step in the final alignment stage instead of 2.5º.

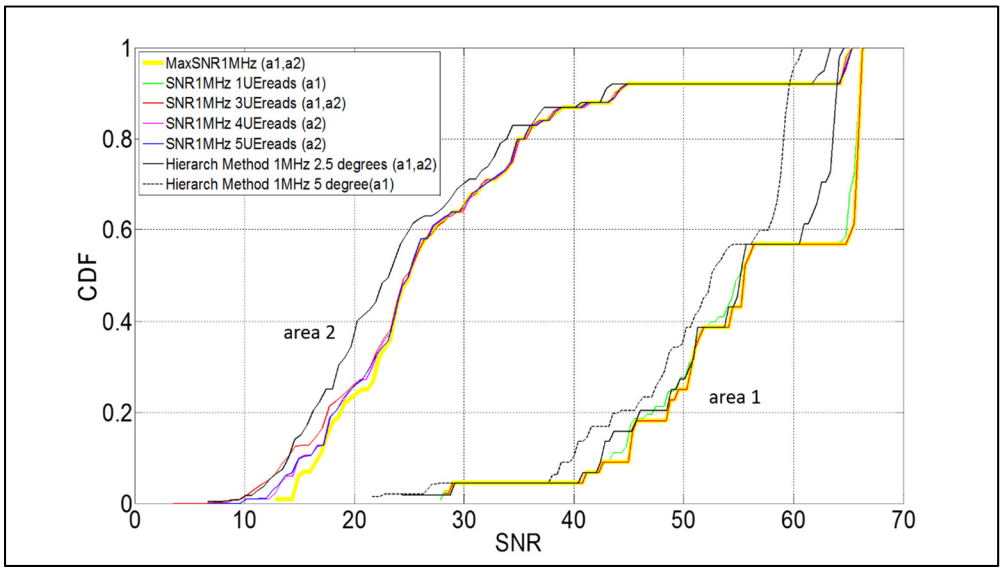

Figure 3.5 Algorithm 3.1 versus modified hierarchical. BS knows the exact UE position

The yellow curve represents the maximum possible power at the UE position considering all combinations of the BS and UE angles. Once the UE determines the angle $\theta_{UEmaxPowRUE}$, a

refinement of three additional power measurements (solid red line) at the angle offsets $[-5^o \;\; 0^o + 5^o]$ are necessary for a user located in $\hat{a}_1$ and five (solid blue line) at the angle offsets $[-10^o \; -5^o \;\; 0^o \; +5^o \;\; 10^o]$ for a user in $\hat{a}_2$. The SNR obtained at $\theta_{UEmaxPowRUE}$ (green curve-one UE read) in $\hat{a}_1$ can be lower than what can be obtained with a modified classical hierarchical method generating the need of a larger number of UE readings. The same situation appears in $\hat{a}_2$ where the performance with just 3 reads would not superior to the reference curve for SNR≤14dB. A special procedure using only 4 UE reads (magenta line) yields similar results as obtained with five reads in $\hat{a}_2$. In the latter procedure, the UE determines the angle of the next power readings based on the tendency of the last two power values.

Case 2: BS knows the exact UE position X_{EP} and has a DB with a resolution (DB_{res}) of d meters

Because it is not possible to collect propagation information for all possible UE positions, the BS must rely on a DB with a finite number of points separated with $DB_{res}=d$ meters (resolution). One possibility is to apply the algorithm 3.1 using the best BS angle for the closest BD point to X_{EP}. Figure 3.6 shows the performance in $\hat{a}_1$ using this criteria for DB_{res} of 1m, 1.5m, 2m, 3m and 4m.

As expected, the lower the resolution of the DB, the lower the received power level at the UE. For this case, given that there are 44 arbitrary fixed UE positions, we simulate the application of the closest point by selecting DB points located within a distance $r \leq \frac{d}{2}\sqrt{2}$ from the reported exact UE location considering that the DB is arbitrarily shifted in x and/or y coordinates. For the specific area $\hat{a}_1$, figure 3.6 indicates that the selection of the best BS angle under the criteria of the 'closest point' in DBs with resolutions larger than 2m basically cannot compete (in term of power delivered) against the modified classical hierarchical beam training (solid black curve). However, the selection of the best angle corresponding to one of the four close BD points located in the vertex of the square enclosing the UE improves the performance to levels very similar to the maximum power possible. This occurs because the

best BS discrete angle for the exact location of the UE is repeated in other nearby points that do not necessarily coincide with the nearest DB point

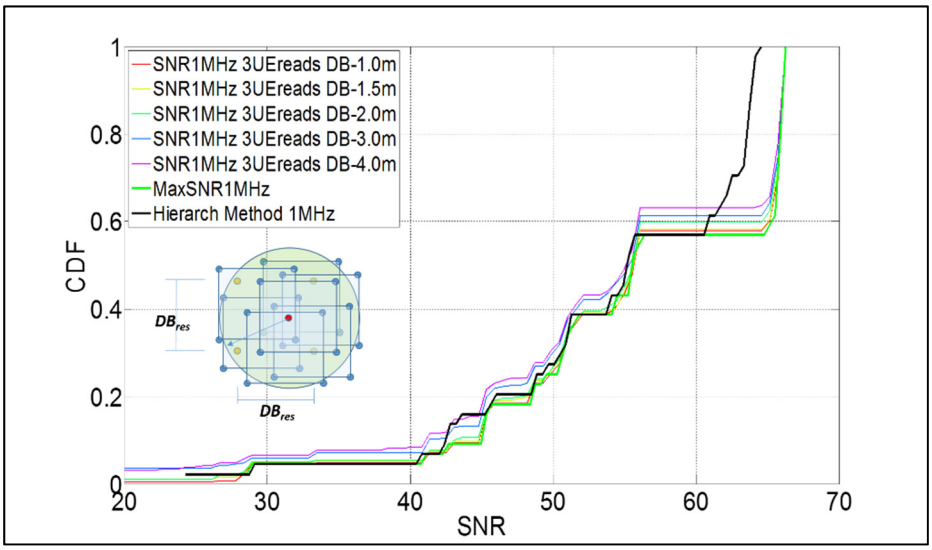

Figure 3.6 SNR of the closest point for different DB resolutions

Case 3: BS knows an inexact UE position X_{RP} and the DB has a DB_{res} of d meters.

The knowledge of X_{EP} is rather an idealistic situation. A Global Positioning System (GPS) normally has an inherent error $e_P = \|X_{RP} - X_{EP}\|_2 \leq e_{pmax}$ that complicates an otherwise straightforward application of algorithm 3.1 because it introduces an uncertainty on the best BS angle to be applied. The information taken directly from the DB closest point to an inexact location can produce a large decrease in the received power. A higher DB_{res} is not useful in this scenario. A circular area $å_{DB}$ (radius D) containing a group of DB points is used as an information base (Figure 3.7).

The geographical distribution of the best discrete BS and UE angles in $\hat{a}_1$ and $\hat{a}_2$ is of interest. These angles repeat themselves at many locations and there are not so many different ones serving the DB points around the positions of the UE.

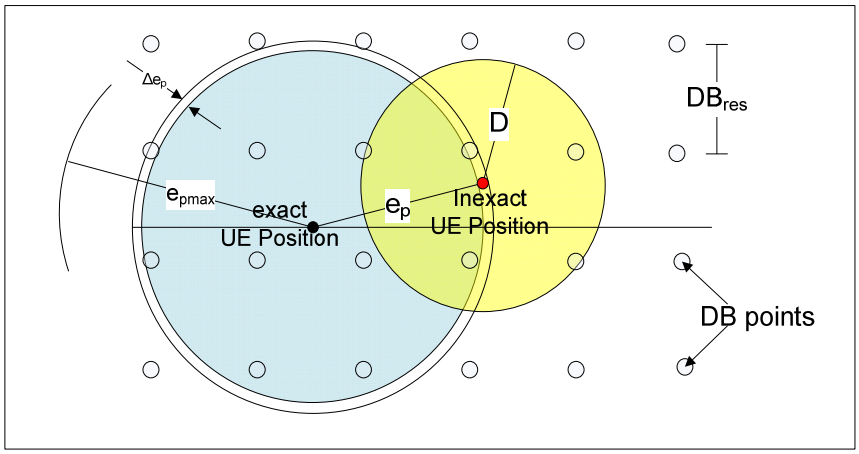

Figure 3.7 Circular area of DB points (radius *D*) around the reported inexact UE position

Figures 3.8 and 3.9 show an example of the group (twelve) of best angle pairs $(\theta_{iBS}, \theta_{jUE})$ serving approximately 800 DB points (blue) that are located within $å_{DB}$ for D=8m and DB_{res}=0.5m. The exact and inexact (reported) positions of the user, and their best BS and UE angles are represented by a small red and green square, respectively. As a reference, Figure 8 also shows all positions of the UE (black dots) and the best BS and UE angles for all DB points in $\hat{a}_1$ and $\hat{a}_2$.

Given a DB_{res}, there is a trade-off between D and the position error e_p of the user. A greater repetition of the best BS angle within $å_{DB}$, the easier becomes its determination and relaxes the knowledge requirement of the exact position of the UE. In contrast, a larger D is not necessarily better since it also increases the number of distant DB points which are best served with very different BS angles complicating the selection of a small group of best BS angles.

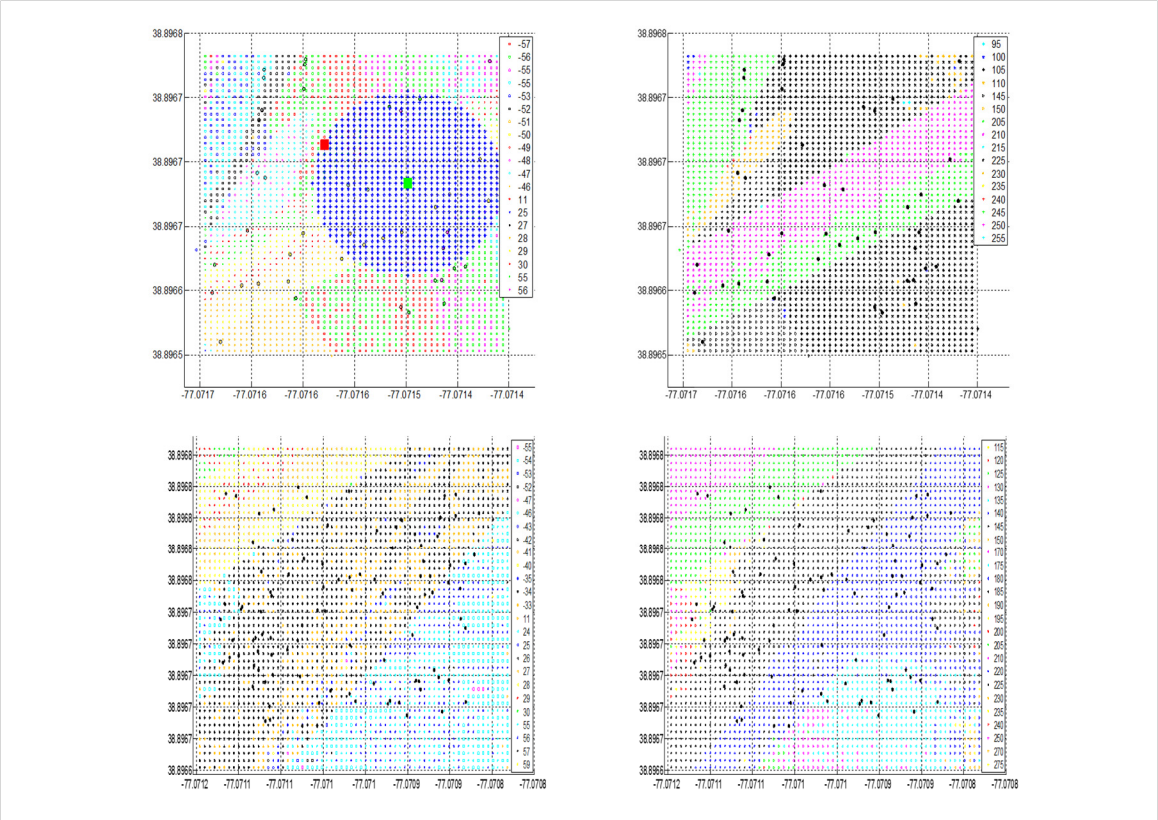

Figure 3.8 Best BS & UE angles in $\hat{a}_1$ (1st row) and $\hat{a}_2$ (2nd row) for DB_{res}=0.5m. UEs are represented as black dots

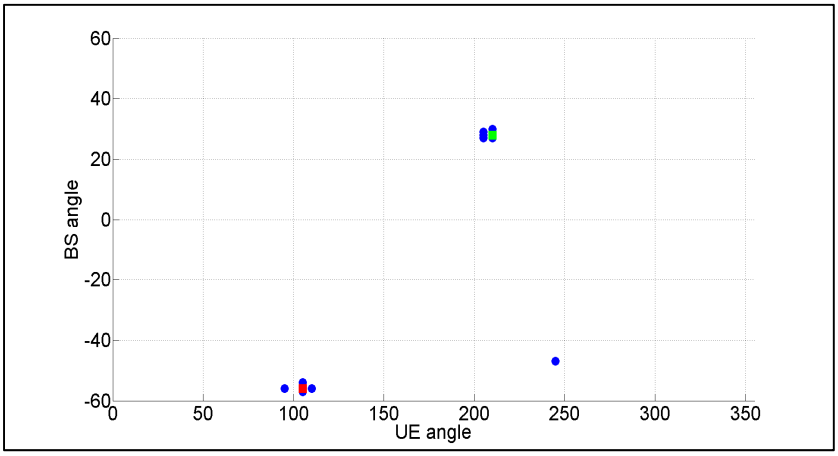

Figure 3.9 Angle pairs (first power lobe) of all DB points and UE (exact e inexact positions) in $\mathring{a}_{DB}$ ($\hat{a}_1$).

To approximate a relationship between e_p and D, we consider the following two cases in which the inexact location reported by the UE ($e_p \neq 0$ in figure 7) is the center of åDB.:

- The probability ($p_{rBestBSang}$) that the best BS angle of the UE repeats in the DB points located within åDB is calculated as D varies. The same DB points are used randomly as candidates for the inexact UE positions. Considering that there are few DB points located at the exact error distance e_p from X_{EP} and it is of interest to obtain adequate statistics, we select DB points with position errors e'_p in the range $[e_p, e_p + \Delta e_p]$ ($\Delta e_p = 0.25$) for $DB_{res} = 0.5$ m. Figure 3.10 and Table 3.1 indicate that the value of $D = D^{(maxprob)}$ that maximizes $p_{rBestBSang}$ is equal or larger than e_p; that is, $D^{(maxprob)} \geq e_p$. For $e_p = 0$ (solid yellow), åDB is centered at the exact position of the UE (Figure 3.7) and $p_{rBestBSang}$ decreases monotonically as D increases. Given that e_p is an unknown variable, its use becomes impractical.

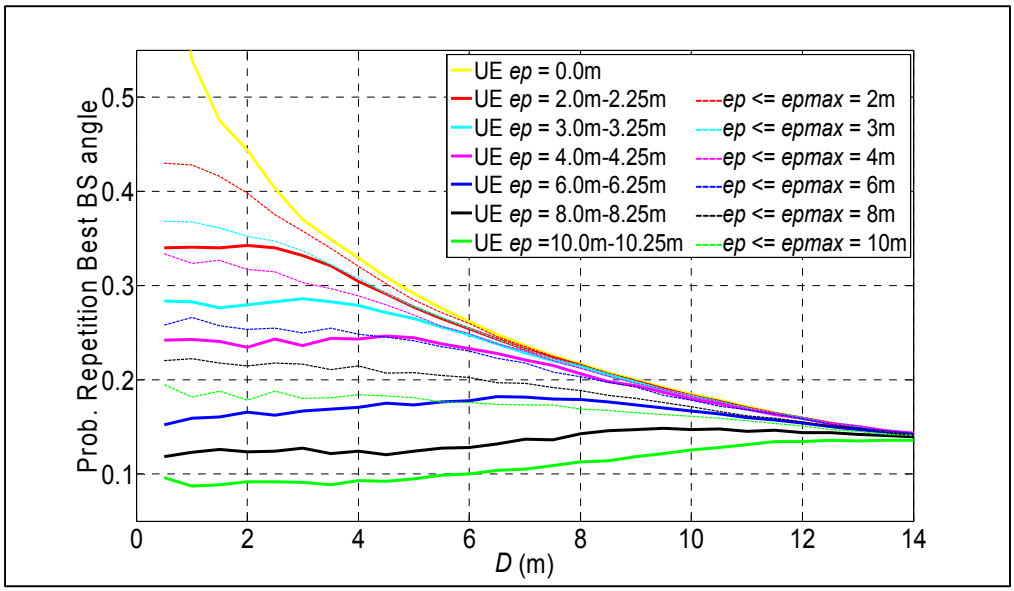

Figure 3.10 Probability of BS angle repetition versus D in åDB ($\hat{a}_1$) for the conditions $e'_p \in [e_p, e_p + \Delta e_p]$ and $e_p \leq e_{pmax}$. $DB_{res} = 0.5$ m

- e_{pmax} is used as a fixed reference and the value of D is determined for which $p_{rBestBSang}$ maximizes under the condition $e_p \leq e_{pmax}$. The parameter e_{pmax} is associated with the accuracy of the positioning system error and is easily available. Figure 10 shows that

$p_{rBestBSang}$ (slotted lines) decreases with D, in which case the minimum value must be selected. The decrease is moderate (fourth column in Table 3.1). Note that the percentages of such variation in the range [0.5, e_{pmax}] become an upper bound because it is likely that on average $e_p \geq 0.5$ for the larger values of e_{pmax}.

Considering both cases, we approximate the radius of åDB as $D \gtrsim e_{pmax}$.

Table 3.1 $D^{(maxprob)} \geq e_p$ and difference in $p_{rBestBSang}$ for $e_p \leq e_{pmax}$

Position error e_p (m)	**D (m) maxProb.**	**Max. position error e_{pmax}**	**Difference in $p_{rBestBSang}$ $0.5\text{m} \leq D \leq e_{pmax}$**
$2.0 \leq e_p \leq 2.25$	2	$e_p \leq e_{pmax} = 2.0$	0.0314 (7.3%)
$3.0 \leq e_p \leq 3.25$	3	$e_p \leq e_{pmax} = 3.0$	0.0320 (8.7%)
$4.0 \leq e_p \leq 4.25$	4.5	$e_p \leq e_{pmax} = 4.0$	0.0443 (14.0%)
$5.0 \leq e_p \leq 5.25$	5.5	$e_p \leq e_{pmax} = 5.0$	0.0361 (12.3%)
$6.0 \leq e_p \leq 6.25$	6.5	$e_p \leq e_{pmax} = 6.0$	0.0273 (10.5%)
$7.0 \leq e_p \leq 7.25$	8.5	$e_p \leq e_{pmax} = 7.0$	0.0159 (6.9%)
$8.0 \leq e_p \leq 8.25$	9.5	$e_p \leq e_{pmax} = 8.0$	0.0320 (14.5%)
$9.0 \leq e_p \leq 9.25$	11.5	$e_p \leq e_{pmax} = 9.0$	0.0256 (12.9%)
$10.0 \leq e_p \leq 10.25$	12.5	$e_p \leq e_{pmax} = 10.0$	0.0334 (17.2%)

The simulation results indicated that the selection of the BS angle based on the combined criteria of maximum power at the DB points and probability of the best BS angle inside åDB became the best approach in terms of power delivery to the UE. Only 3 angles (set G) were sufficient to be competitive relative to the modified classical hierarchical method.

Based on these observations, the following algorithm is proposed:

- Identify all M-DB points located inside a circular area åDB (M-DB points) of radius $D \gtrsim e_{pmax}$ such that this area always includes the exact position of the user;
- Identify the set of N-BS (and L-UE) angles for which each one of the M-DB points ($N \leq L \leq M$) receives the maximum power possible. Because such a set can be large, the set is reduced by a pre-selection procedure based on a received power difference (increasing) and the percentage of the BS angle inside åDB;

a. In pre-selection part 1, the N BS angles are ordered according to the following sum of power differences:

$$\left[\sum_{i=1}^{M}\left|p_{iN}-P_{i,k}\right|\right]_{\theta_{kBS}}; \quad (3.1)$$

$$P_{i,k}=\max\left([P_{i,0^o},P_{i,5^o},\ldots..,P_{i,355^o}]_{\theta_{kBS}}\right);$$

$$p_{iN}=\max\left[P_{i,1},P_{i,2},\ldots,P_{i,N}\right]$$

where $P_{i,k}$ is the maximum power at a DB point i (DB_{pi}) considering all the power values measured when the antenna main beam (10°) is rotated 360° in 5° increments for a particular BS discrete angle θ_{kBS}. P_{iN} corresponds to the 'maximum possible power' at DB_{pi} considering all N BS-angles.

Starting from the first angle in the ordered set and considering that the BS antenna has a beamwidth '*bwdth*', we discard angles within the range $\theta_{iBS}\pm\left(\frac{bwdth}{2}\right)$, except θ_{iBS}. This proposal is reasonable because the eliminated angles would allow the BS to deliver a power level that varies approximately up to 1.5 dB and the largest number of well separated BS angles must be explored;

The angles left after the pre-selection 1 were used directly in the illumination of the UE if the number n_a of them was less than or equal to three ($n_a \leq 3$);

b. In pre-selection part 2 ($n_a > 3$), the reduced set of angles obtained from pre-selection part 1 is ordered again based on their percentage of repetition inside $å_{DB}$. The three most probable angles are considered to illuminate the UE;

- Using a 30° horn antenna, the UE measures the power (for each BS angle in the set G) at θ_{UERUE} = (n-1)π/6; n = 1,2, ….,12 relative to the random initial angle θ_{UEinit};
- UE applies interpolation and curve fitting to each group of power measurements (as in Algorithm 1). This procedure provides 360 power values corresponding to 360 degrees for each BS angle. The best BS and approximate best UE angles are determined by comparing power levels;
- The UE feedbacks the best BS angle;
- Using a higher-gain antenna (10°), the UE determines its final best angle by applying a refinement stage of power measurements at the angle offsets [-10°, -5°, 0°, 5°, 10°].

The algorithm 3.2 is detailed as follows:

Algorithm 3.2 BS and UE beam alignment. BS knows an inexact position of the user and has a DB with resolution DB_{res} of d meters

1 BS identifies all *M-DB* points with coordinates X_i that satisfy:
$H=\{ X_i / \|X_{RP}-X_i\|_2<D\}$; $D \gtrsim e_{pmax}$; $i = 1,2,\dots,M$;

2 BS obtains from DB
$\boldsymbol{A}'_{Mx2}$; $\boldsymbol{A}'(i,1:2) = \left\{(\theta'_{i,vBS}, \theta'_{i,wUE}) / \max_{\theta_{i,vBS}}(P_{i,\theta_{i,wUE}})\right\}$
$\theta'_{vBS}\ \varepsilon\ \{\theta_{1BS}, \theta_{2BS},..,\theta_{121BS}\}$; $\theta'_{wUE}\ \varepsilon\ \{\theta_{1UE}, \theta_{2UE},.., \theta_{72UE}\}$;

3 $\left[\boldsymbol{a}_{\theta_{BS}}\right]_{Nx1} = \text{unique}\left(\boldsymbol{A}'(:,1)\right)$;
$\left[\boldsymbol{a}_{\theta_{UE}}\right]_{Lx1} = \text{unique}(\boldsymbol{A}'(:,2))$; $N \le L \le M$;

4 BS constructs:
$[\boldsymbol{Q}'']_{MxN}$; where each element $q''_{i,k} = \max_{A_{\theta_{kBS}}(k,1)}\left[P_{i,0^o}, P_{i,5^o},., P_{i,355^o}\right]$;
P_i=power at DB_{pi}; $i = 1,2,3,\dots,M$; $k = 1,2,\dots.,N$;
$[\boldsymbol{t}]_{Mx1} = \max(\boldsymbol{Q}''(\text{i},1:N))$;
$[\mathbf{difpow}_{mw}]_{1,k} = \|\boldsymbol{t} - \boldsymbol{Q}''(:,k)\|_1$;

5 BS orders the angles in $\boldsymbol{a}_{\theta_{BS}}$ (set $\boldsymbol{a}^{ord}_{\theta_{BS}}$) according to $\underset{descend}{\text{sort}}[\mathbf{difpow}_{mw}]$;

6 BS generates $\boldsymbol{b}_{\theta_{BS}} = \left[a^{ord}_{\theta_{BS}}(1,1),\dots a^{ord}_{\theta_{BS}}(y,1)\ \dots\right]^T$ by discarding angles in the range $\boldsymbol{a}^{ord}_{\theta_{BS}}(j,1) \pm \left(\frac{bwdth}{2}\right)$, except $\boldsymbol{a}^{ord}_{\theta_{BS}}(j,1)$, where j=1,y,…..
If card($\boldsymbol{b}_{\theta_{BS}}$) ≤ 3 then $G = \boldsymbol{b}_{\theta_{BS}}$;
If card($\boldsymbol{b}_{\theta_{BS}}$)>3 then the BS constructs $\boldsymbol{b}^{ord}_{\theta_{BS}}$ by ordering the angles in $\boldsymbol{b}_{\theta_{BS}}$ according to their percentage (descending) of presence in the *M-DB* points. BS selects $G = \boldsymbol{b}^{ord}_{\theta_{BS}}(1:3)$;

7 BS illuminates the UE using all $\theta_{BS} \in G$;
For each BS angle, the UE measures power at $\theta_{UERUE} = \frac{(n-1)\pi}{6}$; $n = 1:1:12$ relative to the random initial angle θ_{UEinit}. The data set is saved as $\boldsymbol{v}_i(1{:}12,1)$;

8 UE applies interpolation and curve fitting to each extended vector
$\mathbf{v}_{iext}$ = [$\mathbf{v}_i$(7:12,1); $\mathbf{v}_i$(1:12,1); $\mathbf{v}_i$(1:6,1), and determines $[\mathbf{v}''_{iext}]_{720x1}$;
$[\mathbf{v}'_{iext}]_{360x1}=\mathbf{v}''_{iext}(181{:}540,1)$ and $[\mathbf{V}]_{360xq}=\left[\mathbf{v}'_{1ext}, \dots, \mathbf{v}'_{qext}\right]$; q=1,2,3;

9 UE determines $(\theta^b_{BS}, \theta^{1^o}_{UEmaxPowRUE})=\underset{pow}{\text{argmax}}(\mathbf{V})$;

10 UE feeds back the best angle θ^b_{BS};

11 BS applies θ^b_{BS}. UE changes to a narrower beamwidth antenna (horn 10°) and chooses the best θ^u_{UERUE} after measuring power levels at $\theta^{5^o}_{UEmaxPowRUE} + (-10^o, -5^o, 0^o, 5^o, 10^o)$.

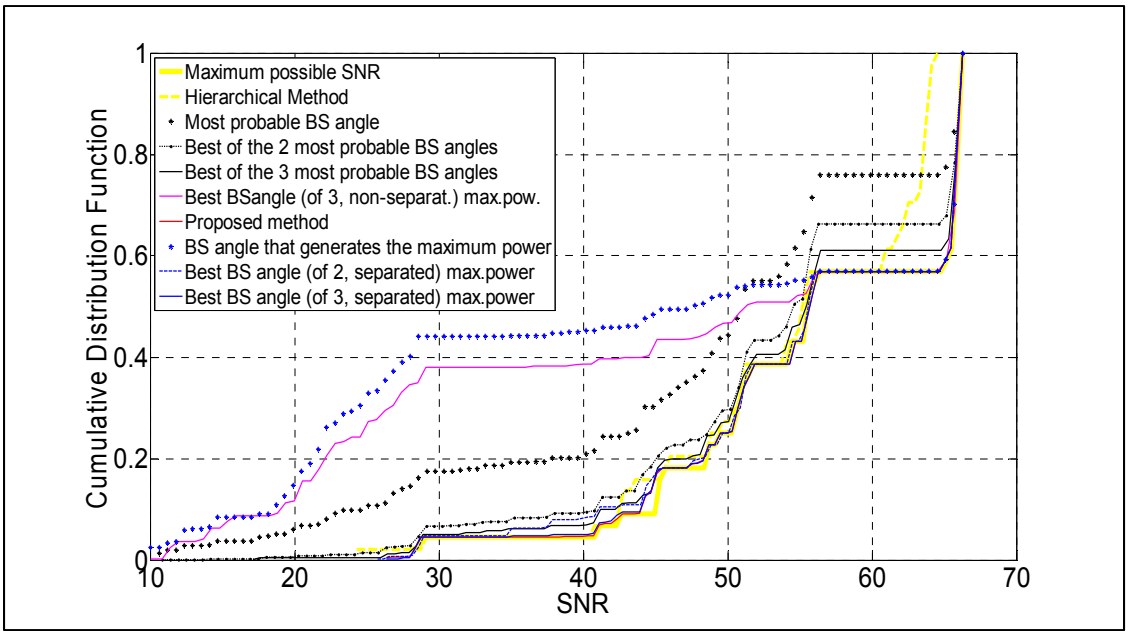

Figure 3.11 SNR obtained ($\hat{a}_1$) from the application of one or the best of two or three BS angles inside $\mathring{a}_{DB}$ (selection based on repetition or power differences)

All 121 BS angles need not be applied in the step 2 of the algorithm 3.2 to determine the best N angles for all M-DB points in $\mathring{a}_{DB}$. The set of best BS angles determined for the entire service area (section 2.3) reduces considerably the DB size. The appropriate number of elements of the set G was determined by searching for the criteria that produced the closest performance to the maximum possible. The simulation results indicated the following:

- The selection (without any processing) of the BS angle that repeats the most inside $\mathring{a}_{DB}$ (among all those used by the DB points) does not offer a viable solution because the performance obtained (black-asterisk line in Figure 3.11) is considerably lower than the maximum possible (solid yellow). The selection of the two most probable BS angles inside $\mathring{a}_{DB}$ (DB points) and the posterior application of the best of the two in terms of power delivery to the UE produces a performance (black dashed line) that is still not better than that of the modified hierarchical alignment method (dashed yellow). A closer result (solid black line) to the maximum possible is obtained by selecting the three most frequent BS angles and the posterior application of the best of the three.

- The application of the BS angle $\boldsymbol{a}_{\theta_{BS}}^{ord}(1,1)$ resulted in a poor performance (asterisk blue, Figure 3.11). The selection of the best of the BS angles $\boldsymbol{a}_{\theta_{BS}}^{ord}(1,1:3)$ (angles not separated in *bwdth*/2 degrees) in terms of power delivery to the BS produced a poor performance as well (magenta solid line).
- The selection of the best BS angle among $\boldsymbol{b}_{\theta_{BS}}(1,1:2)$ or $\boldsymbol{b}_{\theta_{BS}}(1,1:3)$ for the case of $n_a > 3$ produced a closer performance than those selected based on the probability criteria (dashed or solid blue line, Figure 3.11) .
- The combination used in the algorithm 2 provided the closest performance (red) to the maximum possible.

3.3.1 Number of steps

The number of steps necessary in the application of the proposed algorithm 3.2 is lower than that is required in an equivalent classical hierarchical procedure because the BS applies directly a high gain antenna based on the position (exact/non exact) of the UE at the beginning of the alignment task. A simplified comparison is shown in Table 3.2

Table 3.2 Comparison of the number of antenna alignment steps per 180º (UE) angle span

BS H10º/H30º - UE H10º/H30º	**Modified Hierarchical**	**Proposed method**
UE determines best BS sector (30º)	24	18
UE feedbacks information to BS	4	3
UE checks power at θ_{UE} + [-10º -5º 0º 5º 10º]		5
UE determines best BS subsector (10º)	3	
UE feedbacks information to BS	1	
UE determines its best subsector (10º)	3	
UE determines best BS subsector θ_{BS} + [-2.5º +2.5º]	2	
UE feedbacks information to BS	1	
UE determines its best subsector θ_{UE} + [-2.5º +2.5º]	2	
Total (in 180º)	**40**	**26**

Only three additional UE power (angle) reads are sufficient in $\hat{a}_1$ reducing to 24 the total number of steps needed. A more elaborated UE reading mechanism allows to use only 4

instead of 5 additional power readings in $\hat{a}_2$. Note that the number of steps in Table 3.2 is the maximum possible for the proposed method. There are many cases where the number of BS angles in G is less than 3.

3.4 Algorithm performance

3.4.1 Static case

Figures 3.12 and 3.13 show the performance of algorithm 3.2 for $D = e_{pmax}$ =10m, DB_{res}=0.5m. These results are achieved using three and five additional UE power readings in $\hat{a}_1$ and $\hat{a}_2$, respectively The performances basically remain the same compared to *Case 2* (section 3.3) where the BS knows the exact location of the UEs.

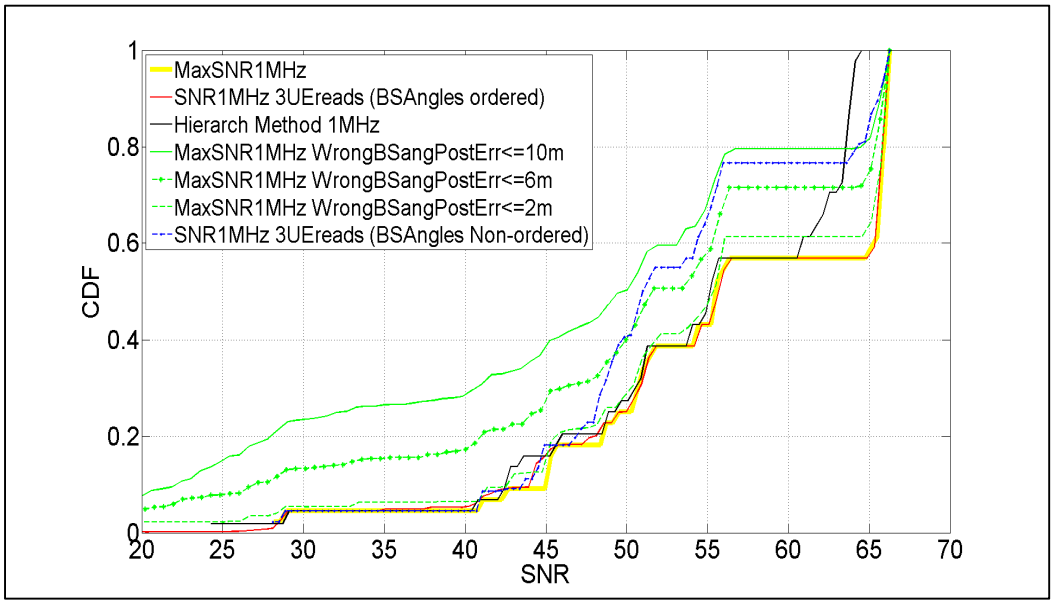

Figure 3.12 Performance of algorithm 3.2 ($\hat{a}_1$). DB_{res}=0.5m, D=e_{pmax}=10m (e_{pmax}=2m,6m,10m, green curves)

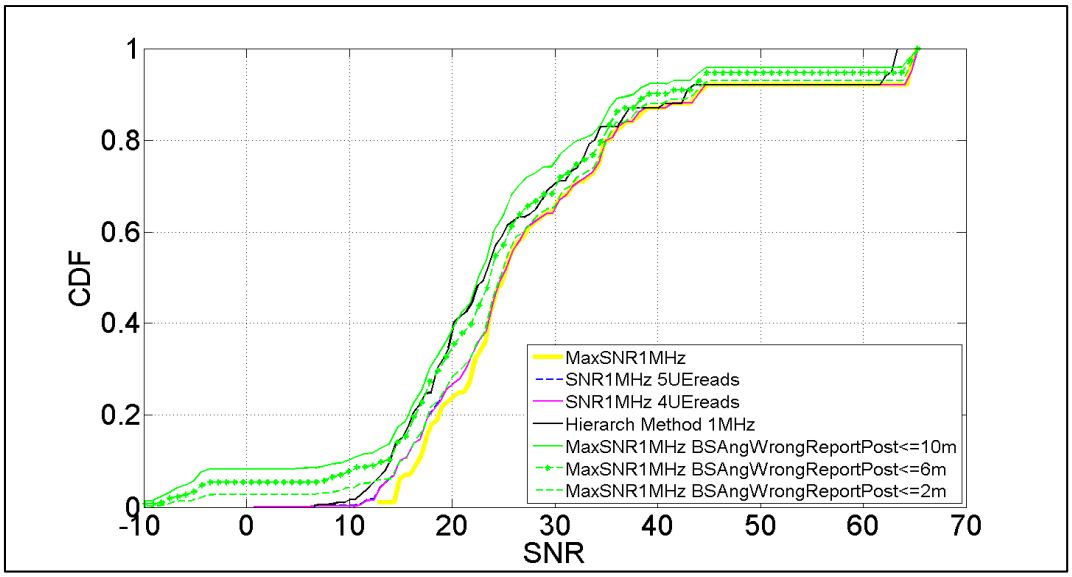

Figure 3.13 Performance of algorithm 3.2 ($\hat{a}_2$). DB_{res}=0.5m, D= e_{pmax} =10m (e_{pmax}=2m,6m,10m, green curves)

The figures also show in green color the SNR at the UE when there is a direct application of the best BS angles obtained from the DB using the inexact location reported by the UE for e_{pmax} of 2m, 6m and 10m. The SNR difference for $e_p \leq e_{pmax}$ relative to the maximum possible reaches 23dB in $\hat{a}_1$ and 8.5 dB in $\hat{a}_2$ (actually is higher for low SNR).

Instead of selecting the angles from set G (step 6 in algorithm 3.2), these can also be chosen simply by picking the ones that are separated in '*bwdth*' degrees. One arbitrary selection of the first three angles in $\boldsymbol{a}_{\theta_{BS}}$ (step 3 in algorithm 3.2) results in a poorer performance (dotted blue line in Figure 3.12). The same simulation for $\hat{a}_2$ (Figure 3.13) is not shown due to the small impact in the received power.

The selection of a larger number of BS angles (e.g. 4) in set G gives a small improvement in performance. For each additional BS angle in set G, the number of steps in the antenna alignment increases in proportion to the number of power level measurements, that is 12.

Figure 3.14 shows the performance of algorithm 3.2 for $e_{pmax} = D$ =10m and different DB_{res} (1m to 4m) for both areas. The repetition of the best BS angles in $\hat{a}_{DB}$ helps maintain the performance with a small change when the DB_{res} decreases. The performances are basically kept without much variation for all the DB resolutions considered in $\hat{a}_1$ and up to 2m in $\hat{a}_2$. In the latter case, a reverse situation begins to appear around SNR=10 for DB_{res} of 3m and 4m. These results become interesting since it gives an opportunity to decrease the number of points needed for the DB. Specifically, for the current 60º x 200m (20,944m2) sector, the number of DB points could be decreased from 86,776 to 9,308 (5,249) if the resolution was decreased from 0.5m to 1.5m (2m) without much impact on performance. The figure also shows the SNR (solid green curves for both areas) at the UE when the BS applies an angle taken from the DB using directly the reported inexact location ($e_{pmax} = 10$m) and $D = 10$m, DB_{res}=4m. The power decrease could reach 22 dB in $\hat{a}_1$ and 8.5 dB in $\hat{a}_2$ (higher for low SNR).

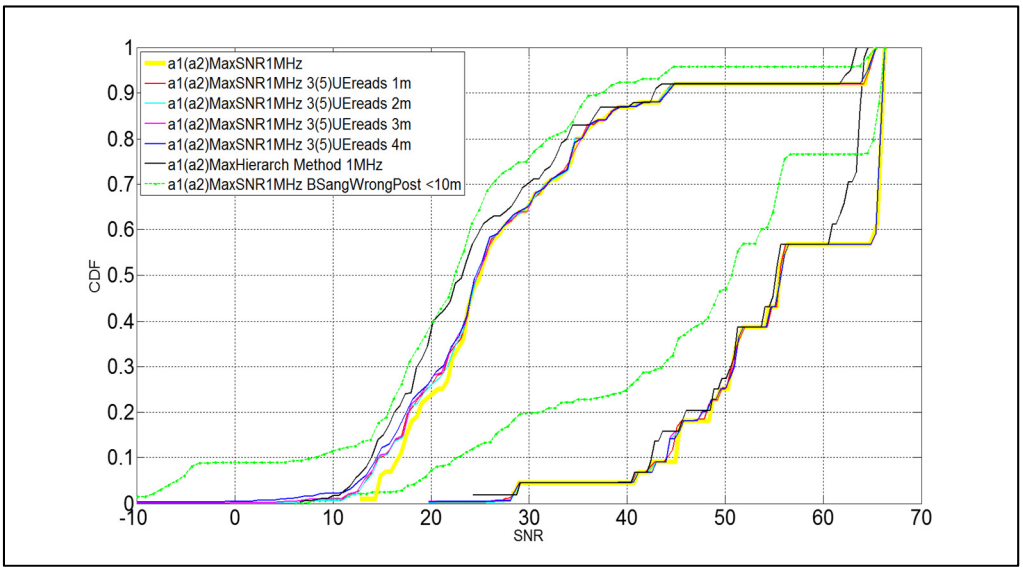

Figure 3.14 Performance of algorithm 3.2 ($\hat{a}_1, \hat{a}_2$).
D=e_{pmax}=10m. DB_{res}= 1m, 2m, 3m, 4m.

3.4.2 Random variation of the maximum received power

To evaluate the performance of algorithm 3.2 for non-static conditions, we emulate a particular channel variation by replacing the PAP (function of the best θ_{BS} and θ_{UE}) at the UE with the one corresponding to a DB point randomly located within a certain radius d_{DBr}, that is, $||X_{new}\text{-}X_{EP}||_2 \leq d_{DBr}$. This replacement can change the received maximum power and the best BS-UE angle combination. Figures 3.15 and 3.16 show the performance of algorithm 3.2 for $D=e_{pmax}$ =10m, $d_{DBr} \leq D$ and particular parameters of DB_{res}=1m,4m in $\hat{a}_1$ and DB_{res}=1m,2m,3m,4m in $\hat{a}_2$.

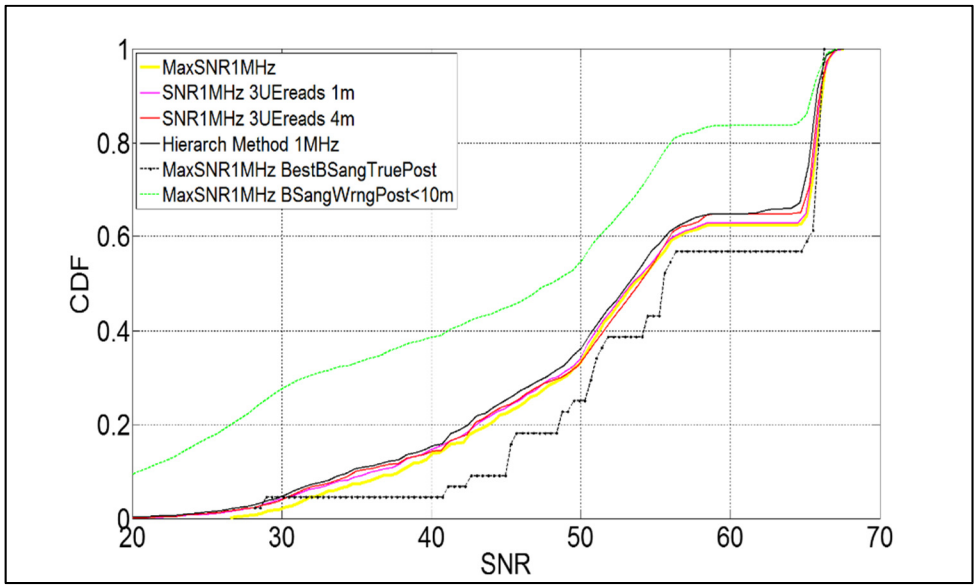

Figure 3.15 SNR comparison ($\hat{a}_1$). Power distribution variation at UE, $D=e_{pmax}$=10m. $d_{DBr} \leq D$, DB_{res}=1 and 4m

As expected, the actual maximum possible SNR (yellow line) has changed compared to the original one (slotted black line), this latter linked to the best BS angle under static conditions. The power variation reaches a maximum value of approximately 10 dB in $\hat{a}_1$. As a reference, the figures also show (green line) the maximum SNR in the case of a direct application of the best BS angle associated with an inexact position information for e_{pmax}=10m and DB_{res}=4m (difference of 17 dB in $\hat{a}_1$ and 4.5 dB in $\hat{a}_2$ relative to the maximum possible). For DB_{res} up to

2m, the proposed algorithm 3.2 has similar performance (excluding some locations in $\hat{a}_2$ where the SNR≥35) as the modified classical hierarchical procedure in both $\hat{a}_1$, $\hat{a}_2$ but uses fewer steps in the antenna alignment procedure (Table 3.2).

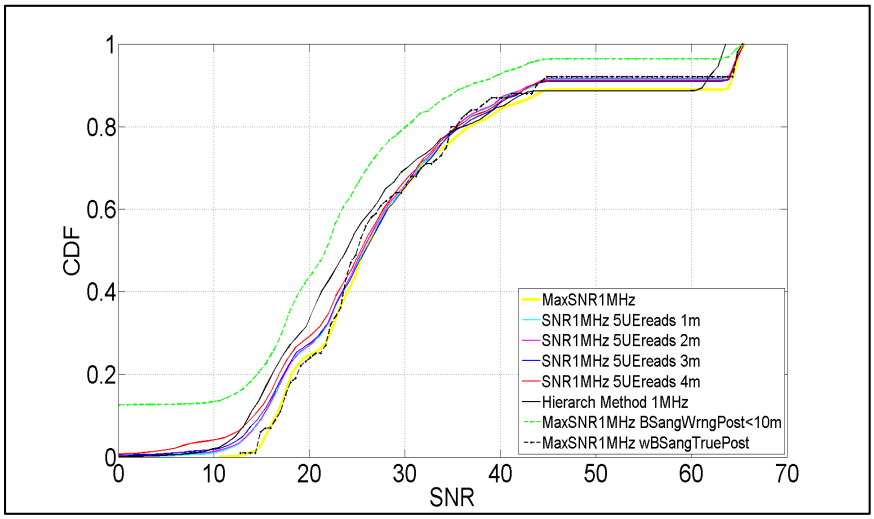

Figure 3.16 SNR comparison ($\hat{a}_2$). Power distribution variation at UE, $D=e_{pmax}$=10m, $d_{DBr} \leq D$, DB_{res}=1m,2m,3m,4m

Simulations using $d_{DBr} > D$ were not considered. An external random event occurring near the UE that can cause a variation in the maximum received power, changes the best UE and BS angle, this latter most likely to a one that belongs to the group of angles best serving all *M*-DB points located in $\mathring{a}_{DB}$. Certainly, the UE angle can change greatly, but this does not have any impact on the performance since the UE determines the best antenna orientation through a sequence of measurements.

To determine if the relation $D \gtrsim e_{pmax}$ was still valid when the power at a UE position varies, a simulation of the relative total sum of power differences (*tspd*) was accomplished in the form:

$$tspd = \frac{ts}{\max(ts)}; \qquad ts = \sum_{i=1}^{M} \left| P_{UEpi} - P_{UEHi} \right| \tag{3.2}$$

where P_{UEpi} and P_{UEHi} represent the maximum power level measured by the UE$_i$ using the algorithm 3.2 and the classical hierarchical method, respectively, for D=6:1:16; e_{pmax}=d_{DBr} =4,6,8m, DB_{res}=2(1.5)m for $\hat{a}_1$ and $\hat{a}_2$.

Figures 3.17, 3.18 and Table 3.3 show that the '*tspd*' in general increases up to a certain D after which it varies with a minimum value higher than the one corresponding to D=e_{pmax}. Moreover, the variation is not sufficiently large to get a benefit by increasing D further. The factor 'max(ts)' in (3.2) was inserted just to accentuate the maximum '*tspd*' values. In all cases the D value corresponding to the first maximum is larger than e_{pmax} at least in 25% for both areas $\hat{a}_1$ and $\hat{a}_2$, without much dependence on DB_{res}. One hundred twenty iterations were applied for each case (R4L30).

The variation in the received power can be due to a sudden partial blocking or deviation (reflection) of the signal power emitted by the BS. The final impact on the performance depends on the difference in the power received by the UE using each angle in the set G and the precision of the UE best angle determination accomplished directly through the sequence of power measurements.

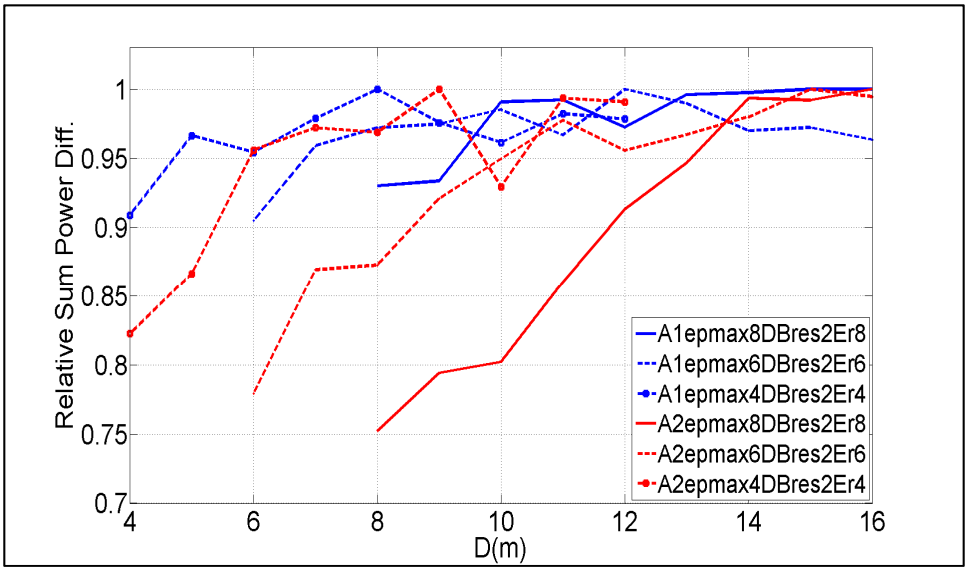

Figure 3.17 Relative sum of power difference versus D for $\hat{a}_1, \hat{a}_2$. DB_{res}=2m

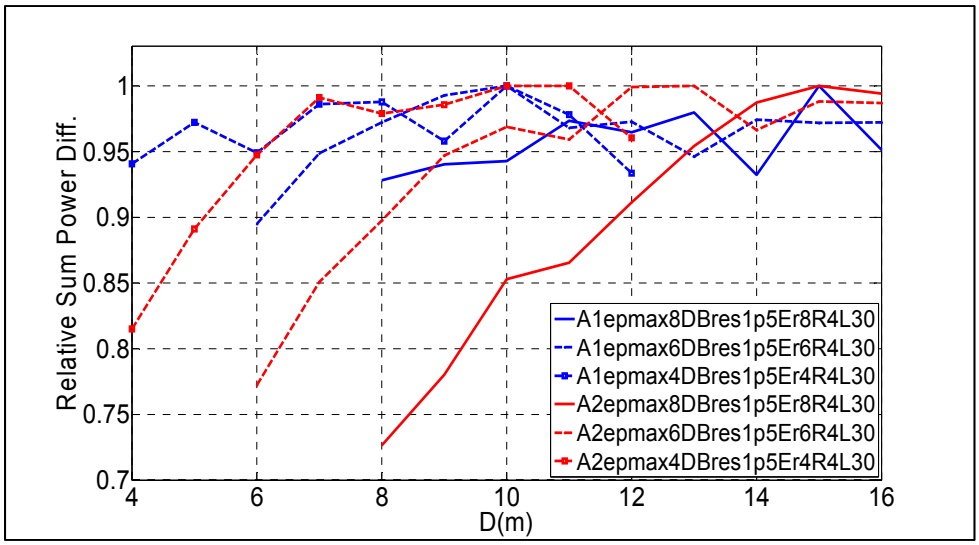

Figure 3.18 Relative sum of power difference versus D for $\hat{a}_1, \hat{a}_2$. DB_{res}=1.5m

Table 3.3 D value for the first maximum '*tspd*'

	D for first *'tspd'* maximum value				
	e_{pmax}	$D(\hat{a}_1)$	$D(\hat{a}_1) > e_{pmax}$	$D(\hat{a}_2)$	$D(\hat{a}_2) > e_{pmax}$
DB_{res} 2m	8	11	38%	14	75%
	6	10	67%	11	83%
	4	5	25%	7	75%
	e_{pmax}	$D(\hat{a}_1)$	$D(\hat{a}_1) > e_{pmax}$	$D(\hat{a}_2)$	$D(\hat{a}_2) > e_{pmax}$
DB_{res} 1.5m	8	11	38%	15	88%
	6	10	67%	10	67%
	4	5	25%	7	75%

3.5 Conclusions

The results from ray tracing simulations in the 28 GHz band indicate that the use of a database can become a resource for a faster antenna lock-on even for the case of non-exact knowledge of the position of a user. In this chapter it is proposed an algorithm that outperforms a modified classical hierarchical procedure in the number of steps and provides

the advantage of an initial larger power for antenna alignment as long as the exact position is located inside the circular area of DB points (radius *D*) around the non-exact position reported by the UE. A practical setting is the use of a *D* value slightly larger than the accuracy of the positioning system. In any case, such value is larger than the accuracy of the positioning system at least in 25%. The specific-site simulations with different position errors up to 10 m and database resolutions indicate that the DB point separation can be increased up to a distance of 2 m without impacting performance considerably. This result relaxes the database resolution requirements to a size that could be easily managed with current computation capabilities. The results show consistency under a random variation of the power levels at the UE.

CHAPTER 4

TAKING ADVANTAGE OF A SECOND PROPAGATION PATH AT 28 GHz UNDER NLOS CONDITIONS

4.1 Introduction

Exploiting more than one of the propagation paths existent in a NLOS communication link whether to increase its reliability or the total capacity is a topic of interest. Research studies include (An et al. 2009) in which two beam switching mechanisms that resolve blockage in the 60 GHz was proposed. In (Tsang and Poon, 2011), it was studied a successive AoA estimation algorithm to reveal a second propagation path (60 GHz) that could be applied to protect the link in case of human blocking. In (Sun et al., 2013), it was shown through field measurements in New York City at 28 GHz that a potential reduction of around 28.1 dB (22.2 dB) in the path loss could be obtained when 4 separate beams were combined coherently (non-coherently). Recent work considered the use of hybrid beamforming to estimate the channel (28 GHz) that facilitated a communication link with more than one data flux, but with the application of many RF chains at the BS and UE sides (Alkhateeb et al., 2014), (Chiang et al., 2016).

As observed in previous chapters, the application of directional antennas at both sides of the link at millimeter frequencies poses many challenges. The identification of the first path using an exhaustive search with only one beam may take a large number of steps and consequently it would be impractical to apply such scheme to search a second path. On the other hand, the classical hierarchical alignment method is focused only on aligning the BS and UE antennas in the main first direction without any attempt to exploit additional paths.

A database with mmW propagation information of the environment in which the system is deployed provides an alternative to exploit a second propagation path. The database can be linked to the position of the user which can be passed to the BS using a separate communication layer working at a lower frequency band. Such method can be practical under NLOS conditions at 28 GHz considering that on average there are 2.5 paths between the Tx

and Rx (Azar et al., 2013; Samimi et al., 2013). Additional related studies to (Capone, et al., 2015, 2016), (Di Taranto, et al., 2014) and (Degli-Esposti, et al., 2014) already considered in previous chapters is that of (Abbas et al., 2016) in which it is shown that analog beamforming with channel information (position of the mobile station) can result in a lower energy consumption and that of (Ferrante, et al., 2015) in which it was studied the effects of the steerable links have on network access, particularly in the presence of UE rotational motion.

In this chapter, we expand our previous work presented in chapter 3 and expand the application of a site-specific propagation characteristics knowledge to increase the link capacity. Given that a DB can have information of most main propagations paths existing at a specific location, the BS can also instruct the UE to take advantage of a second path if such inclusion becomes an advantage (i.e., the total capacity associated with two paths is higher than that of the main path alone).

Through 3D RT simulations in three specific areas, it is shown that a proposed algorithm determines in advance a viable second propagation path for a total capacity increase even in the case of the knowledge of an inexact position of the user. The inaccurate information reported by the UE forces the selection of a reference point in the DB to identify the angles of the second path. Such operation would be trivial if the position of the user was known exactly together with the initial (random) UE antenna angle, that is, the initial direction the UE antenna is pointing to at the moment of the reported position. Given that such is not generally the case, a more elaborated procedure is needed. The total number of alignment steps is kept lower than that compared of a modified hierarchical classical procedure used as a reference.

The remainder of the chapter is organized as follows. Section 4.2 describes the system model and simulation methodology. A description of proposed algorithm is treated in Section 4.3 whereas in Section 4.4 it is considered its performance. Finally, concluding remarks are highlighted in section 4.5.

4.2 System model and simulation methodology

4.2.1 System model

Consider the same one sector TDD cellular system of figures 3.1 and 3.2, operating at 28 GHz in a specific urban environment where the predominant RF propagation corresponds to a street canyon type. A third area $\hat{a}_3$ is considered for the study (Figure 4.1). The system is composed of a Tx and UEs (44, 100 and 39) arbitrarily located at NLOS positions within the three small areas $\hat{a}_1$ (25mx25m), $\hat{a}_2$ (23mx32m) and $\hat{a}_3$ (25mx25m), respectively. The BS has a DB information of 2,652, 2,944 and 3,025 points uniformly distributed in $\hat{a}_1$, $\hat{a}_2$ and $\hat{a}_3$. The DB points are separated 0.5 m (database resolution DB_{res}). Particularly, the DB information includes the average power level received at each point for every combination of the BS and UE angles in which both sides of the link use 10^o horn antennas. Additionally, the BS knows the geographical position of the UE with a maximum error e_{pmax} relative to its exact location. The user position information is assumed to be reported periodically to the BS through the help of a separate control layer using a lower frequency band.

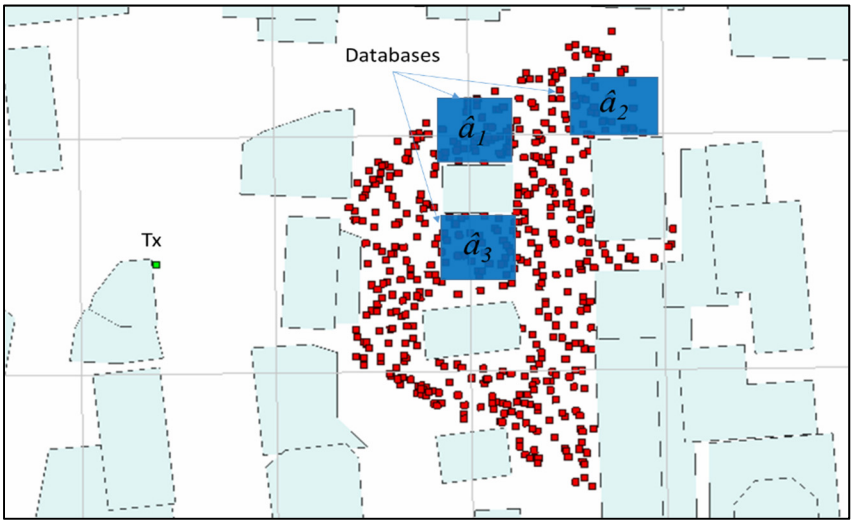

Figure 4.1 Cellular system

4.2.2 Simulation methodology

The same methodology followed in section 3.2.2 is applied in this chapter, except that both BS and UE can now use up to 2 RF chains.

4.3 Proposed method

Given that a DB has information of most BS and UE angle combinations associated to a geographical position, we propose an algorithm that increases the link capacity exploiting a second propagation path even in the case of an inaccurate position information. Such resource is effectively applied only if the total link capacity was higher than that obtained exclusively with the first path.

The algorithm initially uses the technique proposed in Chapter 3 to determine the best BS and UE angle combination (θ^{b}_{1BS},θ^{u}_{1UERUE}) of the first path. For this study, we assume that the UE also feedbacks the approximate UE angle ($\theta^{u}_{2sUERUE}$) of the second path appearing when the BS illuminates the user with θ^{b}_{1BS}. The UE angles θ^{u}_{1UERUE} and θ^{u}_{2UERUE} do not include θ_{UEinit} (random physical rotation).

For simplicity, we name as beam b_1 the combination of beams used in the BS and UE pointing in the direction of a specific propagation path (e.g. b_1 uses θ^{b}_{1BS} and θ^{u}_{1UERUE}, Figure 4.1). The second path can be exploited at least in the following two cases:

- The UE uses two angles with the BS angle (θ^{b}_{1BS}). The second beam (b_2 or b_3) can be located in the first lobe or in a separate lobe (figure 4.1). Such configuration can be applied to increase the total power in a coherent or non-coherent scheme (Sun and Rappaport, 2013). Appendix VIII shows the result of different power signal combinations.

- Both BS and UE use two angles (θ^{b}_{1BS}, θ^{b}_{2BS}) and (θ^{u}_{1UERUE}, θ^{u}_{2UERUE}) intended for two data fluxes serving the same UE (beams b_1 and b_4, separate power lobes). The BS-Tx power is shared in the illumination of the two propagation paths. That sharing can be accomplished as a simple power split[9] or 'water filling' method to maximize the link capacity at the intended UE location (Goldsmith, 2005). Appendix VIII shows the rules and parameters applied to identify the second strongest (separate) power lobe.

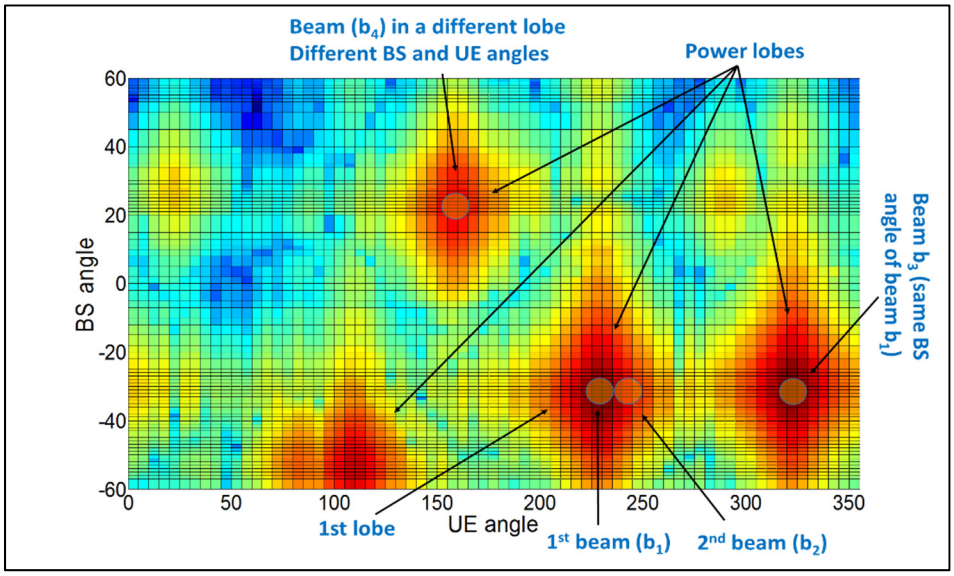

Figure 4.2 Propagation power lobes at a specific location

In chapter 3, the best BS and UE angles ($\theta^{b}_{1BS}, \theta^{u}_{1UERUE}$) associated to the first path were determined at the UE side based on measurements of the power received from the BS using a group of 3 pre-selected angles (set G). Only θ^{b}_{1BS} was reported back. Such information is not sufficient to identify the main angles of the second beam from the DB. The latter task is not straightforward because: 1) the BS does not know the exact location of the UE; 2) there are many neighbor locations to the UE which are best served by the same θ^{b}_{1BS} but with a different UE angle and 3) the BS does not know θ_{UEinit}. Note that θ^{u}_{1UERUE} is the best angle

[9] In (Degli-Esposti et al., 2014) it is considered that the simple splitting of the Tx-Power works better to cope human blocking to the communication links at 60 GHz

determined by the UE relative to its own spatial reference but this is arbitrarily displaced in $\theta_{UEinit.}$

A key step consists to work only with the *M* DB points (set *H*) located inside a circular area åDB of radius *D* ($\gtrsim e_{pmax}$) around the reported inexact position and then select the M_a points (set *F*) according to the following conditions:

$$\theta_{1BS}^{b} - \frac{bwth}{2} < \theta_{1BSDB}^{b} < \theta_{1BS}^{b} + \frac{bwth}{2} \quad (4.1)$$

$$\Delta\theta_{UERUE} - \frac{3*bwth}{2} < \Delta\theta_{UEDB} < \Delta\theta_{UERUE} + \frac{3*bwth}{2} \quad (4.2)$$

where θ_{1BSDB}^{b} is the best BS angle of the first power lobe in the DB, $\Delta\theta_{UERUE} = \theta_{1UERUE}^{u} - \theta_{2sUERUE}^{u}$, and $\Delta\theta_{UEDB} = \theta_{1UERUEDB}^{u} - \theta_{2sUERUEDB}^{u}$. $\theta_{1UERUEDB}^{u}$ and $\theta_{2sUERUEDB}^{u}$ are the UE main angles of the first and second lobe associated to θ_{1BSDB}^{b} that are registered in the DB. The adopted conditions decrease the number of DB point candidates in the selection of the reference point. Condition (4.2) was considered because the application of a 30º antenna in the measurements may displace the angle of the second maximum power level in more than 10 degrees relative to the angle saved in the DB and calculated using 10º beamwidth antennas.

Some of the M_a points may have the same or similar angles of the second beam compared to the one at the UE location but with a different degree of visibility in terms of power levels. The closer the selected DB reference point is to the exact position of the UE, the larger that visibility in terms of power levels. To further reduce the number of DB points, the M_a DB points are ordered in accordance to the maximum power ($p_{w1db} > p_{w2db} > \ldots > p_{wMadb}$) the UE would receive at each of these positions when its antenna is rotated 360º in 5º steps.

$$[\boldsymbol{q}'''']_{M_a\,x\,1}; \quad q_i'''' = \mathrm{p_{widb}} = \max_{\theta_{1BS}^{b}}[P_{i,0^o}, P_{i,5^o}, \ldots\ldots, P_{i,355^o}]; \quad i=1,2,\ldots.,M_a \quad (4.3)$$

$$\boldsymbol{q}''''^{ord} = \underset{descend}{\mathrm{sort}}(\boldsymbol{q}'''') \quad (4.4)$$

We name *criteria 1* the case where the DB point selected has the highest power level p_{w1db} (i.e. the power level $\boldsymbol{q}''''^{ord}(1)$). An alternative is the *criteria 2* in which the DB point

selected belongs to the top percent (p_{erc}) of the ordered M_a points (set F_{sp}) and is closest to the geographical center of all M_a–DB points. Figure 4.3 illustrates the sets H, F and F_{sp}.

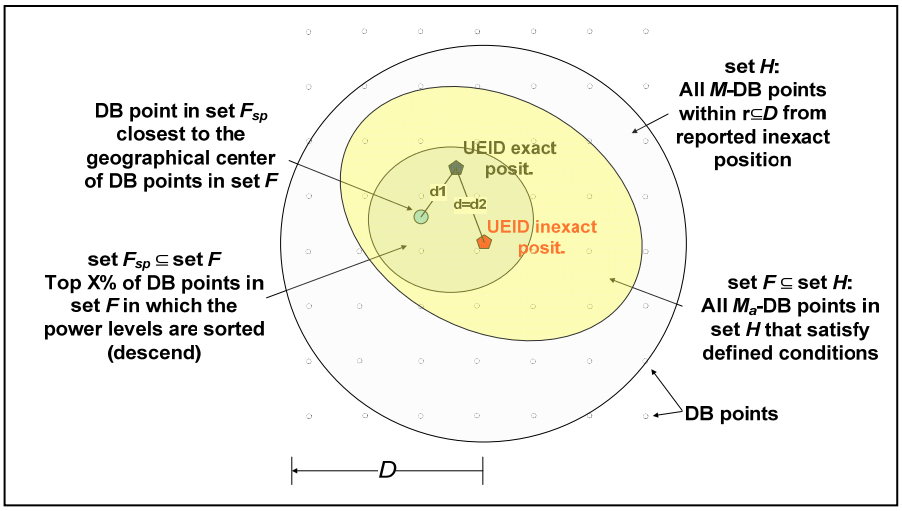

Figure 4.3 Database points used by the proposed algorithm

The selection of the DB point closest to the center of F was adopted because the BS does not know the position of the UE. Simulation results (Figures 4.4 and 4.5) show the advantage of *criteria* 2 over *criteria* 1, where X_{EP}, X_{RP}, X_{BDcr1}, X_{DBcr2} are the geographical positions of the exact, reported (inexact) and of the DB point obtained with *criteria 1* and *2*, respectively, and $\Delta d_1 = \|X_{EP}-X_{DBcr2}\|_2 - \|X_{EP}-X_{BDcr1}\|_2$. The Prob($\Delta d_1 \leq 0$)=0.62, 0.75, 0.60 in $\hat{a}_1$, $\hat{a}_1$, $\hat{a}_3$, respectively, for D=10m, e_{pmax}=8m, DB_{res}=0.5m.

The statistics reveal the DB point selected using *criteria 2* is statistically closer to the exact UE location than the point selected with *criteria 1*. The top fraction p_{erc} (system design factor) of the ordered DB points in set F was determined using the proposed algorithm and testing the percentage of DB ordered points (power) that maximized the total capacity. p_{erc}=20% and 5% were obtained for areas $\hat{a}_1$ (Figure 4.5) and $\hat{a}_3$, respectively, whereas the simulation for area $\hat{a}_2$ did not provide such information.

The simulation was accomplished using 50 iterations of the UEs for every 5% increase in the number of DB points and DB_{res}=0.5m, D=10m, e_{pmax}=8m. A random θ_{UEinit} and an

inaccurate position X_{RP} were applied for the UEs in each iteration. The total capacity was calculated using waterfilling.

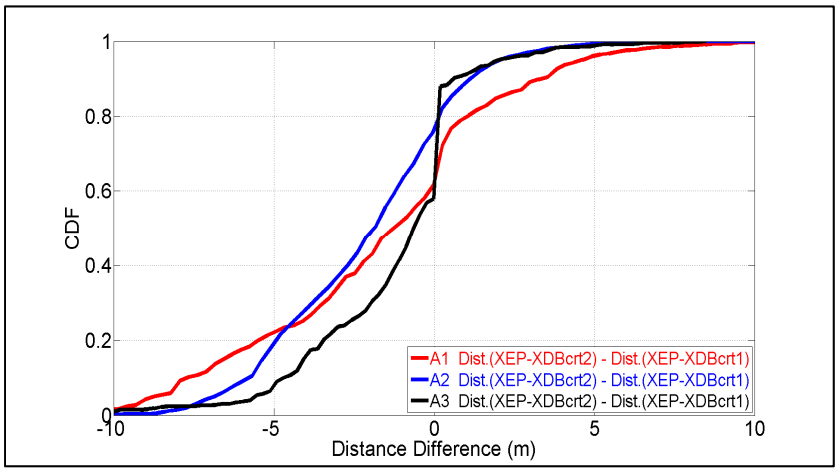

Figure 4.4 Statistics of $\Delta d = dist(X_{DBcr2}\text{-}X_{EP}) \text{-} dist(X_{BDcr1}\text{-}X_{EP})$ in $\hat{a}_1$ and $\hat{a}_2$

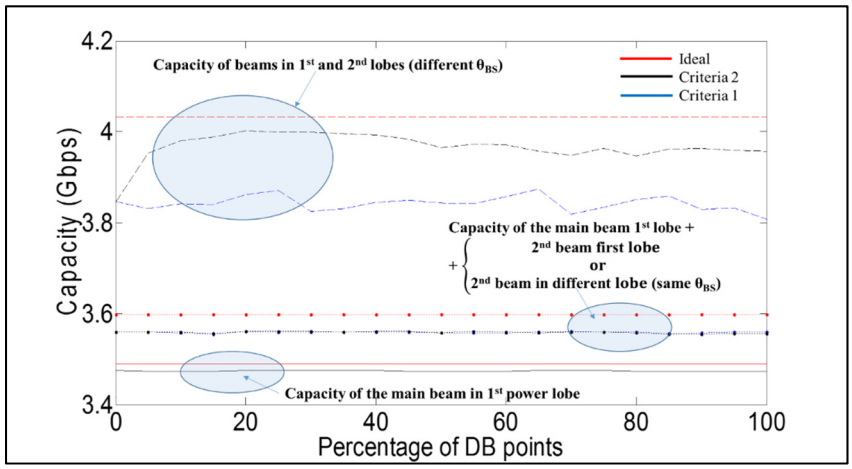

Figure 4.5 ($\hat{a}_1$) Capacity vs percentage of DB points in ordered set F.
DB_{res}=0.5m, D=10m, e_{pmax}=8m

The total capacity difference benefit depended on the area (i.e., viable second power lobes for capacity increase). The plots in red color correspond to the ideal case of a BS with knowledge of the exact position of the UE. Similarly, the plots in black (blue) represent the case of a BS with knowledge of an inexact position of the UE and chooses the reference DB

point based on *criteria 2* (*criteria 1*). The proposed algorithm 4.1 developed under *criteria* 2 is detailed as follows:

Algorithm 4.1 Capacity increase using a second propagation path

1 BS receives $\theta_{1BS}^{b}, \theta_{1UERUE}$ and $\theta_{2sUERUE}$ from the UE

2 BS determines the 'reference' power curve.

a. BS identifies all M_a BD points (set F) in H ($F \subseteq H$) based on the conditions:

- $\theta_{1BS}^{b} - \frac{bwth}{2} < \theta_{1BSDB}^{b} < \theta_{1BS}^{b} + \frac{bwth}{2}$
- $\Delta\theta_{UERUE} - \frac{3*bwth}{2} < \Delta\theta_{UEDB} < \Delta\theta_{UERUE} + \frac{3*bwth}{2}$

b. BS orders the M_a points in set F according to the maximum power received ('descending') and select the first '*perc*' value (group F_{sp})

$p_{wj} = \max_{\theta_{1BS}^{b}} (\mathrm{P}_{j;0^\circ}, \mathrm{P}_{j,5^\circ}, \ldots, \mathrm{P}_{j;355^\circ})$; j=1,2,3,.., M_a.

$\boldsymbol{p_F} = \left[p_{w_1}, p_{w_2}, \ldots p_{w_{M_a}}\right]^T = \underset{descend}{\mathrm{sort}}\left(p_{w^1}, p_{w^2}, \ldots, p_{w^{M_a}}\right)$

$\boldsymbol{p_{F_{sp}}} = \boldsymbol{p_F}(1{:}\,k, 1)$; $k = \lceil p_{erc}\ \mathrm{card}(\boldsymbol{p_F}) \rceil$

c. BS selects the point in F_{sp} that is geographically closest to the mean of coordinates in set F.

3 BS determines from the power lobe distribution of the selected DB point:

a. The best θ_{2BS}^{b} and θ_{2UERBS} based on defined rules and parameters;

b. The best θ_{1UERBS} (relative to the BS reference) in which the maximum power occurs using θ_{1BS}^{b};

c. $\Delta\theta_{UE}$=θ_{2UERBS}-θ_{1UERBS}; θ_{UEInit}=θ_{1UERBS}-θ_{1UERUE};

4 BS instructs the UE with the angle offset $\Delta\theta_{UE}$ in the direction of a second power lobe based on the following decision criteria:

a. Same BS angle θ_{1BS}^{b}

Decision: $\max_{C_{2b}}(C_1 + C_{2b})$;

C_1=$C(snr_{1(main\ beam)})$; C_{2b}=$C(snr_{2(2ndbeam,sameBSangle)})$;

$C_1 = (\beta B')\ \log_2(1 + snr_1)$; $C_{2b} = (\beta B')\ \log_2(1 + snr_2)$;

UE directs the 2nd antenna in the direction $\theta_{2UERUE}^{u} = \theta_{1UERUE}^{u} + \Delta\theta_{UE}$;

b. Different BS angles θ_{1BS}^{b} and θ_{2BS}^{b}.

Decision: $C_{1*}+C_{2c} \geq C_1$;

$C_{1*}+C_{2c} = \max_{P_i:\sum_i P_i \leq P} \sum_{i=1}^{2} (\beta B') \log_2(1 + x_i snr_i) \geq C_1 = B \log_2(1 + snr_1)$;

$\sum_{i=1}^{2} x_i = 1$; $x_i = \frac{P_i}{P}$;

BS applies θ_{2BS}^{b} and the UE directs the 2nd antenna in the direction $\theta_{2UERUE}^{u} = \theta_{1UERUE}^{u} + \Delta\theta_{UE;}$ if applicable.

5 If $\left[\left(\theta_{1BS}^{b} \neq \theta_{2BS}^{b}\right)\&\left(\mathrm{C_T^{UE2d}} < \mathrm{C_T^{UE1d}}\right)\right]$, the UE discards the second path possibility and communicates accordingly to the BS so that it applies full power to first path.

where C represents capacity, $C_1=C(snr_{mainbeam})$ is the link capacity applying the signal-to-noise-ratio (SNR) obtained with b_1 (θ_{1BS}^{b}), $C_{2b}=C(snr_{2beam,sameBSangle,1st\ lobe})$ is the capacity obtained using b_2 (or b_3) whether in the first or separate lobe (same θ_{1BS}^{b}). C_{1*} is the fraction of the capacity associated to the first path when the power sharing is applied. $C_{2c}=C(snr_{2ndlobe,differentBSandUEangles})$ is the capacity calculated applying beam b_4 (θ_{2BS}^{b}) located in a separate lobe. snr_1 is the SNR associated to the i^{th} channel at full power (Goldsmith, 2015) and x_i is the fraction of the total transmitter power assigned to each path. The factor β=(0.5)(0.8) is multiplied to the bandwidth B' in order to account for a TDD operation and 20% control overhead (Barati et al., 2014). If the condition 4b is not met, the link can still work with two RF fronts under the condition 4a; otherwise, both the BS and UE applies one RF front only.

The algorithm 4.1 distinguishes the two exclusive cases considered. In the first one (4a), the BS uses the single angle θ_{1BS}^{b}, whereas the UE applies the second RF chain either to an angle separated at least '$bwth$' degrees (10^o) from θ_{1UERUE}^{u} or in the direction of a separate second power lobe (>10^o), whichever provides the maximum partial capacity The total capacity is obtained as the non-coherent sum of the power levels received by the two UE RF chains. Clearly, the UE can be commanded to test autonomously the power levels at $\theta_{2sUERUE}^{u}, \theta_{1UERBS}-10^o, \theta_{1UERBS}+10^o$ and decide which one is higher to apply the second RF front. However, this procedure would require additional steps compared to that in which the DB commands the UE with the new path information.

In the second case (4b), the decision to exploit a second data flux depends on the estimation of the total capacity obtained using one versus two RF fronts at both BS and UE sides, that is, on which combination delivers more power to the UE. Water-filling power sharing was applied. The condition $\sum_{i=1}^{2} B\log_2(1+x_i snr_i) \geq B\log_2(1+snr_1)$ is equivalent to $\frac{snr_1}{1+x_1 snr_1} \leq snr_2 \leq snr_1$ (Appendix VIII).

Given that the UE has the power measurement values using one path (full BS-Tx power and link capacity C_T^{UE1d}) and two paths (water filling and total link capacity C_T^{UE2d}), it can

evaluate the BS instruction to apply a second path. In case of a non-acceptance, the UE feedbacks that decision to the BS in order to keep the link with just one path.

Figure 4.6 shows the values of the SNR*s* for which the condition $C_{1*}+C_{2c} > C_1$ is satisfied using water-filling. The SNR_1 and its difference relative to SNR_2 determine the viability of the second path. As an example, if SNR_1=10dB, then unless $SNR_2 - SNR_1 \leq 10$dB, it is not worth to search a second path. Such result indicates that not necessarily the presence of a second lobe guarantees it can always be applied for a total capacity increase.

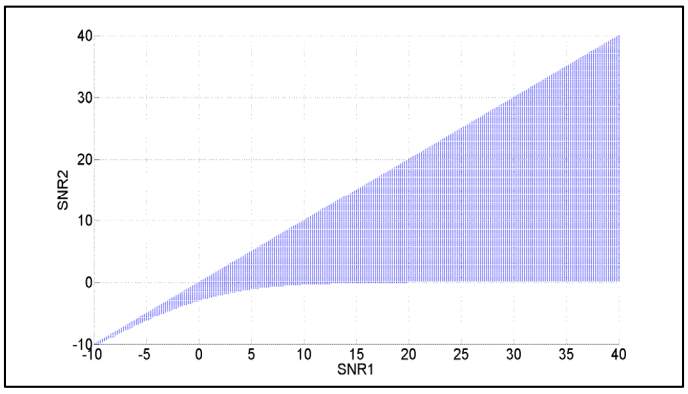

Figure 4.6 Values of of SNR_1 and SNR_2 that satisfy $C_{1*}+C_{2c} \geq C_1$ (waterfilling)

Figure 4.7 shows the DB points with which the algorithm 4.1 operates. The figure is divided into four separate groups in which each one (top to bottom) represents the geographical positions; the best BS and UE (DB point) angle combinations of the first path and; the power lobe distribution, respectively. The exact position X_{EP} of the UE is represented as a small red square, the inexact position X_{RP} reported by the UE as a green square and the DB points in $å_{DB}$ as black dots. The colored dots (background) in Figures 4.7a,b,c,d correspond to the best BS angles for each point in the DB**.** Figure 4.7e show the best angle combination (first path) of the UE with X_{EP} (red) and X_{RP} (green), and of the DB points (black) in $å_{DB}$ centered at $X_{EP.}$ Figure 4.7i shows the propagation power lobes at the exact UE location. Note that although there are many DB points, the number of angles combination pairs is relatively small because of angle repetition. Given that the BS in reality knows X_{RP}, Figures 4.7b,f,j show the corresponding graphs already indicated but relative to this inaccurate position.

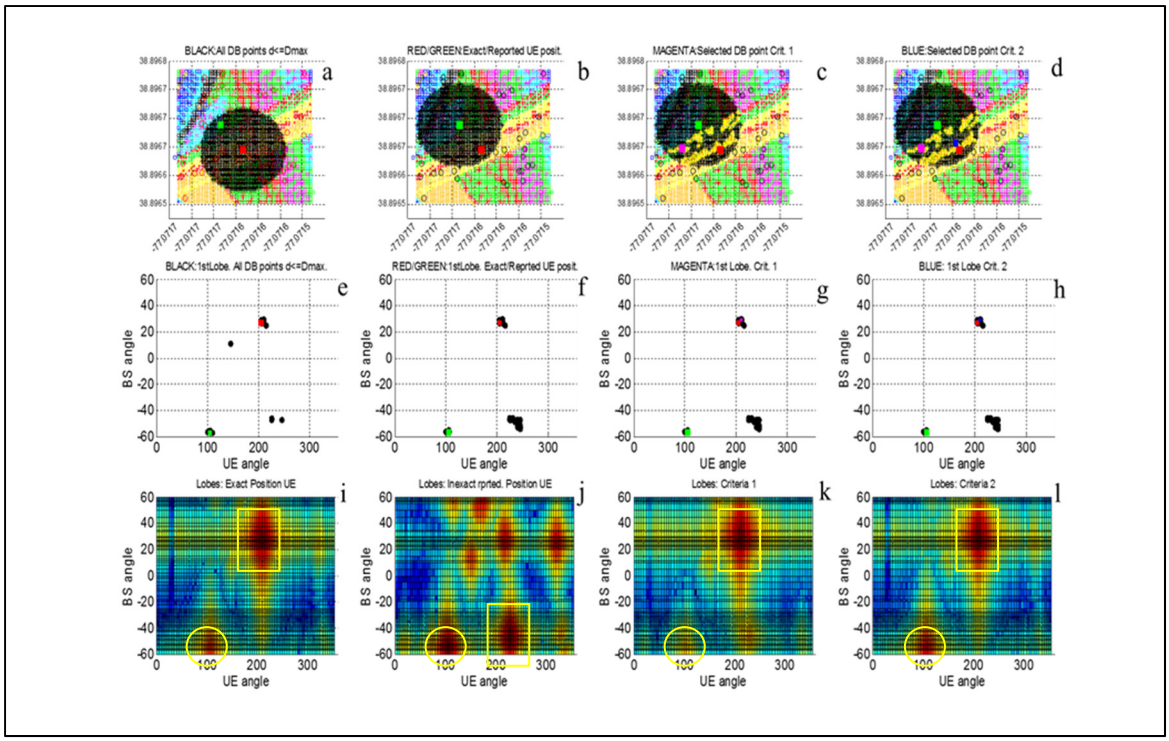

Figure 4.7 BS-UE angle combinations for all DB points in åDB ($\hat{a}_1$)

A DB information based on an erroneous position may lead the BS to direct its main beam to a power lobe different from the most powerful one (figures 4.7e-4.7f and 4.7i-4.7j). Figures 4.7c and 4.7d show additionally the reference DB points selected based on *criteria 1*, *criteria 2* (magenta, blue squares) and the DB points (yellow) that have θ_{1BS}^{b} as its best serving BS angle. Figure 4.7k and 4.7l shows the power lobe distribution of such selected reference DB points, respectively. Figure 4.7l shows a clearer second lobe compared to figure 4.7k.

4.4 Algorithm performance

4.4.1 Static case

Figures 4.8, 4.9 and 4.10 show the performance of the algorithm 4.1 (solid black) for DB_{res}=2m, e_{pmax}=8m and D=10m in areas $\hat{a}_1$, $\hat{a}_2$ and $\hat{a}_3$, respectively. The capacity associated to the main beam in the first lobe is plotted in magenta; the combination of the main and

second beam (same BS angle, first or different lobe) is plotted in blue and the main and second beam (different BS angles) in black. The solid and dashed lines represent the capacity determined using the knowledge of the inexact and exact position of the user, respectively. The capacity (first path) calculated applying directy the inexact position information without any processing (red dashed curve) provided the worst performance.

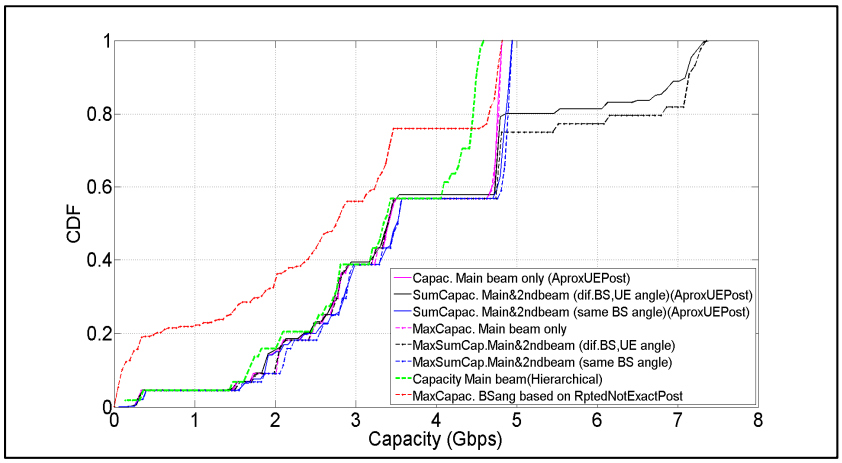

Figure 4.8 ($\hat{a}_1$) Performance of algorithm 4.1. PercBDPoints=20%, DB_{res}=2m, D=10m, e_{pmax}=8m

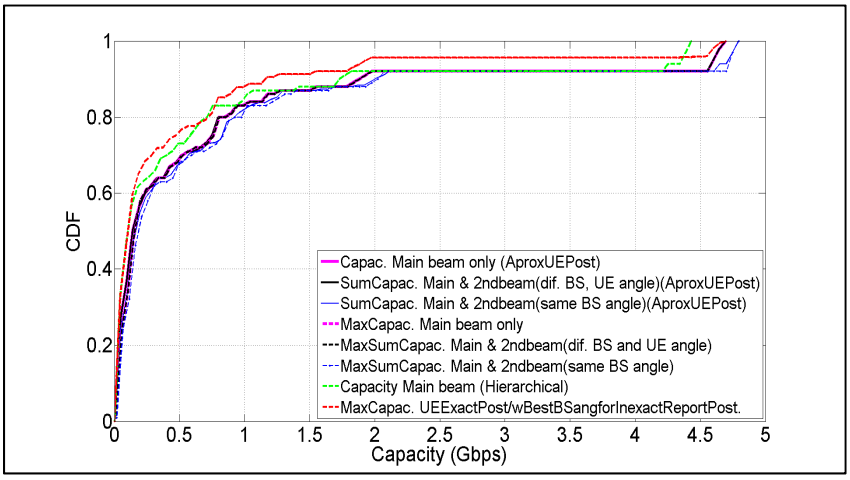

Figure 4.9 ($\hat{a}_2$) Performance of algorithm 4.1. PercBDPoints =20%, DB_{res}=2m, e_{pmax}=8m, D=10m

The figures show a capacity gain (two paths) of more than 2 Gbps relative to the main path only. Clearly, there are more viable second paths in area $\hat{a}_1$ and $\hat{a}_3$ than in $\hat{a}_2$; the latter with lower SNR values. A smaller capacity gain is obtained from the non-coherent power sum of the two beams that have the same BS main angle (solid and dashed blue). As a reference, the Figures 4.8 and 4.9 also show the capacity obtained using a modified classical hierarchical method (green)

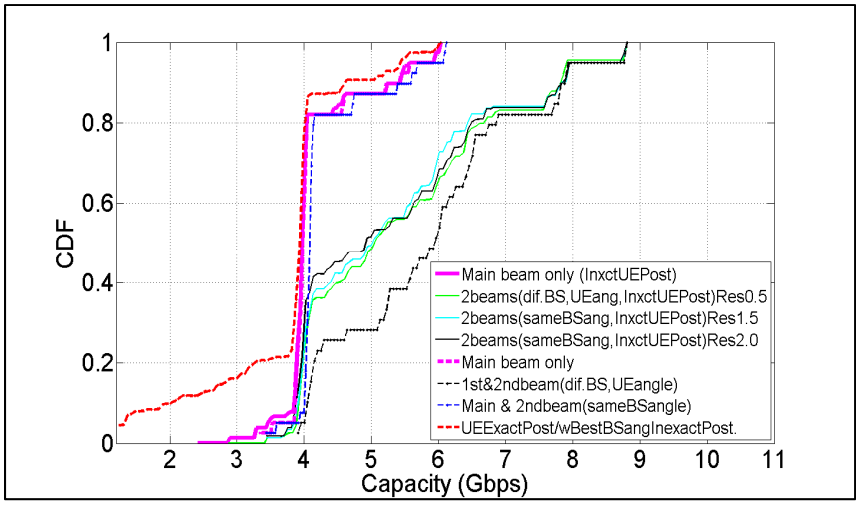

Figure 4.10 ($\hat{a}_3$) Performance of algorithm 4.1. PercBDPoints =5%, DB_{res}=2m (1.5m, 0.5m), D=10m, e_{pmax} =8m

Table 4.1 shows the capacity (average) gain comparison as D and DB_{res} vary in $\hat{a}_1$ without considering the capacity contribution of the main beam. The value of D was set to a value 20% larger than e_{pmax}. The average capacity gain (Gbps) shown corresponds to the second beam using a different or the same BS angle of the first beam, respectively. For the different BS angle case and fixed D, the additional capacity decreases (small slope) with a lower DB_{res} up to 3 m. The slope becomes more pronounced for the DB_{res} between 3 and 4. On the other hand, for a DB_{res}=0.5m,1m,1.5m and 2m, the additional capacity basically does not change with D. Such results were expected since the combination of an appropriate value of D ($\geq e_{pmax}$) and DB resolution provide sufficient DB points in $\mathring{a}_{DB}$ for the operation of the algorithm. The algorithm takes advantage of the repetition of the best BS and UE angles in

the neighborhood of the UE. For a lower DB resolution, the algorithm becomes less predictive.

Table 4.1 Additional average link capacity - second beam, different/same BS angle. Different DB_{res} and D (> e_{pmax})

		DB_{res}					
		0.5 m	**1 m**	**1.5 m**	**2 m**	**3 m**	**4 m**
e_{pmax}	**6 m**	0.5171/0.1048	0.4701/0.1017	0.4898/0.1048	0.4560/0.1015	0.4540/0.1036	0.4251/0.0923
	7 m	0.5229/0.1066	0.5157/0.1050	0.4829/0.1086	0.4425/0.1041	0.4783/0.1062	0.4597/0.0941
	8 m	0.5235/0.1082	0.5150/0.1070	0.5199/0.1085	0.4613/0.1061	0.4857/0.1057	0.4331/0.0949
	9 m	0.5435/0.1077	0.5239/0.1068	0.5091/0.1080	0.4830/0.1061	0.4669/0.1077	0.4074/0.0974
	10 m	0.5421/0.1084	0.5240/0.1081	0.5333/0.1088	0.4872/0.1062	0.4551/0.1092	0.3604/0.0964

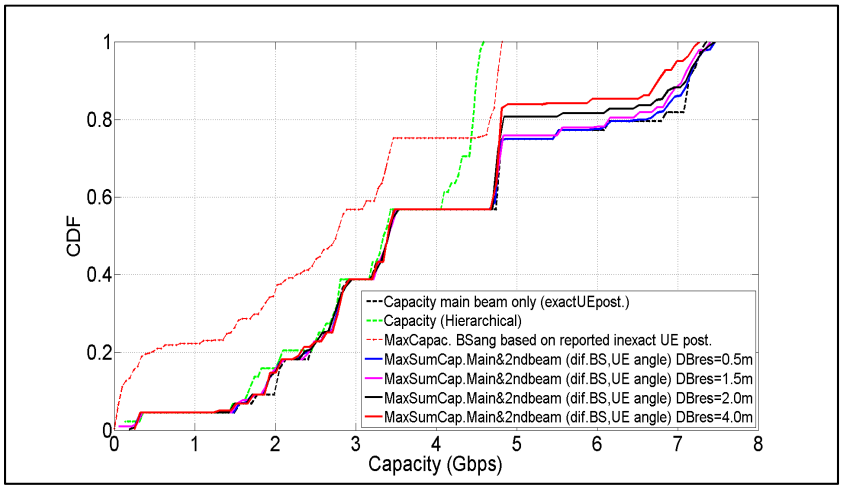

Figure 4.11 ($\hat{a}_1$) Performance of algorithm 4.1. PercBDPoints =20%, DB_{res}=0.5m,1.5m,2.0m,4.0m. D=10m, e_{pmax} =8m

For the case of a second beam using the same BS angle of the first beam, the additional capacity (on average) decreases also slightly with DB_{res} and mostly does not vary with D. The power value in the proximity of the main lobe is normally larger than that of a separate lobe so the performance of the algorithm in this part depends on the correct detection of the first lobe. Figures 4.10 and 4.11 show a performance comparison for different DB_{res} in $\hat{a}_3$ and $\hat{a}_1$, respectively.

4.4.2 Random variation of the maximum received power

To evaluate the algorithm under non-static conditions we generate a channel variation by replacing the power-angle profile $f(\theta_{BS}^{b}, \theta_{UE})$ at the position of the UE with that corresponding to a DB point randomly located within a circular area of radius E_r around X_{EP}. Figures 4.12, 4.13 and 4.14 show the algorithm performance (black line) in $\hat{a}_1$, $\hat{a}_2$ and $\hat{a}_3$, respectively, for the particular settings of D=10m, e_{pmax}=8m, DB_{res}=2m and E_r=8m.

A UE located within $\hat{a}_1$ can receive a power level variation up to 10 dB. The maximum possible SNR at the UE under static conditions is also plotted for reference purposes (dashed red line). The power variation of that magnitude at the UE basically does not have impact on the algorithm performance. The benefit of the second RF front is maintained. The capacity calculated using the inexact position information is also plotted (red slotted-asterisk line) for reference purposes.

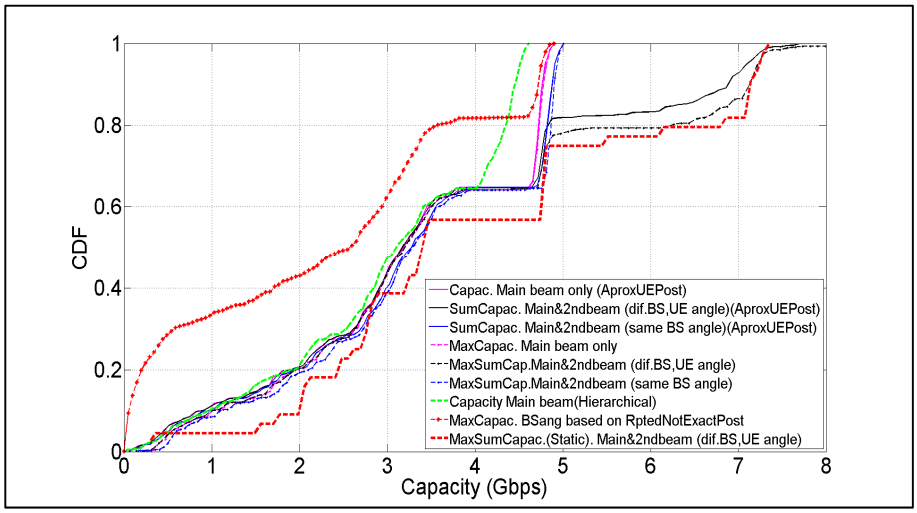

Figure 4.12 ($\hat{a}_1$) Performance of algorithm 4.1. PercBDPoints=20%, DB_{res}=2m, D=10m, e_{pmax}=8m, E_r=8m

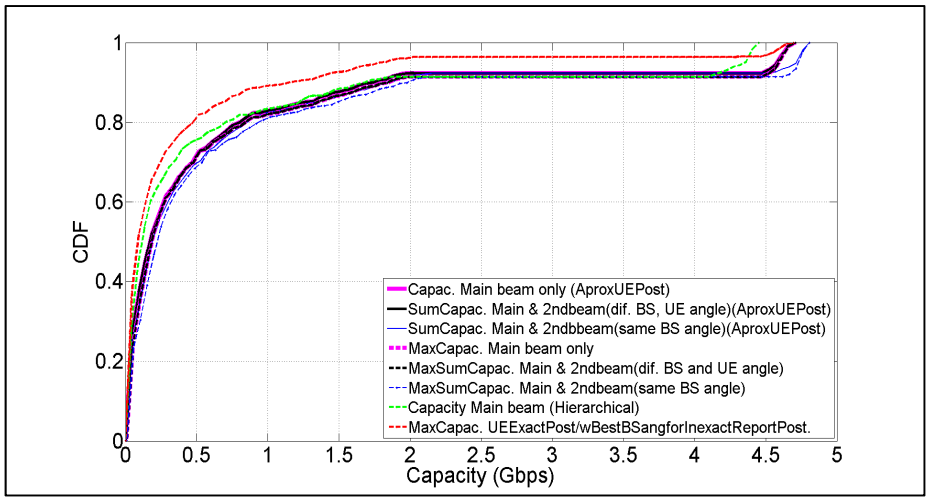

Figure 4.13 ($\hat{a}_2$) Performance of algorithm 4.1. PercBDPoints=20%, DB_{res}=2m, D=10m, e_{pmax}=8m, E_r=8m

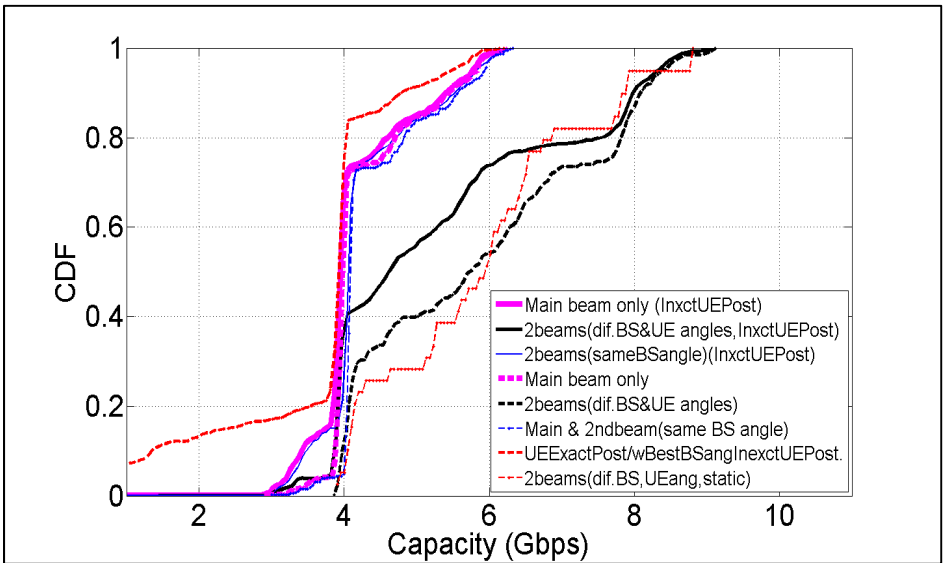

Figure 4.14 ($\hat{a}_3$) Performance of algorithm 4.1. PercBDPoints=5%, DB_{res}=2m, D=10m, e_{pmax}=8m, E_r=8m

Once the UE feedbacks the best BS and UE angles, the BS processes the information extracted from the DB and instructs the UE with the angle offset $\Delta\theta_{UE}$ necessary to align the second beam. Three to five additional steps would be required at the UE side to identify the main angle of the second path after the beam alignment of the first path. In that case, the

maximum total number of steps would reach the value of 32 (=26+6), which is still lower compared to the modified classical hierarchical alignment method (Table 3.2). Note that these additional steps are only necessary whenever the second RF front is applied.

4.5 Conclusions

Ray tracing simulations in the 28 GHz band indicate that the use of a database linked to the location of a user can be applied advantageously to increase the total link capacity by exploiting a second propagation path even in the case of an inexact position information. A modified algorithm that identifies a neighbor DB point with an angle power distribution of similar characteristics to that existing at the UE position is proposed for the determination of the new set of second best BS-UE angles and an advanced assessment of the potential link capacity benefit. The application of $D \gtrsim e_{pmax}$ and a DB resolution up to 1.5 m allow the algorithm to approximate the total capacity obtained when the BS knows the exact position of the user. Because only one additional step is needed for the BS to communicate the UE on the viability of the second path, the duration of an alignment procedure based on database information still demands a smaller total number of steps compared to the modified classical hierarchical method that can identify the approximate best propagation path only. The algorithm outcomes are sustained when the power level at the UE is varied.

CONCLUSION

Millimeter bands have become strong candidates to provide 5G cellular services. It is expected that their potential larger spectrum availability can meet the ever increasing capacity demand that have saturated current microwave bands. The inherent large propagation path loss associated to mmW carrier frequencies impose high gain antennas (directional) at both sides of the link which introduces many challenges especially at NLOS locations. Research efforts have been devoted to field measurements, channel modeling and estimation using analog and hybrid beamforming. The latter technique is applied as an alternative to digital beamforming which, although the best option, becomes too costly in terms of the number of Digital to Analog Converters required. Compressed sensing techniques used with analog or hybrid beamforming show promising results but more research is still needed for locations with a low SNR. The hierarchical antenna alignment method already standardized in the 60 GHz band needs a redesign for its application in the 28 GHz band to cope with the larger propagation path loss.

One line of research that has not been fully explored in mmW bands is to exploit the knowledge of the propagation characteristics of a specific site. This information can be stored in a database linked to the position of a user but it cannot be applied directly at least for the following two reasons: 1) the geographical position reported by the user normally has an error that must be considered in the determination of the best BS and UE angles (even a moderate position error can generate a large impact in the received power); 2) there is an initial random rotation of the UE antenna that cannot be registered in the database.

Results from ray tracing simulations in the 28 GHz band presented in chapter 2 indicated that a prior knowledge of the RF illumination efficacy of some discrete BS angles to deliver the maximum power possible at NLOS locations can be exploited in a directional search. This knowledge is beneficial especially for the cases where the BS and UE apply analog beamforming. It is shown that a performance gain of more than 2 dB can be accomplished

when both the BS and UE switch their antenna beam orientations randomly in a defined period of time but this result depends on:

- The street canyon propagation severity. The larger the street canyon condition, the lower the number of the best BS angles needed for the NLOS locations, that is, more positions use the same best BS angles.
- The probability of the angle use. A larger performance gain is obtained when the angles are selected using a non-uniform CDF related to the RF coverage. The CDFs are based on the unequal percentage of positions served by the best BS and UE angles within the service area.

A larger average power at the user locations reduces the number of steps needed in an antenna alignment. The approximate identification of the best BS angles is accomplished using a proposed RT procedure. The subset of the best angles reduces the extension of the database needed for the service area.

The algorithm 3.2 introduced in chapter 3 shows that a user position-dependent database can be applied successfully for RF illumination even in the case of a reported inexact UE position or under a moderate variation of the received power level. This result is obtained as long as the exact-positioned UE is located within the circular area of database points around the inexact position. Moreover, it is found that there is not much performance impact if the radius of the considered circular area is set a little larger that the accuracy of the GPS. The algorithm takes advantage of the repetition of the best BS angles in the circular area of database points considered. Given that the UE can experience a random rotation not registered in the database, the algorithm 3.2 allows the UE to find its best angle (antenna beam) based on a sequence of power level measurements. The proposed hierarchical-like antenna alignment scheme provides the benefit of a larger initial antenna gain and a lower number of antenna alignment steps than that obtained from a modified classical hierarchical method considered for comparison.

An extension of the previous algorithm is presented in chapter 4 where the database information is applied to exploit a second propagation path to increase the total capacity of the link based on defined rules. For this part the BS needs to determine the random initial rotation of the UE so that it can identify a reference DB point to approximate the main angles associated with the second path. Two criteria are explored for the determination of the reference point.

FUTURE WORK

The research work addressed the problem of how to exploit propagation characteristics to improve a communication link for a user that reports periodically its inexact location. Some questions that contribute for further research on the topic of this thesis are:

- How to apply site-specific propagation cognition to a mobile user? Is it possible to determine the periodicity of the position report based on a prediction of the future location of the user?
- Can a database application be helpful to overcome the potential link intermittency that may be present in outdoors communication using mmW frequency carriers? Is it worth to apply two RF chains both at BS and UE for link reliability purposes? Is it possible to quantify the blocking effect of moving cars and persons?
- Is it possible to exploit the propagation characteristics of a site in the compressed sensing techniques to cope with the need of more BS transmitter power at NLOS positions of the user?
- What is the benefit of a (mmW) database application in a multiuser system?

APPENDIX I

DISTRIBUTION FUNCTION OF MAXIMUM POWER IN *L* READINGS

Assumptions:

- User located at position x from BS
- For each discrete BS angle θ_{iBS} there is only one MPC arriving at the UE with an amplitude $\tilde{A}_i$ and AoA equal to $\theta_{UEalign}$.
- The gain of the UE antenna $Y=g_u(\theta^\Delta)$ has the form shown in Fig. 2.4 (equation 2.1) where $\theta^\Delta = (\theta_{UEalig} - \theta_{UE}) \sim U(-\pi, \pi]$ is the UE azimuth angle difference between $\theta_{UEalign}$ and an arbitrary UE antenna orientation. θ^Δ takes values according to a uniform distribution in (-π,π].

Distribution and Density function of UE antenna gain - $g_u(\theta^\Delta)$

The CDF $F_Y(y)$ can be calculated (Papoulis, 2002) as:

$$\boldsymbol{y < 0} \quad F_Y(y) = 0 \tag{A I-1a}$$

$$\boldsymbol{y \geq 1} \quad F_Y(y) = P\{g_u(\theta^\Delta) \leq y\} = 1 \tag{A I-1b}$$

$$\boldsymbol{0 \leq y < 1} \quad F_Y(y) = P\{g_u(\theta^\Delta) \leq y\} = 2P\{\theta^\Delta > \theta_a\} = 2P\left\{\theta^\Delta > \frac{y-b}{m}\right\}$$

$$F_Y(y) = 1 + \frac{1}{\pi}\left[2y\left(\theta_{3dB}^\Delta - \theta_a^\Delta\right) - \left(2\theta_{3dB}^\Delta - \theta_a^\Delta\right)\right] \tag{A I-1c}$$

$$F_Y(0) = 1 - \frac{1}{\pi}\left(2\theta_{3dB}^\Delta - \theta_a^\Delta\right) = 1 - \frac{\theta_b^\Delta}{\pi} \tag{A I-1d}$$

where we applied the following relations obtained from Fig. 2.4:

$$\frac{1/2}{\left(\theta_{3dB}^\Delta - \theta_a^\Delta\right)} = \frac{1}{\theta_b^\Delta - \theta_a^\Delta} \tag{A I-2}$$

$$y = m\theta^\Delta + b = -\frac{\theta^\Delta}{\theta_b^\Delta - \theta_a^\Delta} + \frac{2\theta_{3dB}^\Delta - \theta_a^\Delta}{2\left(\theta_{3dB}^\Delta - \theta_a^\Delta\right)} \tag{A I-3}$$

and:

$$2P\left\{\theta^{\Delta} > \frac{y-b}{m}\right\} = \frac{2}{2\pi}\left(\pi - \frac{y-b}{m}\right) = 1 - \frac{1}{\pi}\left(\frac{y - \frac{2\theta^{\Delta}_{3dB} - \theta^{\Delta}_{a}}{2\left(\theta^{\Delta}_{3dB} - \theta^{\Delta}_{a}\right)}}{-\frac{1}{\theta^{\Delta}_{b} - \theta^{\Delta}_{a}}}\right) \quad \text{(A I-4)}$$

Taking the first derivative of (A I-1) and using (A I-2), the Probability Density Function (PDF) of y becomes (Figure-A I-1):

$$f_Y(y) = \left(1 - \frac{\theta^{\Delta}_{b}}{\pi}\right)\delta(y) + \left(\frac{\theta^{\Delta}_{b} - \theta^{\Delta}_{a}}{\pi}\right)\mathrm{rect}(y - 1/2) + \frac{\theta^{\Delta}_{a}}{\pi}\delta(y-1) \quad \text{(A I-5)}$$

where $\mathrm{rect}(v) = \begin{Bmatrix} 1 & |v| \le 1/2 \\ 0 & |v| > 1/2 \end{Bmatrix}$ and $\delta(y)$ is an impulse function

Distribution function of an individual UE power reading $F_{\mathbf{z}}(z)$

If the BS uses θ_{iBS} with $p_{\theta_{iBS}}$ and the maximum possible power level (UE and BS with their antenna beams aligned) at a UE located at x=x$_i$ is a random variable $\tilde{A}$ taking values from the set $\{\tilde{A}_1, \tilde{A}_2, \dots, \tilde{A}_i, .., \tilde{A}_N\}$ with Prob($\tilde{A}_i$)=Prob(θ_{iBS}), then the CDF of the power Z = $\tilde{A}$ $g_u(\theta^{\Delta})$ read by the UE for any antenna orientation is computed (Papoulis, 2002) as:

$$F_z(z) = \int_0^{\infty}\int_0^{\frac{z}{w}} f_W(w)\, f_y(y) dw dy \quad \text{(A I-6)}$$

where: $f_W(w) = \sum_i p_{\tilde{A}_i}\, \delta\left(w - \tilde{A}_i\right)$ (A I-7)

$\tilde{A}$, $g_u(\theta^{\Delta})$ are considered independent random variables.

Replacing (A I-5) in (A I-6), we obtain:

$$F_Z(z) = \int_0^{\infty} p_{\tilde{A}_1}\, \delta\left(w - \tilde{A}_1\right)\int_0^{\frac{z}{w}} f_Y(y) dy dw + \int_0^{\infty} p_{\tilde{A}_2}\, \delta\left(w - \tilde{A}_2\right)\int_0^{\frac{z}{w}} f_Y(y)\, dy dw + \cdots$$

$$\dots\dots + \int_0^{\infty} p_{\tilde{A}_N}\delta\left(w - \tilde{A}_N\right)\int_0^{\frac{z}{w}} f_Y(y)\, dy dw\,. \quad \text{(A I-8)}$$

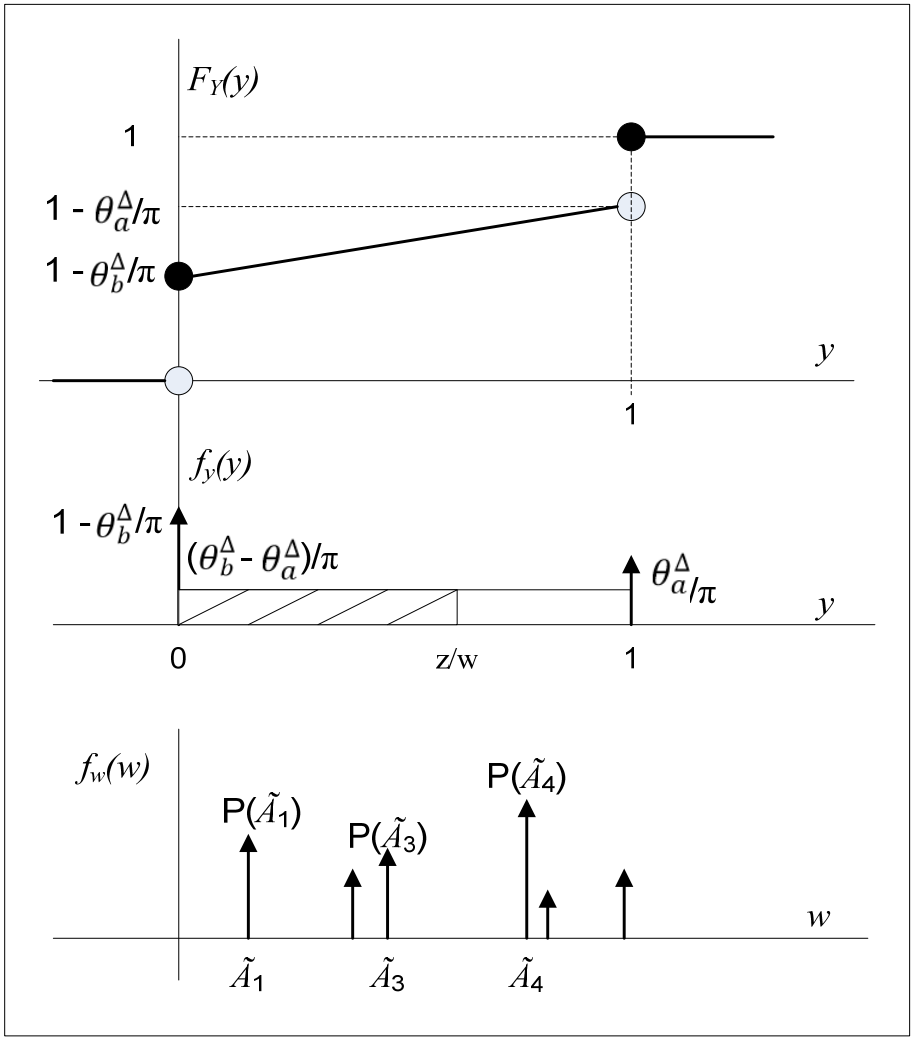

Figure-A I-1 CDF and PDF of $y=g_u(\theta^{\Delta})$.

The first term exists only for $w=\tilde{A}_1$. A similar condition applies for the remaining terms. $F_Z(z)$ is explicitly calculated as :

For $z < \tilde{A}_1$:

For this case, $f_Y(y)$ in the first term of (A I-8) does not include the impulse $\frac{\theta_a^{\Delta}}{\pi}\delta(y-1)$ because this term is different from zero only for $w=\tilde{A}_1$ and $z < \tilde{A}_1$, which results in $y=z/w<1$. The same applies for the remaining terms, given that $\tilde{A}_1<\tilde{A}_2<\tilde{A}_3<\ldots<\tilde{A}_N$.

$$F_Z(z) = \int_0^{\infty} p_{\tilde{A}_1}\,\delta(w-\tilde{A}_1)\left[\left(1-\frac{\theta_b^{\Delta}}{\pi}\right)+\left(\frac{\theta_b^{\Delta}-\theta_a^{\Delta}}{\pi}\right)\frac{z}{w}\right]dw +$$

$$+\int_0^{\infty} p_{\tilde{A}_2}\,\delta(w-\tilde{A}_2)\left[\left(1-\frac{\theta_b^{\Delta}}{\pi}\right)+\left(\frac{\theta_b^{\Delta}-\theta_a^{\Delta}}{\pi}\right)\frac{z}{w}\right]dw +\ldots.$$

$$\ldots..+\int_0^{\infty} p_{\tilde{A}_N}\,\delta(w-\tilde{A}_N)\left[\left(1-\frac{\theta_b^{\Delta}}{\pi}\right)+\left(\frac{\theta_b^{\Delta}-\theta_a^{\Delta}}{\pi}\right)\frac{z}{w}\right]dw$$

$$F_Z(z) = \left(1-\frac{\theta_b^{\Delta}}{\pi}\right)+\left(\frac{\theta_b^{\Delta}-\theta_a^{\Delta}}{\pi}\right)z\left[\sum_{i=1}^{N}\frac{p_{\tilde{A}_i}}{\tilde{A}_i}\right] \qquad \text{(A I-9)}$$

For $\tilde{A}_1 \le z < \tilde{A}_2$

$f_Y(y)$ in the first term of (A I-8) must include the second impulse component $\frac{\theta_a^{\Delta}}{\pi}\delta(y-1)$ because $z/w>1$. For the remaining terms, $z/w<1$, then:

$$F_Z(z) = p_{\tilde{A}_1} + \int_0^{\infty} p_{\tilde{A}_2}\,\delta(w-\tilde{A}_2)\int_0^{\frac{z}{w}}\left[\left(1-\frac{\theta_b^{\Delta}}{\pi}\right)\delta(y)+\left(\frac{\theta_b^{\Delta}-\theta_a^{\Delta}}{\pi}\right)\mathrm{rect}(y-1/2)\right]dydw +$$

$$+\cdots\ldots\ldots\ldots\ldots..+$$

$$+\int_0^{\infty} p_{\tilde{A}_N}\,\delta(w-\tilde{A}_N)\int_0^{\frac{z}{w}}\left[\left(1-\frac{\theta_b^{\Delta}}{\pi}\right)\delta(y)+\left(\frac{\theta_b^{\Delta}-\theta_a^{\Delta}}{\pi}\right)\mathrm{rect}(y-1/2)\right]dydw.$$

$$F_Z(z) = p_{\tilde{A}_1} + \sum_{i=2}^{N} p_{\tilde{A}_i}\left[\left(1-\frac{\theta_b^{\Delta}}{\pi}\right)+\left(\frac{\theta_b^{\Delta}-\theta_a^{\Delta}}{\pi}\right)\frac{z}{\tilde{A}_i}\right], \quad \text{and}$$

$$F_Z(z) = \left(1-\frac{\theta_b^{\Delta}}{\pi}\right)+\left(\frac{\theta_b^{\Delta}}{\pi}\right)p_{\tilde{A}_1}+\left(\frac{\theta_b^{\Delta}-\theta_a^{\Delta}}{\pi}\right)z\left[\sum_{i=2}^{N}\frac{p_{\tilde{A}_i}}{\tilde{A}_i}\right]. \qquad \text{(A I-10)}$$

For $\tilde{A}_2 \le z < \tilde{A}_3$

$$F_Z(z) = \left(1-\frac{\theta_b^{\Delta}}{\pi}\right)+\left(\frac{\theta_b^{\Delta}}{\pi}\right)\left(p_{\tilde{A}_1}+p_{\tilde{A}_2}\right)+\left(\frac{\theta_b^{\Delta}-\theta_a^{\Delta}}{\pi}\right)z\left[\sum_{i=3}^{N}\frac{p_{\tilde{A}_i}}{\tilde{A}_i}\right]. \qquad \text{(A I-11)}$$

……..

In general, for $\tilde{A}_{j-1} \le z < \tilde{A}_j$,

$$F_Z(z) = \left(1-\frac{\theta_b^{\Delta}}{\pi}\right)+\left(\frac{\theta_b^{\Delta}}{\pi}\right)\sum_{i=1}^{j-1}p_{\tilde{A}_i}+\left(\frac{\theta_b^{\Delta}-\theta_a^{\Delta}}{\pi}\right)z\left[\sum_{i=j}^{N}\frac{p_{\tilde{A}_i}}{\tilde{A}_i}\right]. \qquad \text{(A I-12)}$$

For $z \ge \tilde{A}_N$, $F_Z(z) = 1$ because all terms in (A I-8) include the second impulse $\frac{\theta_a^{\Delta}}{\pi}\delta(y-1)$.

For simplicity of notation, the equation (A I-12) includes the case of j=1. We assume the first summation $\sum_{i=1}^{j-1} p_{\tilde{A}_i}$=0 and $\tilde{A}_0$=0 although this power level does not exist.

Distribution Function of the maximum power in L readings - $F_z(z)$

If Z_i was the power obtained at the UE location in one reading, then the CDF of the maximum power level $\hat{Z} = \max[Z_1 \quad Z_2 \ldots\ldots \quad Z_L]$ obtained in L independent readings corresponds to the $F_{\hat{Z}}(\hat{z}) = F_{Z1}(\hat{z})F_{Z2}(\hat{z}) \ldots F_{Zi}(\hat{z}) \ldots F_{ZL}(\hat{z})$ where each $F_{Z_l}(\hat{z})$ is given by (A I-12).

Statement 1:

If $\boldsymbol{F_Z^{(1)}(z)}$ and $\boldsymbol{F_Z^{(2)}(z)}$ are the CDFs of z using $\boldsymbol{p_{\tilde{A}_i}^{(1)} = \frac{1}{N}; \quad i = 1, 2, 3, \ldots\ldots, N;}$ and $\boldsymbol{p_{\tilde{A}_i}^{(2)} = \begin{cases} 0 & i = 1, 2, 3, \ldots . n_0 \\ \frac{1}{N - n_0}; & i = n_0 + 1, n_0 + 2, \ldots\ldots, N \end{cases}}$, respectively, then $\boldsymbol{F_Z^{(1)}(z) \geq F_Z^{(2)}(z)}$

Proof:

Replacing $C_1 = \left(1 - \frac{\theta_b^{\Delta}}{\pi}\right), \quad C_2 = \left(\frac{\theta_b^{\Delta}}{\pi}\right)$ and $C_3 = \left(\frac{\theta_b^{\Delta} - \theta_a^{\Delta}}{\pi}\right)$ in (A I-12), then

for j=1,2,3,…..,n_0

$$F_Z^{(1)}(z) = C_1 + C_2 \sum_{i=1}^{j-1} p_{\tilde{A}_i}^{(1)} + C_3 z \left[\sum_{i=j}^{N} \frac{p_{\tilde{A}_i}^{(1)}}{\tilde{A}_i}\right]; \quad F_Z^{(2)}(z) = C_1 + 0 + C_3 z \left[\sum_{i=n_0+1}^{N} \frac{p_{\tilde{A}_i}^{(2)}}{\tilde{A}_i}\right]$$

$$\Delta F_Z^{(1,2)} = F_Z^{(1)}(z) - F_Z^{(2)}(z) = C_2 \sum_{i=1}^{j-1} p_{\tilde{A}_i}^{(1)} + C_3 z \left[\sum_{i=j}^{N} \frac{p_{\tilde{A}_i}^{(1)}}{\tilde{A}_i}\right] - C_3 z \left[\sum_{i=n_0+1}^{N} \frac{p_{\tilde{A}_i}^{(2)}}{\tilde{A}_i}\right]$$

$$\Delta F_Z^{(1,2)} = C_2 \sum_{i=1}^{j-1} p_{\tilde{A}_i}^{(1)} + C_3 z \left[\sum_{i=j}^{n_0} \frac{p_{\tilde{A}_i}^{(1)}}{\tilde{A}_i} + \sum_{i=n_0+1}^{N} \frac{p_{\tilde{A}_i}^{(1)}}{\tilde{A}_i}\right] - C_3 z \left[\sum_{i=n_0+1}^{N} \frac{p_{\tilde{A}_i}^{(2)}}{\tilde{A}_i}\right]$$

$$\Delta F_Z^{(1,2)} = C_2 \left(\frac{j-1}{N}\right) + \frac{C_3 z}{N} \left[\sum_{i=j}^{n_0} \frac{1}{\tilde{A}_i} - \frac{n_0}{(N - n_0)} \sum_{i=n_0+1}^{N} \frac{1}{\tilde{A}_i}\right]$$

$$\Delta F_Z^{(1,2)} = \frac{C_3}{N} \left[\frac{C_2}{C_3}(j-1) + z \left(\sum_{i=j}^{n_0} \frac{1}{\tilde{A}_i} - \frac{n_0}{(N - n_0)} \sum_{i=n_0+1}^{N} \frac{1}{\tilde{A}_i}\right)\right]$$

Applying the lower and upper bound to the second and third terms, respectively:

$\Delta F_Z^{(1,2)} = \frac{C_3}{N}\left[\frac{C_2}{C_3}(j-1) + z\left(\frac{n_0-j+1}{\tilde{A}_{n_0}} - \frac{n_0}{\tilde{A}_{n_0+1}}\right)\right] = \frac{C_3}{N}\left[(j-1)\left(\frac{C_2}{C_3} - \frac{z}{\tilde{A}_{n_0}}\right) + zn_0\left(\frac{1}{\tilde{A}_{n_0}} - \frac{1}{\tilde{A}_{n_0+1}}\right)\right]$

The first term $\left(\frac{C_2}{C_3} - \frac{z}{\tilde{A}_{n_0}}\right) > 0$ since $\frac{C_2}{C_3} > 1$ and for any $j \leq n_0$, $\frac{z}{\tilde{A}_{n_0}} < 1$ given that $\tilde{A}_{j-1} \leq z < \tilde{A}_j$; the second term $\left(\frac{1}{\tilde{A}_{n_0}} - \frac{1}{\tilde{A}_{n_0+1}}\right) > 0$, since $\frac{1}{\tilde{A}_{n_0}} > \frac{1}{\tilde{A}_{n_0+1}}$ assuming $\tilde{A}_1 < \tilde{A}_2 < \tilde{A}_3 < \ldots < \tilde{A}_N$, then $F_Z^{(1)}(z) - F_Z^{(2)}(z) \geq 0$

for $j = n_0 + 1, n_0 + 2, \ldots\ldots, N$

$F_Z^{(1)}(z) = C_1 + C_2\left[p_{\tilde{A}_1}^{(1)} + p_{\tilde{A}_2}^{(1)} + \cdots + p_{\tilde{A}_{j-1}}^{(1)}\right] + \frac{C_3 z}{N}\left[\sum_{i=j}^{N}\frac{1}{\tilde{A}_i}\right]$

$F_Z^{(1)}(z) = C_1 + C_2\left(\frac{(j-1)-1+1}{N}\right) + \frac{C_3 z}{N}\left[\sum_{i=j}^{N}\frac{1}{\tilde{A}_i}\right]$;

$F_Z^{(2)}(z) = C_1 + C_2\left[p_{\tilde{A}_{n_0+1}}^{(2)} + p_{\tilde{A}_{n_0+2}}^{(2)} + \cdots + p_{\tilde{A}_{j-1}}^{(2)}\right] + C_3 z\left(\frac{1}{N-n_0}\right)\left[\sum_{i=j}^{N}\frac{1}{\tilde{A}_i}\right]$

$F_Z^{(2)}(z) = C_1 + C_2\left(\frac{(j-1)-(n_0+1)+1}{N-n_0}\right) + C_3 z\left(\frac{1}{N-n_0}\right)\left[\sum_{i=j}^{N}\frac{1}{\tilde{A}_i}\right]$

$\Delta F_Z^{(1,2)} = C_2\left(\frac{j-1}{N}\right) + \frac{C_3 z}{N}\left[\sum_{i=j}^{N}\frac{1}{\tilde{A}_i}\right] - C_2\left(\frac{j-n_0-1}{N-n_0}\right) + C_3 z\left(\frac{1}{N-n_0}\right)\left[\sum_{i=j}^{N}\frac{1}{\tilde{A}_i}\right]$

$\Delta F_Z^{(1,2)} = \frac{n_0}{N(N-n_0)}\left[C_2(N-j+1) - C_3 z\left(\sum_{i=j}^{N}\frac{1}{\tilde{A}_i}\right)\right]$

using the upper bound in the second term:

$\Delta F_Z^{(1,2)} \geq \frac{n_0}{N(N-n_0)}\left[C_2(N-j+1) - C_3 z(N-j+1)\frac{1}{\tilde{A}_j}\right]$

$\Delta F_Z^{(1,2)} \geq \frac{n_0(N-j+1)}{N(N-n_0)} C_3\left(\frac{C_2}{C_3} - \frac{z}{\tilde{A}_j}\right) \geq 0$ for any $j > n_0$ and $\tilde{A}_{j-1} \leq z < \tilde{A}_j$

Statement 2:

If $F_Z^{(1)}(z)$, $F_Z^{(2)}(z)$ and $F_Z^{(3)}(z)$ are the CDFs of z using:

$p_{\tilde{A}_i}^{(1)} = \frac{1}{N}; \quad i = 1, 2, 3, \ldots\ldots, N; \qquad p_{\tilde{A}_i}^{(2)} = \begin{cases} 0 & i = 1, 2, 3, \ldots . n_0 \\ \frac{1}{N-n_0} & i = n_0+1, n_0+2, \ldots, N \end{cases}$, and

$p_{\tilde{A}_i}^{(3)} = \begin{cases} 0 & i = 1, 2, 3, \ldots, n_0+1 \\ \frac{1}{N-(n_0+1)} & i = n_0+2, n_0+3, \ldots, N \end{cases}$, respectively,

then $F_Z^{(1)}(z) - F_Z^{(3)}(z) \geq F_Z^{(1)}(z) - F_Z^{(2)}(z)$

Proof:

for j=1,2,3,…..,n_0

$$\Delta F_Z^{(1,2)} = C_2\left(\frac{j-1}{N}\right) + \frac{C_3 z}{N}\left[\sum_{i=j}^{n_0}\frac{1}{\tilde{A}_i} - \frac{n_0}{(N-n_0)}\sum_{i=n_0+1}^{N}\frac{1}{\tilde{A}_i}\right]$$

$$\Delta F_Z^{(1,3)} = C_2\left(\frac{j-1}{N}\right) + \frac{C_3 z}{N}\left[\sum_{i=j}^{n_0+1}\frac{1}{\tilde{A}_i} - \frac{n_0+1}{(N-n_0-1)}\sum_{i=n_0+2}^{N}\frac{1}{\tilde{A}_i}\right]$$

$$\Delta F_Z^{(1,3)} - \Delta F_Z^{(1,2)} = \frac{C_3 z}{N}\left(\left[\sum_{i=j}^{n_0}\frac{1}{\tilde{A}_i} + \frac{1}{\tilde{A}_{n_0+1}} - \frac{n_0+1}{(N-n_0-1)}\sum_{i=n_0+2}^{N}\frac{1}{\tilde{A}_i}\right] - \left[\sum_{i=j}^{n_0}\frac{1}{\tilde{A}_i} - \frac{n_0}{(N-n_0)}\frac{1}{\tilde{A}_{n_0+1}} - \frac{n_0}{(N-n_0)}\sum_{i=n_0+2}^{N}\frac{1}{\tilde{A}_i}\right]\right)$$

$$\Delta F_Z^{(1,3)} - \Delta F_Z^{(1,2)} = \frac{C_3 z}{N}\left(\left[\frac{1}{\tilde{A}_{n_0+1}} - \frac{n_0+1}{(N-n_0-1)}\sum_{i=n_0+2}^{N}\frac{1}{\tilde{A}_i}\right] + \left[\frac{n_0}{(N-n_0)}\frac{1}{\tilde{A}_{n_0+1}} + \frac{n_0}{(N-n_0)}\sum_{i=n_0+2}^{N}\frac{1}{\tilde{A}_i}\right]\right)$$

$$\Delta F_Z^{(1,3)} - \Delta F_Z^{(1,2)} = \frac{C_3 z}{N-n_0}\left[\frac{1}{\tilde{A}_{n_0+1}} - \frac{1}{(N-n_0-1)}\sum_{i=n_0+2}^{N}\frac{1}{\tilde{A}_i}\right]$$

Using the upper bound in the second term:

$$\Delta F_Z^{(1,3)} - \Delta F_Z^{(1,2)} = \frac{C_3 z}{N-n_0}\left[\frac{1}{\tilde{A}_{n_0+1}} - \frac{1}{\tilde{A}_{n_0+2}}\right] \geq 0$$

for j=n_0+1, n_0+2,…..,N

$$\Delta F_Z^{(1,3)} - \Delta F_Z^{(1,2)} =$$

$$= \frac{n_0+1}{N(N-n_0-1)}\left[C_2(N-j+1) - C_3 z\left(\sum_{i=j}^{N}\frac{1}{\tilde{A}_i}\right)\right] - \frac{n_0}{N(N-n_0)}\left[C_2(N-j+1) - C_3 z\left(\sum_{i=j}^{N}\frac{1}{\tilde{A}_i}\right)\right]$$

$$\Delta F_Z^{(1,3)} - \Delta F_Z^{(1,2)} = \left[\frac{n_0+1}{N(N-n_0-1)} - \frac{n_0}{N(N-n_0)}\right]\left[C_2(N-j+1) - C_3 z\left(\sum_{i=j}^{N}\frac{1}{\tilde{A}_i}\right)\right]$$

$$\Delta F_Z^{(1,3)} - \Delta F_Z^{(1,2)} = \frac{1}{(N-n_0)(N-n_0-1)}\left[C_2(N-j+1) - C_3 z\left(\sum_{i=j}^{N}\frac{1}{\tilde{A}_i}\right)\right]$$

$$\Delta F_Z^{(1,3)} - \Delta F_Z^{(1,2)} = \frac{1}{(N-n_0)(N-n_0-1)}\left[C_2(N-j+1) - C_3 z(N-j+1)\frac{1}{\tilde{A}_j}\right]$$

$$\Delta F_Z^{(1,3)} - \Delta F_Z^{(1,2)} = \frac{(N-j+1)}{(N-n_0)(N-n_0-1)} C_3\left[\frac{C_2}{C_3} - \frac{z}{\tilde{A}_j}\right] \geq 0$$

APPENDIX II

SPATIAL FILTERING ON PROPAGATION DATA

The best BS angles to illuminate users located within a defined service sector can be identified by applying data scanning to the propagation information obtained from the RT tool in which the BS and UE are equipped with a sector antenna (e.g. horn 60º) and isotropic antenna, respectively. Such simplified method saves much time compared to that using exclusively directional antennas with a small beamwidth.

Figure-A II-1 shows the BS power-angle profile at a specific UE for the cases of a BS equipped with a 10º directional antenna (yellow), 10º horn antenna (red), ULA-10 (dashed cyan), ULA-32 (solid cyan), URA-10x10 (solid green) in the range [-30º:1º:30º]. Additionally it shows the results of data scanning (using an ULA-10 (dashed black) and ULA-32 (solid black) of the RT result obtained when the BS and UE were equipped with a 60º directional and isotropic antenna, respectively.

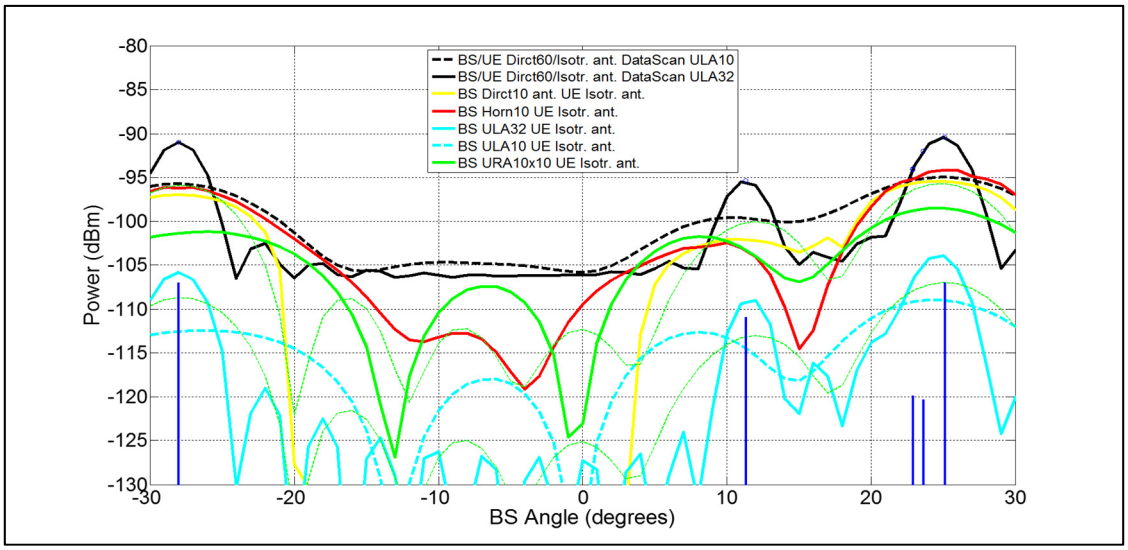

Figure-A II-1 BS angle-power profile for various BS antennas (UE with an isotropic antena).

The parameters of the ULA-N and URA-NxM were obtained from (Van Trees, 2002, chapters 2, 4). Table-A II-1 indicates the BS angles where a maximum power level occurs and the power levels. The BS angles corresponding to the two main propagation paths for each type of antenna are identified with blue color.

The application of an ULA-32 to scan the propagation data (BS and UE with directional and omnidirectional antennas, respectively) gives very good results in the identification of the first and second main BS antenna directions with an angle error less or equal than 1º in all cases. The direct selection of the best angle simply by inspection of the highest power of a particular MPC gives an angle precision error of around 5% of the cases compared to the value obtained through data scanning.

Table-A II-1 BS angle identification and UE power levels

BS antenna	**(BS) Tx Longitude: -77.0730068799 Tx Latitude: 38.8962065033 (UE) Rx Longitude: -77.0712819668 Rx Latitude: 38.8968777921 UE equipped with isotropic antenna**											
Direct10 (30dBm)	**-28º** -97.0								11º -102.1	17º -101.9	**25º** -95.4	
Horn10 (30dBm)	**-28º** -96.2				-9º -112.7			7º -113.4	10º -102.5		**26º** -94.2	
ULA32	**-28º** -105.8	-22º -119.0	-18º -122.5	-14º -124.7	-10º -126.3	-7º -126.8	-3º -126.8 0º -126.9	4º -126.5 7º -124.1	12º -109.0	16º -116.2	**25º** -103.9	30º -120.0
ULA16	**-28º** -108.7		-16º -121.6			-8º -125.0	0º -125.2		12º -113.0		**25º** -107.0	
ULA10		**-26º** -112.5				-6º -118.0		8º -112.6			**24º** -109.0	
URA 10x10 (30dBm)		**-26º** -101.2				-7º -107.4		8º -101.7			**24º** -98.5	
URA 16x16 (30 dBm)	**-28º** -95.9		-16º -108.8			-8º -112.3	0º -112.3		12º -100.0		**25º** -95.7	
BS angle identification (RT data scanning). Antennas: BS (60º horn), UE (isotropic)												
Data scan (ULA32)	**-28º** -91.0	-22º -102.5	-18º -104.8	-15º -105.6	-11º -105.86	-7º -106.1	-4º -106.1 -1º -106.1	2º -105.8 6º -104.6	11º -95.5	16º -103.5	**25º** -90.4	
Data scan (ULA10)	**-28º** -95.7				-10º -104.71				10º -99.6		**25º** -95.0	

APPENDIX III

BS ANGLE IDENTIFICATION

BS angle identification and comparison in setups 1 and 3

Table-A III-1 BS angle identification in setups 1 and 3

Set *A*		Set *B*		Set *A*		Set *B*	
Angle	**Prctg (%)**	**Angle**	**Prctg (%)**	**Angle**	**Prctg (%)**	**Angle**	**Prctg (%)**
		-58	0.20			-27	1.20
-57	0.88	-57	0.40			-26	0.40
-56	1.03	-56	3.60	-25	1.10	-25	0.20
-55	1.99	-55	4.00			-24	0.20
-54	6.03	-54	4.40	-18	2.98		
-53	4.49	-53	3.60			-17	0.20
-52	1.00	-52	0.80	11	0.22	11	0.20
-51	0.26	-51	0.80			12	0.20
-50	0.35	-50	0.60			19	0.40
-49	0.57	-49	0.60	20	0.05	20	2.60
-48	0.44			21	3.84	21	2.00
-47	2.69	-47	0.80	22	2.07	22	2.40
-46	2.85	-46	0.60	23	2.45	23	2.60
		-45	0.20	24	3.58	24	1.60
-43	0.01			25	4.09	25	4.80
-42	0.05			26	8.66	26	1.20
-41	0.03	-41	0.20	27	0.70	27	3.00
-40	1.93			28	0.89	28	4.40
-39	0.06	-39	1.60	29	0.73	29	1.00
-38	0.08			30	0.06	30	2.00
-37	0.06					32	0.20
-36	0.09					34	0.40
-35	0.09	-35	0.20	35	1.35		
-34	3.56	-34	4.00			36	0.40
-33	2.58	-33	2.80			54	0.20
-32	2.15	-32	2.00	55	1.99	55	1.00
-31	2.72	-31	4.20	56	0.15	56	3.60
-30	3.55	-30	8.40	57	0.03		
-29	23.95	-29	12.20	58	0.01		
-28	0.64	-28	6.00	59	0.03	59	0.20
				60	0.92	60	1.20
Set *A* 49 angles		**11 angles from set *A* do not belong to set *B* (7.01%)**					
Set *B* 50 angles		**12 angles from set *B* do not belong to set *A* (4.2%)**					

BS angle identification and comparison in setups 2 and 4

Table-A III-2 BS angle identification in setups 2 and 4

Set *F*		Set *E*		Set *F*		Set *E*	
Angle	**Prctg (%)**	**Angle**	**Prctg (%)**	**Angle**	**Prctg (%)**	**Angle**	**Prctg (%)**
30	1.19	30	3.31	74	1.09	74	1.26
31	0.70	31	0.63	75	0.50	75	0.63
32	1.07	32	1.10	85	0.41	85	0.63
33	0.52	33	1.10	86	0.63	86	0.63
34	0.71	34	0.63	87	0.91	87	0.63
35	0.89	35	0.16	88	1.03	88	0.95
36	0.02			89	1.07	89	0.32
		38	0.32			90	0.47
40	1.29	40	1.58			102	0.16
41	0.80	41	0.32	103	0.37	103	0.16
42	1.02	42	0.95	104	0.56	104	0.16
43	0.78	43	0.16			114	0.32
44	0.42	44	0.95	115	0.26	115	1.42
45	0.29	45	0.32	116	2.05	116	0.95
46	0.34	46	0.63	117	1.68	117	2.05
47	0.53	47	0.47	118	1.66	118	1.58
48	1.22	48	0.95	119	2.57	119	2.21
49	0.81	49	0.47	120	2.27	120	2.84
50	0.71	50	0.79	121	2.08	121	2.37
51	1.54	51	1.58	122	2.16	122	2.68
52	2.36	52	3.31	123	2.20	123	2.05
53	3.53	53	3.15	124	2.24	124	1.58
54	3.41	54	2.68	125	0.43	125	0.95
55	4.36	55	3.79	126	1.95	126	1.58
56	2.84	56	2.68	127	1.04	127	0.79
		57	0.95	128	0.57	128	1.26
58	1.09	58	0.63	129	1.14	129	1.89
59	2.57	59	2.52	130	0.96	130	0.79
60	1.13	60	1.58	131	0.87	131	0.63
61	1.05	61	1.42	132	0.77	132	0.47
62	1.06	62	0.95	133	0.58	133	0.79
63	1.17	63	1.58	134	0.56	134	0.47
64	0.86	64	0.32	135	0.42	135	0.47
		66	0.32	136	0.29	136	0.32
67	1.62	67	0.95	137	0.23	137	0.32
68	1.24	68	1.10	138	0.24	138	0.32
69	1.19	69	1.26	139	0.15	139	0.16
70	1.10	70	1.26	140	0.15	140	0.16
71	2.78	71	9.15	141	0.10		
72	13.15	72	3.79	142	0.06		
73	2.35	73	2.68	143	0.04	143	0.16

Set *F*	**76 angles**	**3 angles from set *F* do not belong to set *E***	**(0.18%)**
Set *E*	**79 angles**	**6 angles from set *E* do not belong to set *F***	**(2.52%)**

BS angle identification and comparison in setups 5 and 3

Figure-A III-1 Simulation scenario 1, setup 5 (grid of 6,004 Rxs)

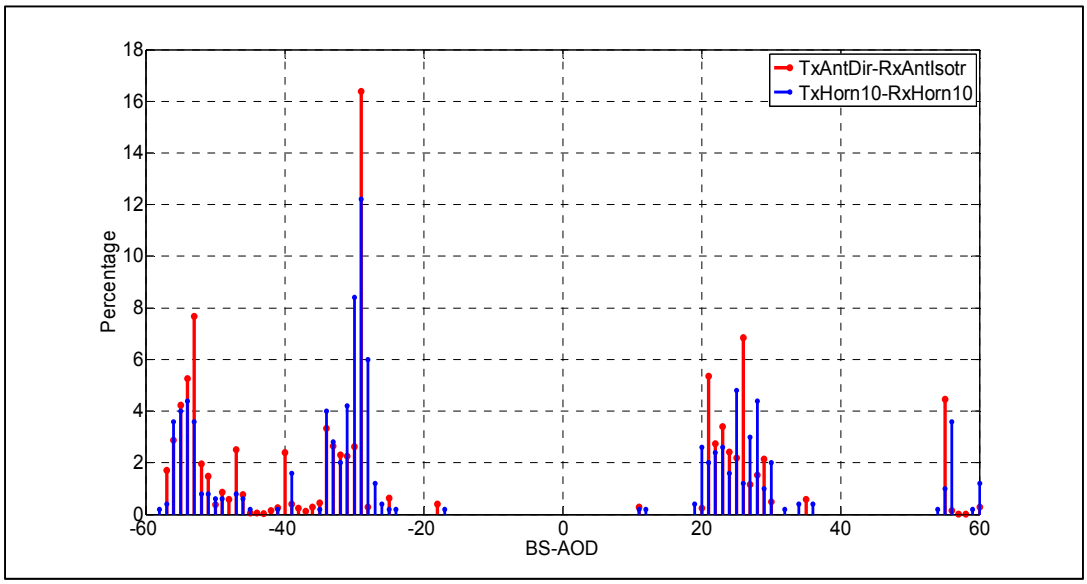

Figure-A III-2 Percentage of UEs per BS angle reaching max. power (setups 5,3)

Table-A III-3 BS angle identification in setups 5 and 3

Set $\tilde{A}$		Set B		Set $\tilde{A}$		Set B	
Angle	**Prctg (%)**	**Angle**	**Prctg (%)**	**Angle**	**Prctg (%)**	**Angle**	**Prctg (%)**
		-58	0.20			-27	1.20
-57	1.70	-57	0.40			-26	0.40
-56	2.88	-56	3.60	-25	0.63	-25	0.20
-55	4.22	-55	4.00			-24	0.20
-54	5.26	-54	4.40	-18	0.40		
-53	7.68	-53	3.60			-17	0.20
-52	1.97	-52	0.80	11	0.30	11	0.20
-51	1.49	-51	0.80			12	0.20
-50	0.38	-50	0.60			19	0.40
-49	0.86	-49	0.60	20	0.25	20	2.60
-48	0.60			21	5.36	21	2.00
-47	2.52	-47	0.80	22	2.73	22	2.40
-46	0.76	-46	0.60	23	3.41	23	2.60
-45	0.07	-45	0.20	24	2.42	24	1.60
-44	0.07			25	2.20	25	4.80
-43	0.03			26	6.85	26	1.20
-42	0.15	-41	0.20	27	1.16	27	3.00
-41	0.26			28	1.52	28	4.40
-40	2.40			29	2.14	29	1.00
-39	0.40	-39	1.60	30	0.50	30	2.00
-38	0.25					32	0.20
-37	0.13					34	0.40
-36	0.28			35	0.58		
-35	0.45	-35	0.20			36	0.40
-34	3.33	-34	4.00			54	0.20
-33	2.65	-33	2.80	55	4.45	55	1.00
-32	2.30	-32	2.00	56	0.15	56	3.60
-31	2.27	-31	4.20	57	0.02		
-30	2.63	-30	8.40	58	0.02		
-29	16.39	-29	12.20			59	0.20
-28	0.28	-28	6.00	60	0.28	60	1.20
Set $\tilde{A}$	**50 angles**	**12 angles from set $\tilde{A}$ do not belong to set B**				**(5.03%)**	
Set B	**50 angles**	**12 angles from set B do not belong to set $\tilde{A}$**				**(4.2%)**	

APPENDIX IV

ORDERED (ASCENDING) $\widetilde{A}_i$ VALUES PER EACH UE IN SERVICE AREAS

Service area 1, setup 3: 500 positions, 49 BS angles.
Service area 2, setup 4: 644 positions, 76 BS angles.
BS and UE equipped with 10^o horn antennas

In order to appreciate the impact of selecting the best angles for the entire service area we proceed as follows:

- The power levels that the UE measures are associated to each BS angle (the values considered are arbitrary).

	θ_{1BS}	θ_{4BS}	..	θ_{10BS}	….	θ_{50BS}	…	θ_{81BS}	θ_{82BS}	….	θ_{120BS}	θ_{121BS}
UE₁	-85.2	-95.2	….	-90.1	….	-68.3	….	-73.3	-64.3	….	-65.0	-65.7
UE₂	-73.4	-69.4	….	-70.1	….	-67.3	….	-62.3	-66.7	….	-55.0	-63.3
….	….						…	….				….

- The 121 power levels of each UE are sorted in ascending order:
  $\tilde{A}_1 < \tilde{A}_2 < \cdots < \tilde{A}_{50} < \cdots .. \tilde{A}_{121}$

	$\widetilde{A}_1$	$\widetilde{A}_2$		$\widetilde{A}_{10}$		$\widetilde{A}_{50}$		$\widetilde{A}_{81}$	$\widetilde{A}_{82}$		$\widetilde{A}_{120}$	$\widetilde{A}_{121}$
UE₁	θ_{4BS}	θ_{10BS}	…	θ_{1BS}	…	θ_{81BS}	…	θ_{50BS}	θ_{121BS}	…	θ_{120BS}	θ_{82BS}
	-95.2	-90.1	….	-85.2	….	-73.3	….	-68.3	-65.7	….	-65.0	-64.3
UE₂	θ_{1BS}	θ_{10BS}	….	θ_{4BS}	….	θ_{50BS}	….	θ_{82BS}	θ_{121BS}	….	θ_{81BS}	θ_{120BS}
	-73.4	-70.1	…..	-69.4	….	-67.3	….	-66.7	-63.3	….	-62.3	-55.0
….	….						….	….				….

- The power levels corresponding to the 49 best BS angles are kept whereas the remaining are set to zero

	$\tilde{A}_1$	$\tilde{A}_2$		$\tilde{A}_{10}$		$\tilde{A}_{50}$		$\tilde{A}_{81}$	$\tilde{A}_{82}$		$\tilde{A}_{120}$	$\tilde{A}_{121}$
UE₁	θ_{4BS}	θ_{10BS}	….	θ_{1BS}	…	θ_{81BS}	…	θ_{50BS}	θ_{121BS}	…	θ_{120BS}	θ_{82BS}
	-95.2	-90.1	…..	0	….	-73.3	….	0	-65.7	….	-65.0	-64.3
UE₂	θ_{1BS}	θ_{10BS}	….	θ_{4BS}	….	θ_{50BS}	…	θ_{82BS}	θ_{121BS}	….	θ_{81BS}	θ_{120BS}
	0	-70.1	….	-69.4	….	0	….	-66.7	-63.3	….	-62.3	-55.0
….	….							….	….			….

- The angle references are discarded and the places with power values different from zero are shaded.

	$\tilde{A}_1$	$\tilde{A}_2$		$\tilde{A}_{10}$		$\tilde{A}_{50}$		$\tilde{A}_{81}$	$\tilde{A}_{82}$		$\tilde{A}_{120}$	$\tilde{A}_{121}$
UE₁	-95.2	-90.1	…..	0	….	-73.3	….	0	-65.7	….	-65.0	-64.3
UE₂	0	-70.1	….	-69.4	….	0	….	-66.7	-63.3	….	-62.3	-55.0
….	….							….	….			….

Note that: a) the BS angles are not ordered; b) each UE has different set of ordered $\tilde{A}_i$ values; c) each UE line has 72 (=121-49) blanks corresponding to the $\tilde{A}_i$ that do not contribute to the CDF $F_{\hat{Z}}(\hat{z})$. Figures-A IV-1 and A IV-2 show the distribution of the 49 $\tilde{A}_i$ values (color) and blanks (no color) for each UE in the service areas 1 and 2, respectively. Clearly, there is a pattern that depends on the scenario.

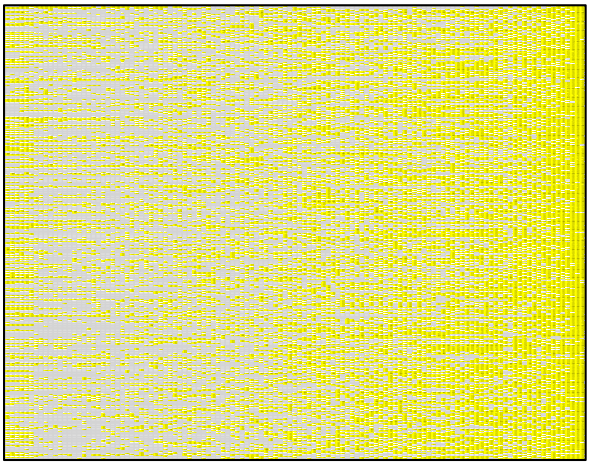

Figure-A IV-1 Area 1, Setup 3

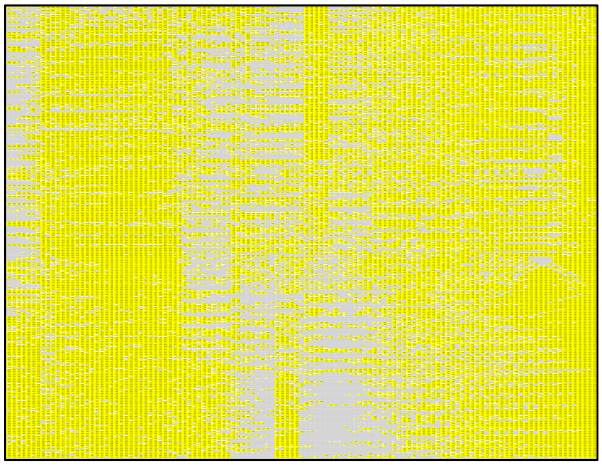

Figure-A IV-2 Area 2, Setup 4

APPENDIX V

SNR COMPARISON

In contrast to a classical hierarchical procedure in the 60 GHz band, where a beam alignment process starts in transmit or receive mode with one of the sides using an omnidirectional antenna, its direct implementation in the 28 GHz band becomes problematic due to a large propagation path loss not fully compensated with the antenna gains. This can be observed by considering as a reference the maximum SNR_o ($=SNR_{1GHzTH10UEH10}$) obtained in a system comprised of a BS serving one user that can be located at 500 arbitrary NLOS positions (Figure-A V-1), all equipped with 3dB-10º horn antennas and operating with a bandwidth (ΔW) of 1 GHz. For this task, we let the BS use the best angles (section 2.3) found in the range [-60º:1º:60º] whereas the UE angle varies in [0º:5º:355º]. Figure-A V-2 shows (solid black) the maximum SNR_o when both BS and UE antenna beams are completely aligned.

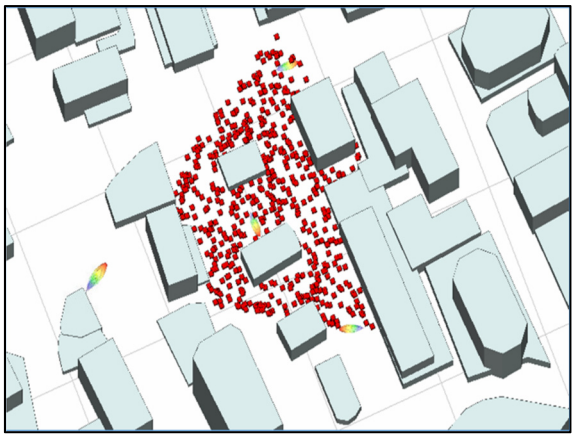

Figure-A V-1 System: 1Tx, 500 UEs

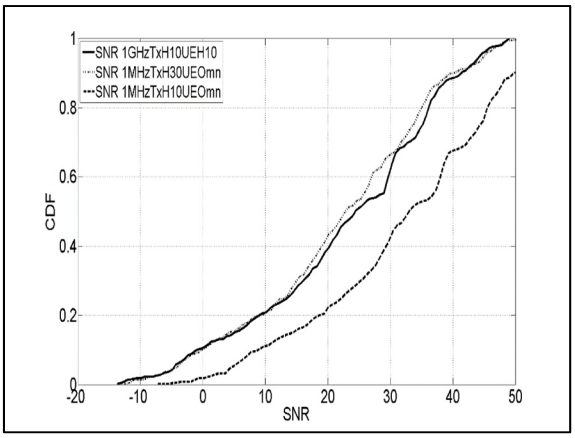

Figure-A V-2 SNR comparison

Based on this reference, a new SNR with a different bandwidth and antenna gain can be calculated as $SNR_{\text{New}} = SNR_o - (G_{Txo} + G_{Rxo}) + (G_{TxNew} + G_{RNew}) + G_F$, where $G_{Txo}, G_{Rxo}(G_{TxNew}, G_{RxNew})$ represent the Tx and Rx antenna gains used in the calculation of the reference SNR_o (SNR_{New}) and G_F the gain due to a change in the bandwidth.

Table-A V-1 shows the quantity in dBs that must be added in the approximate calculation of the new SNR. The last 2 lines correspond to BS and UE equipped with planar arrays. Figure-A V-1 and Table-A V-1 show that $SNR_{1GHzTH10UEH10}$ is basically equivalent to $SNR_{1MHzTH30UEOmn}$ (same system with the BS and UE equipped with a (3dB-beamwidth) 30º horn antenna (15 dB) and omnidirectional antenna, respectively, and operating with a bandwidth of 1 MHz).

Table-A V-1 SNR approximation for different antenna gain and frequency

G_{TH10}=24.45dB, G_{TH30}=15dB, $G_{Omn(dipole)}$=2.15dB, G_F=30dB			
$SNR_{1MHzTH30UEOmn}$	$= SNR_{1GHzTH10UEH10}$	-	1.75
$SNR_{1MHzTH10UEOmn}$		+	7.70
$SNR_{1MHzTH30UEH30}$		+	11.10
$SNR_{1MHzTH10UEH30}$		+	20.55
$SNR_{1MHzTH10UEH10}$		+	30.00
$SNR_{1MHzTA2x8UEA2x4}$		+	1.17
$SNR_{1MHzTA2x10UEA2x10}$		+	6.12

Applying the relation $R = \beta \Delta W \log_2(1 + \text{SNR})$, SNR= $P_i G_T G_R/(N_o \Delta W)$ (Barati et al., 2014) where $\beta = (0.5)(0.8)$ for half-duplexing TDD constraints and 20% control overhead, ΔW=1GHz and P_i the received power without the antenna gain, we computed that the minimum equivalent *SNR* needed for a target rate of 10 Mbps corresponds to -17.57 dB. The figure shows that the configuration 1GHzTH10UEH10 offers a minimum *SNR* of -13.5 dB allowing all UE positions meet the rate requirement. That would not be the case if the BS or UE used an antenna with a lower gain (e.g., 30º horn antenna).

In order to make a fair comparison between the proposed and the reference method, it is required that the UE can be connected at all positions inside the service area. The lower antenna gain normally applied in the first stage of the classical hierarchical alignment can be compensated by decreasing the bandwidth and the target rate assuming a minimal data exchange. A bandwidth of 1 MHz and target rate of 100 Kbps impose a minimum equivalent *SNR* of -7.23 dB. Figure-A V-2 and Table-A V-1 show that the configuration 1MHzTH30UEOmn cannot provide this minimum value for all UE positions whereas the

configuration 1MHzTH10UEOmn barely meets the requirement. A larger margin is preferred. The configurations 1MHzTH30UEH30, 1MHzTH10UEH30 and 1MHzTxH10UEH10 provide more margin than the minimum necessary. Table-A V-1 also shows that the application of an array of 2 antenna elements for the beam steering in azimuth (beamwidth of 52.9^{o} (Van Trees, 2002)) that could decrease the number of steps in a hierarchical alignment procedure does not either facilitate an initial link possibility for all UE positions.

APPENDIX VI

DATABASE GENERATION

One basic part in the actual research work was the propagation database generation using a RT tool (Wireless Insite, Remcom).

In general, the procedure applied was the following:

- Selection of the service area: extension, building and streets layout, foliage. These models can be edited directly or imported as DXF files, KMZ files, Raster data;
- RT parameter settings: frequency, number of rays, ray spacing, electrical characteristics of the building and street materials, number of reflections, transmissions and diffractions, waveforms, propagation model (Full 3D, X3D, Urban Canyon,…), selection of data output (recvd. power, path loss, propagation paths, time of arrival, ..);
- Setup of the transmitter (BS) parameters: power, height, and antenna characteristics;
- Selection of a line, grid or individual receivers (UE) inside the service area and its individual parameters: height, NF and antenna characteristics;
- Simulate and obtain propagation data for each combination of the BS discrete angles and the 72 UE angles (separated in 5^o). The data included the AoD, AoA, ToA and power of each individual MPC, received average power, path loss. The software facilitated the simultaneous calculation of propagation data for a group of receivers. Such feature saved much simulation time. The results of the simulation was output in the form of text tables.

Due to the large number of simulations involved (switching the BS and UE angles in 1^o and 5^o steps, respectively) for each receiver, it was necessary to design a Matlab interfase with the Wireless Insite software in order to automate the database generation. Each system required a new set of databases. Simplified tables were obtained from the propagation data for posterior Matlab performance simulations.

Particularly, the modified hierarchical antenna alignment procedure demanded the generation of many databases due to the different antenna beamwidth and angle combinations needed.

The database generation demanded long periods of time and a large computer memory capacity. The computing time depends on the PC processor speed, parallel processing capabilities, communication system setup (distribution and number of transmitters and receivers) and the simulation parameters (number of reflections, diffractions, etc). As an example it can be indicated that the generation of a data base (using just one PC processor core, 6 reflections, 1 diffraction, 25 propagation paths and full output data, except the power delay profile) for a specific scenario using every combination of 49 BS angles and 72 UE angles for 1,119 receivers (line points) takes approximately 7.5 days (3.14 minutes/simulation x 72 x 49) and demands a memory capacity of 0.388 Terabyte (110 Mb/simulation x 72 x 49). Similarly, a simulation using a single combination of a BS and UE angles for a group of 500 receiver points (arbitrarily located) takes 12 minutes approximately so the total database generation is completed in 29 days and requires a memory space of 107 Gbytes (30.3 Mbyte/simulation x 72 x 49). The application of parallel processing using many PC processors decreases substantially the computing time.

The databases generated in the research work were:

Table-A VI-1 Linear sets and grids of receivers for setups 1, 2 and 5

TxPower=30dBm, h_{tx}=8m, h_{rx}=1.5m			
NRxs	**Tx/Rx antenna**		**Identification of angles after data scanning**
21 linear routes (setup 1) 10,465	Direct. 150º /Isotropic	NLOS	BS:-60º:1º:60º UE:0º:1º:359º
3 grids of Rx (setup 2) 11,354 (1m separation)	Direct. 150º /Isotropic	NLOS	BS:30º:1º:150º UE:0º:1º:359º
1 grid of Rx (setup 5) 6,004 (1.5m separation)	Direct. 150º /Isotropic	NLOS	BS:-60º:1º:60º UE:0º:1º:359º

Table-A VI-2 Individual receivers in setup 3 and 4 and grid of receivers in $\hat{a}_1$ and $\hat{a}_2$

TxPower=30dBm, h_{tx}=8m, h_{rx}=1.5m (NLOS)			
NRxs	**Tx/Rx antenna**	**Description**	**Angles**
500 (setup 3)	Horn10º/Horn10º	UEs located arbitrarily	BS:-60º:1º:60º UE:0º:5º:355º
634 (setup 4)	Horn10º/Horn10º	Grid of points separated 4m	BS:30º:1º:150º UE:0º:5º:355º
44 ($\hat{a}_1$) DB_{res}=0.5m	Horn30º/Horn30º	UEs located arbitrarily	BS:-45º:30º:45º UE:0º:5º:355º
44 ($\hat{a}_1$) DB_{res}=0.5m	Horn10º/Horn30º	UEs located arbitrarily	BS:-55º:10º:55º UE:0º:5º:355º
44 ($\hat{a}_1$) DB_{res}=0.5m	Horn10º/Horn10º	UEs located arbitrarily	BS:-57.5º:5º:57.5º UE:0º:5º:355º
44 ($\hat{a}_1$) DB_{res}=0.5m	Horn10º/Horn10º	UEs located arbitrarily	BS:-57.5º:5º:57.5º UE:2.5º:5º:375.5º
2,652 ($\hat{a}_1$) DB_{res}=0.5m	Horn10º/Horn10º	Grid of points separated 0.5m	Best BS angles UE:0º:5º:355º
2,652 ($\hat{a}_1$) DB_{res}=0.5m	Horn30º/Horn30º	Grid of points separated 0.5m	BS:-45º:30º:45º UE:0º:5º:355º
2,652 ($\hat{a}_1$) DB_{res}=0.5m	Horn10º/Horn30º	Grid of points separated 0.5m	BS:-55º:10º:55º UE:0º:5º:355º
2,652 ($\hat{a}_1$) DB_{res}=0.5m	Horn10º/Horn30º	Grid of points separated 0.5m	Best BS angles UE:0º:5º:355º
2,652 ($\hat{a}_1$) DB_{res}=0.5m	Horn10º/Horn10º	Grid of points separated 0.5m	BS:-57.5º:5º:57.5º UE:0º:5º:355º
2,652 ($\hat{a}_1$) DB_{res}=0.5m	Horn10º/Horn10º	Grid of points separated 0.5m	BS:-57.5º:5º:57.5º UE:2.5º:5º:375.5º
100 ($\hat{a}_2$) DB_{res}=0.5m	Horn30º/Horn30º	UEs located arbitrarily	BS:-45º:30º:45º UE:0º:5º:355º
100 ($\hat{a}_2$) DB_{res}=0.5m	Horn10º/Horn30º	UEs located arbitrarily	BS:-55º:10º:55º UE:0º:5º:355º
100 ($\hat{a}_2$) DB_{res}=0.5m	Horn10º/Horn10º	UEs located arbitrarily	BS:-57.5º:5º:57.5º UE:0º:5º:355º
100 ($\hat{a}_2$) DB_{res}=0.5m	Horn10º/Horn10º	UEs located arbitrarily	BS:-57.5º:5º:57.5º UE:2.5º:5º:375.5º
2,944 ($\hat{a}_2$) DB_{res}=0.5m	Horn10º/Horn10º	Grid of points separated 0.5m	Best BS angles UE:0º:5º:355º
2,944 ($\hat{a}_2$) DB_{res}=0.5m	Horn30º/Horn30º	Grid of points separated 0.5m	BS:-45º:30º:45º UE:0º:5º:355º
2,944 ($\hat{a}_2$) DB_{res}=0.5m	Horn10º/Horn30º	Grid of points separated 0.5m	BS:-55º:10º:55º UE:0º:5º:355º
2,944 ($\hat{a}_2$) DB_{res}=0.5m	Horn10º/Horn30º	Grid of points separated 0.5m	Best BS angles UE:0º:5º:355º
2,944 ($\hat{a}_2$) DB_{res}=0.5m	Horn10º/Horn10º	Grid of points separated 0.5m	BS:-57.5º:5º:57.5º UE:0º:5º:355º
2,944 ($\hat{a}_2$) DB_{res}=0.5m	Horn10º/Horn10º	Grid of points separated 0.5m	BS:-57.5º:5º:57.5º UE:2.5º:5º:375.5º
44 ($\hat{a}_1$)	Horn10º/Horn30º	UE located arbitrarily	Best BS angles UE:0º:5º:355º

100 ($\hat{a}_2$)	Horn10º/Horn30º	UE located arbitrarily	Best BS angles UE:0º:5º:355º
100 ($\hat{a}_2$)	Horn10º/Horn10º	UE located arbitrarily	Best BS angles UE:0º:5º:355º
60 points - 0.04m 10 linear routes ($\hat{a}_1$)	Horn10º/Horn10º	Lines located arbitrarily	Best BS angles UE:0º:5º:355º
39 ($\hat{a}_3$)	Horn10º/Horn30º	UE located arbitrarily	Best BS angles UE:0º:5º:355º
3,025 ($\hat{a}_3$) DB_{res}=0.5m	Horn10º/Horn10º	Grid of points separated 0.5m	Best BS angles UE:0º:5º:355º

APPENDIX VII

MODIFIED CLASSICAL HIERARCHICAL PROCEDURE SIMULATION

Instead of using an omnidirectional antenna in one of the sides of link as in the classical hierarchical antenna alignment procedure, this is modified by using only directional antennas (beamwidth of 30º and 10º) at the Tx and Rx sides. The assumed arbitrary initial θ_{UEinit} forced the generation of propagation data for the UE angles in the range [0º:5º:355º) to cover all possibilities. Figure-A V-1 and Table-A V-1 show the angle variation scheme used in the database generation for the simulation of the modified hierarchical procedure.

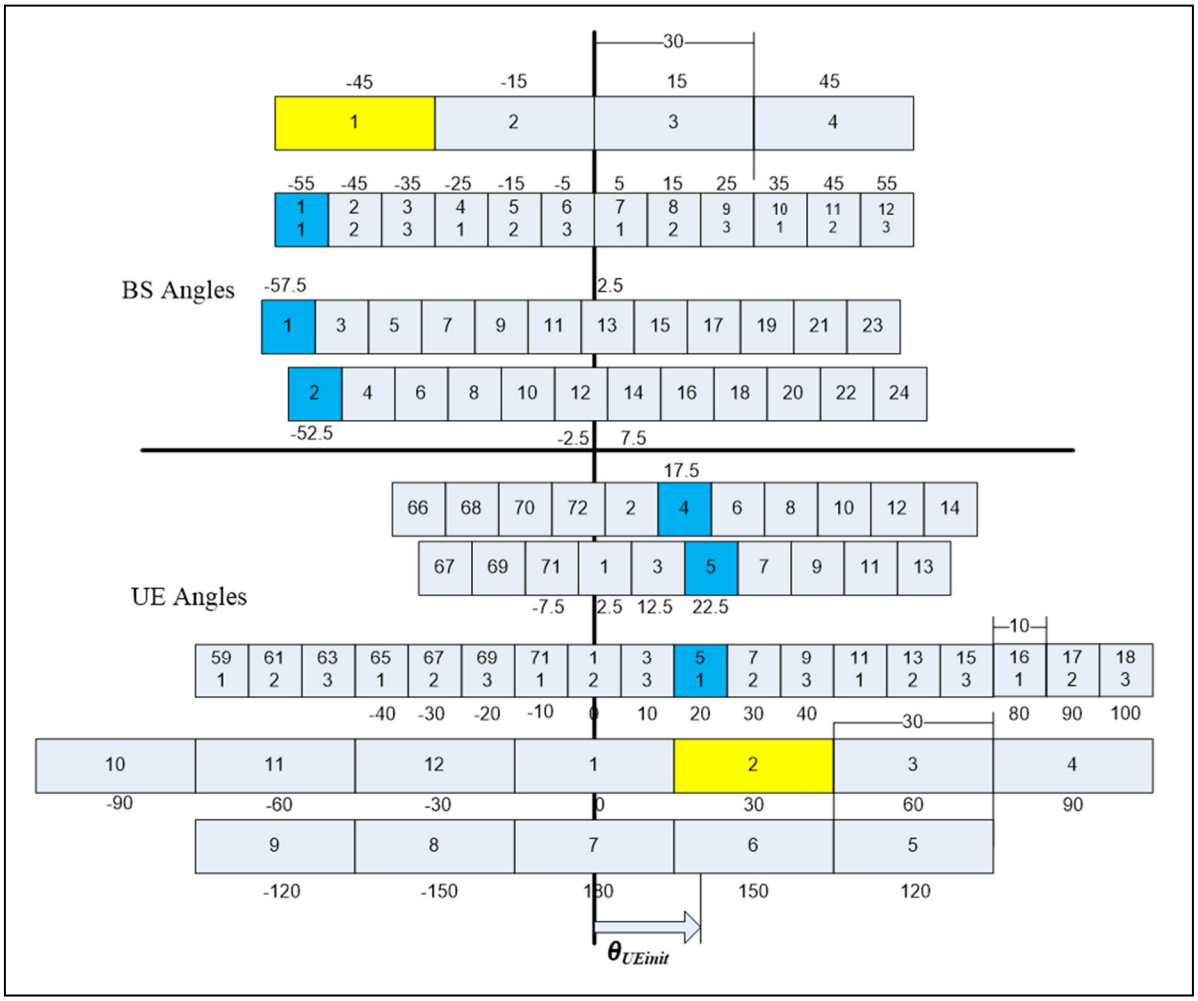

Figure-A VII-1 BS and UE angles and beamwidth used in simulation

Table-A VII-1 BS-UE angles applied in modified hierarchical alignment simulation

BS-Tx angles θ_{BS}	**UE-Rx angles θ_{UE}**
H30: -45º,-15º, 15º, 45º	H30: 0º, 30º, 60º, 90º, 120º,……...330º H30: 5º,10º,15º,20º,25º,35º,40º,45º,50º,55º,65º,…..
H10: -55º,-45º,-35º,….., 35º, 45º, 55º	H30: 0º, 30º, 60º, 90º, 120º,……..….330º H30: 5º,10º,15º,20º,25º,35º,40º,45º,50º,55º,65º,…..
H10: -55º,-45º,-35º,….., 35º, 45º, 55º	H10: 0º, 10º, 20º, 30º, 40º, 50º,……..330º H10: 5º,10º,15º,20º,25º,35º,40º,45º,50º,55º,65º,…..
H10: -57.5º,-52.5º,-47.5º,….., 52.5º, 57.5º	H10: 0º, 10º, 20º, 30º, 40º, 50º,……..,330º H10: 5º,10º,15º,20º,25º,35º,40º,45º,50º,55º,65º,…..
H10: -57.5º,-52.5º,-47.5º,….., 52.5º, 57.5º	H10: 2.5º, 7.5º, 12.5º, 17.5º,…...…..357.5º
H30/H10=Horn antenna 30º/10º For each BS angle θ_{BS}, the final UE angle = $\theta_{UE} + \theta_{UEinit}$; where θ_{UEinit} ε {0º, 5º,…….,355º}	

Modified hierarchical algorithm

The BS starts the alignment steering its 30º beam in the direction -45º, -15º, 15º, 45º. For each BS angle, the 30º UE beam is switched sequentially in the range [θ_{UEinit}+0º:30º:θ_{UEinit}+330º]. The initial total BS-UE antenna gain is 30dB. Once the UE reports back the best BS angle $\theta^i_{stage1BS}$, the UE fixes its 30º beam to the corresponding best direction $\theta^j_{stage1UE}$. In the following stage, the BS changes its antenna beamwidth to 10º and switches in the range [$\theta^i_{stage1BS}$-10º:10º: $\theta^i_{stage1BS}$+10º]. The UE reports back the best $\theta^i_{stage2BS}$ which is fixed by the BS for the following part. The UE changes its antenna beamwidth to 10º and switches its angle in the range [$\theta^j_{stage1UE}$-10º:10º:$\theta^j_{stage1UE}$+10º] and find the best $\theta^k_{stage2UE}$. In order to get a fair comparison using antennas up to 10º beamwidth, UE fixes $\theta^k_{stage2UE}$ and let the BS beam move $\theta^i_{stage2BS} \pm 2.5^{\mathrm{o}}$. The UE feedbacks the best BS angle $\theta^l_{stage3BS}$ which is fixed for the next stage. Finally the UE finds the best angle $\theta^k_{stage3UE}$ from $\theta^k_{stage2UE} \pm 2.5^{\mathrm{o}}$. The best combination corresponds to $\theta^l_{stage3BS}, \theta^k_{stage3UE}$. A 2.5º step was applied instead of the correct 5º. The main purpose was to have a more strict reference for the comparison.

APPENDIX VIII

LINK WITH TWO PROPAGATION PATHS

Procedure to identify a separate (second strongest) power lobe for a DB point or UE

From the information in the DB:

- The power-angle profile at the UE side $\boldsymbol{a}'_{72x1}$ corresponding to each θ_{iBS} (curve *i*) is converted to $\boldsymbol{a}_{360X1}$ (smoothed) using interpolation.
- The angles $(\theta_{UE1}, \theta_{UE2}, \ldots., \theta_{UEn})$ where the power peaks $(\mathrm{Pow}_1, \mathrm{Pow}_2, \ldots., \mathrm{Pow}_n)$ occur can be obtained using a derivative function. Each curve *i* has different number of peaks but only n (=5) were chosen so that the same number of lobes are considered for each BS angle θ_{iBS}. Generally the power of the lobes decreases greatly with n.
- A matrix **B'** is constructed in which each column has the UE angles and power values corresponding to $\theta_{i'BS}$, *i*=1,2,3,…,*N*

  B'=

$$\begin{pmatrix} [\theta_{1'BS}\ (\theta_{UE1})_{1'}\ (\mathrm{Pow}_1)_{1'}\ (\theta_{UE2})_{1'}\ (\mathrm{Pow}_2)_{1'}\ \ldots\ (\theta_{UEn})_{1'}\ (\mathrm{Pow}_n)_{1'}]^T \\ [\theta_{2'BS}\ (\theta_{UE1})_{2'}\ (\mathrm{Pow}_1)_{2'}\ (\theta_{UE2})_{2'}\ (\mathrm{Pow}_2)_{2'}\ \ldots.(\theta_{UEn})_{2'}\ (\mathrm{Pow}_n)_{2'}]^T \\ \ldots \\ [\theta_{N'BS}\ (\theta_{UE1})_{N'}\ (\mathrm{Pow}_1)_{N'}\ (\theta_{UE2})_{N'}\ (\mathrm{Pow}_2)_{N'}\ \ldots(\theta_{UEn})_{N'}\ (\mathrm{Pow}_n)_{N'}]^T \end{pmatrix} \quad \text{(AVIII-1)}$$

  $(\theta_{UEn})_{1'}$ represents the UE angle n in which the peak power value $(\mathrm{Pow}_n)_{1'}$ occurs for $\theta_{1'BS}$. On the other hand, $(\theta_{UE1})_{k_1}$ and $(\theta_{UE2})_{k_2}$ represent the UE angles of the first and second power lobe associated to the BS angles θ_{k_1BS} and θ_{k_1BS}, respectively.

  A new matrix **B** is constructed by sorting (descend) **B'**(3,:), that is, sorting the maximum power values of the main first lobe associated to each BS angle.

- A data comparison is established between **B**(:,1) and each of the columns **B**(:,k); k=2,3,.,*N* according to the rules of Table-A VIII-1 and the parameters of Table-A VIII-2. The objective is to identify the UE angle of a lobe that has the second highest power

value (2nd lobe). Initially, the comparison is accomplished only between the sets **B**(1:5,1) and **B**(1:5,k), that is, the angles and power values of the first and second power lobes.

- Once the BS and UE angle of the second lobe are identified, it becomes necessary to determine if their application generates (receive) an interference to (from) the first path (e.g. Figure-A VIII-1d). It is considered ΔP=$\mathrm{Pow}_1 - \mathrm{Pow}_k \geq 15$ dB as a reference value for the interference value (design parameter). If the value of ΔP is not met, the initially selected BS and UE angles of the second lobe are discarded and the search continues on **B**(6:11,1) and **B**(6:11,k), that is, the remaining power lobes (n=3,4,5).

Table-A VIII-1 Rules to determine the BS and UE angles of the second power lobe

Angle conditions $\Delta\theta_{BS} \neq 0$	**Power conditions**
$\lvert(\theta_{UE1})_1 - (\theta_{UE1})_k\rvert \geq \Delta\theta_{UE}$; $\lvert(\theta_{UE1})_1 - (\theta_{UE2})_k\rvert \geq \Delta\theta_{UE}$ $\lvert(\theta_{UE2})_1 - (\theta_{UE2})_k\rvert \geq \Delta\theta_{UE}$; $\lvert(\theta_{UE2})_1 - (\theta_{UE1})_k\rvert \geq \Delta\theta_{UE}$	None
$\lvert(\theta_{UE1})_1 - (\theta_{UE1})_k\rvert < \Delta\theta_{UE}$; $\lvert(\theta_{UE1})_1 - (\theta_{UE2})_k\rvert \geq \Delta\theta_{UE}$ $\lvert(\theta_{UE2})_1 - (\theta_{UE2})_k\rvert \geq \Delta\theta_{UE}$; $\lvert(\theta_{UE2})_1 - (\theta_{UE1})_k\rvert \geq \Delta\theta_{UE}$	$(\mathrm{Pow}_1)_k < (\mathrm{Pow}_1)_1$ $\lvert(\mathrm{Pow}_1)_k - (\mathrm{Pow}_1)_1\rvert > \Delta P$
$\lvert(\theta_{UE1})_1 - (\theta_{UE1})_k\rvert \geq \Delta\theta_{UE}$; $\lvert(\theta_{UE1})_1 - (\theta_{UE2})_k\rvert < \Delta\theta_{UE}$ $\lvert(\theta_{UE2})_1 - (\theta_{UE2})_k\rvert \geq \Delta\theta_{UE}$; $\lvert(\theta_{UE2})_1 - (\theta_{UE1})_k\rvert \geq \Delta\theta_{UE}$	$(\mathrm{Pow}_2)_k < (\mathrm{Pow}_1)_1$ $\lvert(\mathrm{Pow}_2)_k - (\mathrm{Pow}_1)_1\rvert > \Delta P$
$\lvert(\theta_{UE1})_1 - (\theta_{UE1})_k\rvert \geq \Delta\theta_{UE}$; $\lvert(\theta_{UE1})_1 - (\theta_{UE2})_k\rvert \geq \Delta\theta_{UE}$ $\lvert(\theta_{UE2})_1 - (\theta_{UE2})_k\rvert < \Delta\theta_{UE}$; $\lvert(\theta_{UE2})_1 - (\theta_{UE1})_k\rvert \geq \Delta\theta_{UE}$	None
$\lvert(\theta_{UE1})_1 - (\theta_{UE1})_k\rvert \geq \Delta\theta_{UE}$; $\lvert(\theta_{UE1})_1 - (\theta_{UE2})_k\rvert \geq \Delta\theta_{UE}$ $\lvert(\theta_{UE2})_1 - (\theta_{UE2})_k\rvert \geq \Delta\theta_{UE}$; $\lvert(\theta_{UE2})_1 - (\theta_{UE1})_k\rvert < \Delta\theta_{UE}$	$(\mathrm{Pow}_2)_1 < (\mathrm{Pow}_1)_k$ $\lvert(\mathrm{Pow}_2)_1 - (\mathrm{Pow}_1)_k\rvert > \Delta P$
$\lvert(\theta_{UE1})_1 - (\theta_{UE1})_k\rvert \geq \Delta\theta_{UE}$; $\lvert(\theta_{UE1})_1 - (\theta_{UE2})_k\rvert < \Delta\theta_{UE}$ $\lvert(\theta_{UE2})_1 - (\theta_{UE2})_k\rvert \geq \Delta\theta_{UE}$; $\lvert(\theta_{UE2})_1 - (\theta_{UE1})_k\rvert < \Delta\theta_{UE}$	$(\mathrm{Pow}_2)_k < (\mathrm{Pow}_1)_1$ $\lvert(\mathrm{Pow}_2)_k - (\mathrm{Pow}_1)_1\rvert > \Delta P$ $(\mathrm{Pow}_2)_1 < (\mathrm{Pow}_1)_k$ $\lvert(\mathrm{Pow}_2)_1 - (\mathrm{Pow}_1)_k\rvert > \Delta P$

Figure-A VIII-1a,b,c show three examples of the identification of the second power lobe based on the adopted rules. Figure-A VIII-1d show the case of an interference that can be avoided. According to the power levels, the second lobe (A) should be selected. Nevertheless

the UE antenna oriented in θ_{2UE} receives power not only from the BS using the angle θ_{2BS} but also using the angle θ_{1BS}. Unless $\Delta P \geq 15$ dB, the combination $(\theta_{3BS}, \theta_{3UE})$ would be selected instead of the $(\theta_{2BS}, \theta_{2UE})$. The variation of the parameters of Table-A VIII-2 changes the identification of the second lobe.

Table-A VIII-2 Parameters applied for the second beam identification

Second beam	BS angle difference	UE angle difference	Power difference ΔP
Same BS angle	0^o	$\geq 10^o$	
Different BS angles	$\geq 20^o$	$\geq 20^o$	15 dB

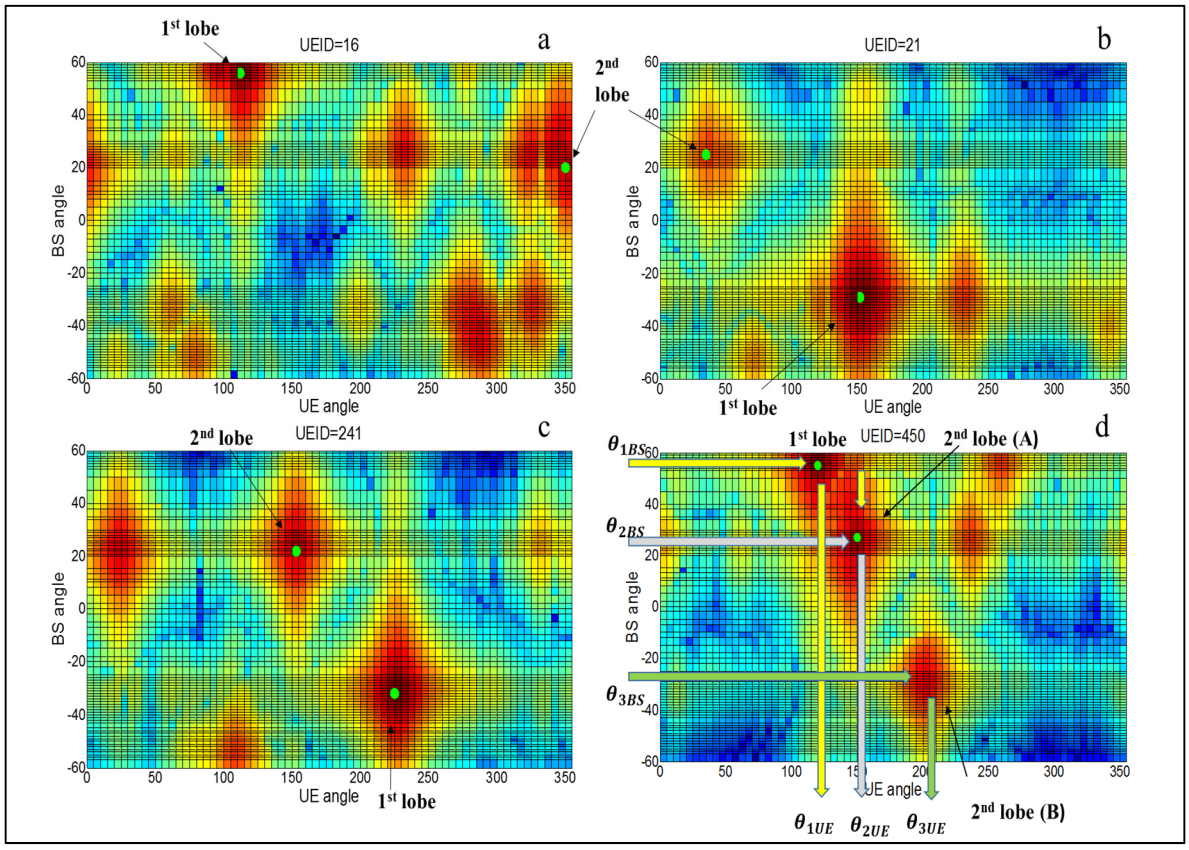

Figure-A VIII-1 Power lobes for different UEs

SNR and capacity of two paths

System: Figure-A V-1
Parameters: Tx power=30 dBm, htx=8m, hrx=1.5m
Tx, Rx antenna=horn 10º (3dB - beamwidth).

Figures-A VIII-2 and 3 show a comparison of SNRs and capacity associated to two paths in a system using 1 BS-Tx and 500 arbitrary positions, respectively, Specifically, Figure-A VIII-2 shows the SNR associated to the first path (blue), second path (magenta) and their difference (black). An average SNR difference of 9.8 dB is observed when the selection of the second path was taken only if its associated power level was at most 20 dB below that of the first path. In such a case, it was possible to identify second power lobes in 54.8% of the 500 UEs. Using a difference equal to or lower than 25 (30) dB, the number of UEs with identified second lobes increased to 66.4 (76.2)%, respectively.

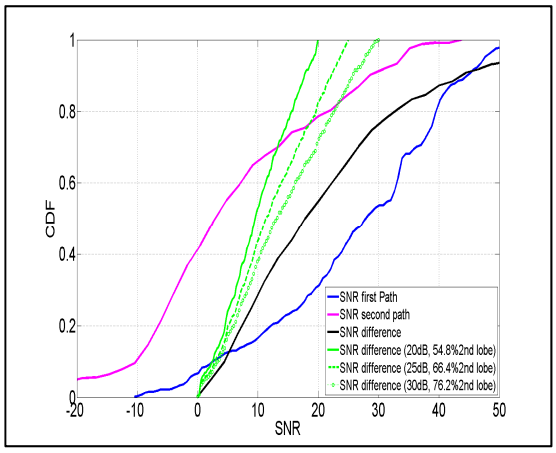

Figure-A VIII-2 SNR comparison

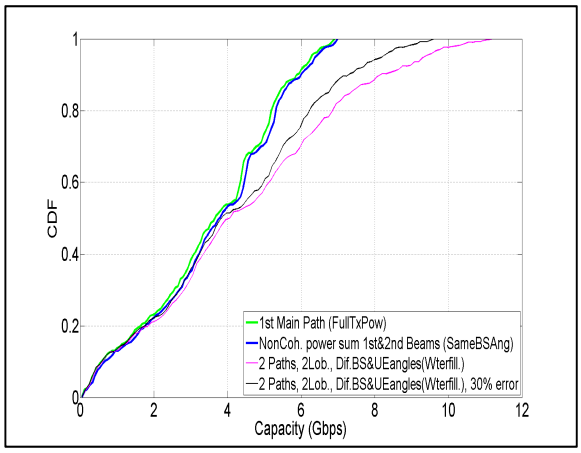

Figure-A VIII-3 Capacity comparison

For the link capacity comparison, Figure-A VIII-3 shows the capacity obtained using the main propagation path (green), the total capacity (blue) obtained by the non-coherent sum of the power levels of the two paths using the same BS angle and different UE angles (whether in the same first lobe or in a separate one), and the total capacity (magenta) of two separate propagation paths in which the BS and UE angles are different (different lobes). For such

system, the total capacity obtained by combining non-coherently the power levels (one data flux) and that from two separate data fluxes serving the same UE (different BS and UE angles) are both higher than the capacity obtained using exclusively the main propagation path. The increase using two separate data fluxes is noticeably higher for larger SNR values. Water filling was applied to get the largest total capacity when the Tx power was shared in the two paths.

Figure-A VIII-3 also shows the case in which it is assumed that the variable conditions of the environment change the angles of the second lobe randomly (uniform) in 30% of the cases. Given that for those events such information is not available in the DB, the algorithm provides an inaccurate information to the UE which result in a decreased total power (the fraction assigned to the main beam). Nevertheless, the system still gets a capacity increase benefit. The algorithm that determines the angle combination for the main beam in the first power lobe is less prone to this type of error given that it can be designed to determine the best BS angle from the position information and assign the UE the task to discover its best angle through power measurements

Equivalence

$\sum_{i=1}^{2} B\log_2(1 + x_i snr_i) \geq B\log_2(1 + snr_1)$;

$\log_2(1 + x_1 snr_1) + \log_2(1 + x_2 snr_2) \geq \log_2(1 + snr_1)$; $\quad x_1 + x_2 = 1$

$(1 + x_1 snr_1)(1 + x_2 snr_2) \geq (1 + snr_1)$

$(1 + x_1 snr_1) + (1 + x_1 snr_1)(1 - x_1) snr_2 \geq (1 + snr_1)$

$(1 + x_1 snr_1)(1 - x_1) snr_2 \geq (1 - x_1) snr_1$

$snr_2 \geq \frac{snr_1}{(1+x_1 snr_1)}$ (AVIII-2)

Coherent versus Non-Coherent sum of powers from two propagation paths for a single data flux.

The illumination of the UE using two separate antennas both at BS and UE intended to increase the capacity of a single data flux works only for the coherent combination of the two path signals in the case of an equal splitting of the Tx power. Such effect can be observed assuming a simplified scenario where there are two propagation paths with only one multipath component in each path and P_{1dB}, P_{2dB} ($P_{1dB} \geq P_{2dB}$) represent the maximum powers read by the UE when the Tx applies full power in each direction. The total combined coherent and non-coherent power at the UE position becomes:

$$P_c = \left(\sqrt{\frac{1}{2}10^{P1dB/10}} + \sqrt{\frac{1}{2}10^{P2dB/10}}\right)^2 = \frac{1}{2}\left(1 + \frac{1}{10^{(P1dB-P2dB)/20}}\right)^2 10^{P1dB/10} \qquad \text{(AVIII-3)}$$

$$P_{nc} = \frac{1}{2}10^{P1dB/10} + \frac{1}{2}10^{P2dB/10} = \frac{1}{2}\left(1 + \frac{1}{10^{(P1dB-P2dB)/10}}\right)10^{P1dB/10} \qquad \text{(AVIII-4)}$$

The application of the conditions $P_c \geq P_{1dB}$ and $P_{nc} \geq P_{1dB}$ gives:

$$\left\{\begin{array}{ll} 3.83\text{dB} \geq \Delta P_{12} = P_{1dB} - P_{2dB} \geq 0\text{dB} & \text{for } P_c \geq P_{1dB} \\ P_{1dB} = P_{2dB} & \text{for } P_{nc} \geq P_{1dB} \end{array}\right\} \qquad \text{(AVIII-5)}$$

For the coherent combination, the result indicates that unless there is a $\Delta P_{12} \leq 3.83$dB in the received power between the first and second path, it is not worth it to apply two RF fronts. Such purpose is not valid for the non-coherent case because the conditions $P_{1dB}=P_{2dB}$ and $P_{1dB}>P_{2dB}$ imply $P_{nc} = P_{1dB}$ and $P_{nc} < P_{1dB}$, respectively.

On the other hand, if the BS used only one antenna and the UE seeks two propagation paths, then:

$$P_c = \left(\sqrt{10^{P1dB/10}} + \sqrt{10^{P2dB/10}}\right)^2 = \left(1 + \frac{1}{10^{(P1dB-P2dB)/20}}\right)^2 10^{P1dB/10} \qquad \text{(AVIII-6)}$$

$$P_{nc} = 10^{P1dB/10} + 10^{P2dB/10} = \left(1 + \frac{1}{10^{(P1dB-P2dB)/10}}\right)10^{P1dB/10} \qquad \text{(AVIII-7)}$$

In all cases there is an advantage to use two RF fronts at the UE side

BIBLIOGRAPHY

Abbas, Waqas and Michele Zorzi. 2016. "Context Information Based Initial Cell Search for Millimeter Wave 5G Cellular Networks". [Online]. Available: https://arxiv.org/abs/1605.01930v1, Cornell University Library.

Abbas, Waqas and Michele Zorzi. 2016. "Towards an Appropriate Beamforming Scheme for Initial Cell Discovery in mmW 5G Cellular Networks". [Online]. Available: https://arxiv.org/abs/1605.00508v1, Cornell University Library.

Abouelseoud, Mohamed and Gregg Charlton. 2013. "System level perforrmance-wave access link for outdoor coverage". In *IEEE Wireless Communications and Networking Conference (WCNC)*. p. 4146-4151.

Akdeniz, M., Y. Liu, S. Sun, S. Rangan, and E. Erkip. 2013. "Millimeter Wave PicoCellular System Evaluation for Urban Deployments". [Online]. Available: https://arxiv.org/abs/1304.3963v1, Cornell University Library.

Akdeniz, M., Y. Liu, S. Sun, S. Rangan, T. Rappaport, and E. Erkip. 2013. "Millimeter Wave Channel Modeling and Cellular Capacity Evaluation". [Online]. Available: https:// arxiv.org/abs/1312.4921, Cornell University Library.

Akoum, Salam, Omar El Ayach, and Robert W. Heath. 2012. "Coverage and capacity in mmWave cellular systems". In *Conference Record of the 46th Asilomar Conference on Signals, Systems and Computers (ASILOMAR)*. p. 688-692.

Alkhateeb, A., O. El Ayach, G. Leus, and R.W. Heath. 2013. "Hybrid precoding for millimeter wave cellular systems with partial channel knowledge". In *Information Theory and Applications Workshop (ITA), IEEE*. p. 1-5.

Alkhateeb, A., O. El Ayach, G. Leus, and R.W. Heath. 2014. "Channel Estimation and Hybrid Precoding for Millimeter Wave Cellular Systems". *IEEE Journal of Selected Topics in Signal Processing', Vol. 8, No. 5*, p. 831-846.

Alkhateeb, A., El Ayach O., Leus G., and R. W. Heath. 2015. "Compressed Sensing Based Multi-User Millimeter Wave Systems: How many measurements are needed?". [Online]. Available: https://arxiv.org/abs/1505.00299v1.

An, X., C. Sum, R. Prasad, J. Wang, Z. Lan, J. Wang, R. Hekmat, H. Harada, and I. Niemegeers. 2009. "Beam switching support to resolve link-blockage problem in 60 GHz WPANs". In *IEEE 20th International Symposium on Personal, Indoor and Mobile Radio Communications.* p. 309-394.

Aviles, Juan and Ammar Kouki. 2016. “Exploiting site-specific propagation characteristics in directional search at 28 GHz”. *IEEE Access*, vol. 4, p. 3894-3906.

Aviles, Juan and Ammar Kouki. 2016. “Position-Aided mm-Wave Beam Training under NLOS Conditions”. *IEEE Access*, vol. 4, pp. 8703–8714.

Azar, Y., G.N. Wong, K. Wang, R. Mayzus, H. Zhao, F. Gutierrez, D. Hwang, and T.S. Rappaport. 2013. “28GHz propagation measurements for outdoor cellular communications using steerable beam antennas in New York City”. In *International Conference on Communications (ICC)*. p. 5143 – 5147.

Balanis, Constantine. 2005. *Antenna Theory. Analysis and Design.* 3rd ed., John Wiley & Sons, Inc., 2005, 1072 p.

Baek, S., Y. Chang, H. Kim, and A. Agiwal. 2014. “Comparison Analysis of Outdoor Channel Characteristics at 28 Ghz and 2 GHz using 3D Ray-Tracing Technique”. In *IEEE 80th Vehicular Technology Conference (VTC2014-Fall)*. p. 1-5.

Barati, C., S. Hosseini, S. Rangan, P. Liu, T. Korakis, and S. Panwar. 2014. “Directional Cell Search for Millimeter Wave Cellular Systems”. [Online]. Available: https://arxiv.org/abs/1404.5068.

Berger, C., Z. Wang, J. Huang, and S. Zhou. 2010. “Application of Compressive Sensing to Sparse Channel Estimation”. *IEEE Communications Magazine*, vol. 48, nº 11, p. 164-174.

Berraki, D.E., S.M.D Armour, and A.R. Nix. 2014. “Application of compressive sensing in sparse spatial channel recovery for beamforming in mmWave outdoor systems”. In *IEEE Wireless Communications and Networking Conference (WCNC)*. p. 887-892.

Caichana, P., P. Uthansakul, and M. Uthansakul. 2104. “GPS-Aided Opportunistic Space-Division Multiple Access for 5G Communications”. In *The 20th Asia-Pacific Conference on Communications (APCC)*. p. 468-472.

Candes, Emmanuel and Michael Wakin. 2008. “An introduction to compressive sampling”, *IEEE Signal Processing Magazine,* vol. 25, nº 2, p. 21-30.

Capone, A., I. Filippini, and V. Sciancalepore. 2015. “Context-based Cell Search in Millimeter Wave 5G Networks”. [Online]. Available: https://arxiv.org/abs/:1501.02223v1.

Capone, A., I. Filippini, V. Sciancalepore, and D. Tremolada. 2015. “Obstacle avoidance cell discovery using mm-waves directive antennas in 5G Networks”. In *IEEE 26th Personal, Indoor, and Mobile Radio Communications (PIMRC)*, p. 2349-2353.

Cisco. 2016. “Cisco Visual Networking Index: Global Mobile Data Traffic Forecast Update, 2015-2020, white paper”.

Chiang, H.L., W. Rave, T. Kadur, and G. Fettweis. 2016. “Full Rank Spatial Channel Estimation at Millimeter Wave Systems”. In *Proceedings of the International Symposium on Wireless Communication Systems (ISWCS'16)*.

Choi, Jinho. 2015. “Beam Selection in mm-Wave Multiuser MIMO Systems Using Compressive Sensing”, *IEEE Transactions on Communications*, Vol. 63, nº 8, p. 2936-2947.

Degli-Esposti, F. Fuschini, E. M. Vitucci, M. Barbiroli, M. Zoli, L. Tian, X. Yin, D. Dupleich, R. Müller, C. Schneider, and R. S. Thomä. 2014. “Ray-tracing based mm-wave beamforming assessment”. *IEEE Access*, vol. 2, p. 1314 – 1325.

Desai, V., L. Krzymien, P. Sartori, W. Xiao, A. Soong, and A. Alkhateeb. 2014. “Initial Beamforming for mmWave communications”. In *48th Asilomar Conference on Signals, Systems, and Computers*. p. 1926-1930.

El Ayach, O., R.W. Heath, S. Abu-Surra, S. Rajagopal, and Z. Pi. 2012. “Low complexity precoding for large millimeter Wave MIMO systems”. In *IEEE International Conference on Communications (ICC)*. p. 3724-3729.

El Ayach, O., S. Rajagopal, S. Abu-Surra, Z. Pi, and R.W. Heath. 2013. “Spatially Sparse Precoding in Millimeter Wave MIMO Systems”. [Online]. Available: https://arxiv.org/abs/1305.2460v1.

Eliasi, P., S. Rangan, and T. Rappaport. 2014. “Low-Rank Spatial Channel Estimation for Millimeter Wave Cellular System”. [Online]. Available: https://arxiv.org/abs/1410.4831v1.

Endeshaw, T., A. Haghighat, and L. Bao. 2014. “Hybrid Analog-Digital Beamforming: How Many RF Chains and Phase Shifters Do We Need?, In *arXiv:1410.2609v1 [cs.IT]*.

Federal Aviation Administration. 2014. “Global Positioning System (GPS) Standard Positioning Service (SPS) Performance Analysis Report, July 2014”. http://www.gps.gov/systems/gps/performance/accuracy/

Goldsmith, Andrea. 2005. *Wireless Communications*. Cambridge University Press, 572 p.

Guibene, Wael and Dirk Slock. 2013. “Degrees of Freedom of Downlink Single and Multi-Cell Multi-User MIMO Systems With Location Based CSIT”. *2013 IEEE 77th Vehicular Technology Conference (VTC Spring)*. p. 1-5.

Haupt, Rand and Sue Haupt. 2004. *Practical Genetic Algorithms*, 2nd edition, Hoboken, New Jersey, John Wiley & Sons, 2004, Inc. 272 p.

Heath, R.W., N. Gonzalez-Prelcic, S. Rangan, W. Roh, and A. Sayeed. 2015. "An Overview of Signal Processing Techniques for Millimeter Wave MIMO Systems". [Online]. Available: https://arxiv.org/abs/1512.03007v1.

Hur, S., T. Kim, D. Love, J. Krogmeier, T. Thomas, and A. Ghosh. 2013. "Millimeter Wave Beamforming for Wireless Backhaul and Access in Small Cell Networks", *IEEE Transactions on Communications*, vol. 61, nº 10, p. 4391-4403.

Hur, S., S. Baek, B. Kim, J. Park, A. Molisch, K. Haneda, and M. Peter. 2015. "28 GHz Channel Modeling Using 3D Ray-Tracing in Urban Environments". *9th European Conference on Antennas and Propagation (EuCAP)*. p. 1-5.

Hur, S., Y. Cho, L. Lee, J. Ko, and J. Park. 2014. "Millimeter-wave Channel Modeling based on Measurements in In-building and Campus Environments at 28 GHz". *European Cooperation in the field of Scientific and Technical Research. DMC R&D Samsung Electronics.*

IEEE 802.15.3c Specification, Part 15.3: Wireless medium access control (MAC) and physical layer (PHY) specifications for high rate wireless personal area networks (WPANs). 2009. https://standards.ieee.org/about/get/802/802.15.html.

Jeong, C., J. Park, and H. Yu. 2015. "Random access in millimeter-wave beamforming cellular networks: issues and approaches". *IEEE Communications Magazine*, vol.53, nº 1, p.180-185.

Kaya, A. O., W. Trappe, L.J. Greenstein, and D. Chizhik. 2012. "Predicting MIMO Performance in Urban Microcells Using ray Tracing to Characterize the Channel", *IEEE Transactions on Wireless Communications*, vol. 11, nº 7, p. 2402-2411.

Khan, F. and Z. Pi. 2011. "mmWave Mobile Broadband (MMB): Unleashing the 3-300 GHz Spectrum" *34th IEEE Sarnoff Symposium*, pp. 1-6, May 2011.

Kim, Joongheon and Andreas Molisch. 2014. "Fast Millimeter-Wave Beam Training with receive Beamforming". *Journal of Communications and Networks*, vol. 16, nº 5, p. 512-522.

Kwon, G., Y. Shim, H. Park, and H. Kwon. 2014. "Design of Millimeter Wave Hybrid Beamforming Systems", *2014 IEEE 80th Vehicular Technology Conference*. p. 1-5.

Li, Qian, Huaning Niu, Geng Wu, and Rose Hu. 2013. "*Anchor-booster based heterogeneous networks with mmWave capable booster cells*". 2013 IEEE Globecom Workshops (GC Wkshps). p. 93-98.

MacCarney, G., J. Zhang, S. Nie, and T. Rappaport. “Path Loss Models for 5G Millimeter Wave Propagation Channels in Urban Microcells”. *IEEE Global Communication Conference, Exhibition & Industry Forum (GLOBECOM)*. p. 3948-3953.

Mathworks. 2013. "MATLAB (R2013b)". https://www.mathworks.com.

Međedović, P., and D. Šuka. 2012. “Software for urban electromagnetic wave propagation modeling”. Infotech-Jahorina 2012. Vol. 11, p. 422-427.

Mendez-Rial, R., C. Rusu, N. Gonzalez-Prelcic, A. Alkhateeb, and R.W. Heath. 2015. “Hybrid MIMO Architectures for Millimeter Wave Communications: Phase Shifters or Switches?”. [Online]. Available: https://arxiv.org/abs/1512.03032v1.

Michalski, A. and J. Czajewski. 2004. “The accuracy of the global positioning systems”. *IEEE Instrumentation and Measuring Magazine*, vol. 7, nº 1, p. 56-60.

Molisch, A., A. Karttunen, R. Wang, C. Umit Bas, S. Hur, J. Park, and J. Zhang J. 2016. “Millimeter-Wave Channels in Urban Environments”. *10th European Conference on Antennas and Propagation (EuCAP)*. p. 1-5.

Molisch, A., A. Karttunen, S. Hur, J. Park, and J. Zhang. 2016. “Spatially consistent path loss modeling for millimeter-Wave channels in Urban Environments”. *10th European Conference on Antennas and Propagation (EuCAP)*. p. 1-5.

Noh, Song, Michael Zoltowsky, and David J. Love. 2015. “Multi-Resolution Codebook and Adaptive Beamforming Sequence Design for Millimeter Wave Beam Alignment”. [Online]. Available: http://docs.lib.purdue.edu/ecetr.

Oesteges, C. and Vanhoenacker-Janvier. 2000. “Experimental validation and system applications of ray-tracing model in built-up areas”. *IEEE Electronics Letters*, vol. 36, nº 5, p. 461-462.

Papadogiannis, Agisilaos and Alister Burr. 2011. “Multi-beam assisted MIMO – A novel approach to fixed beamforming”. *IEEE Conference Future Network & Mobile Summit (FutureNetw)*. p. 1-8.

Papoulis, Athanasios and S. Unnikrishna Pillai. 2002. *Probability, Random Variables, and Stochastic Processes*, 4th edition, Mcgraw Hill, 433 p.

Perahia E., C. Cordeiro, M. Park, and L. Yang. 2010. “IEEE 802.11ad: Defining the Next Generation Multi-Gbps Wi-Fi”. *7th IEEE Consumer Communications and Networking Conference*. p. 1-5

Pi, Zhouyue and Farroq Khan. 2011, “An Introduction to Millimeter-Wave Mobile Broadband Systems”, *IEEE Communications Magazine*, vol. 49, nº 6, p. 101-107.

Rajagopal, S., S. Abu-Surra, Z. Pi, and F. Khan. 2011. "Antenna Array Design for Multi-Gbps mmWave Mobile Broadband Communication", *Global Telecommunications Conference (GLOBECOM 2011)*. p. 1-6.

Rajagopal, S., S. Abu-Surra, and M. Malmirchegini. 2012. "Channel Feasibility for Outdoor Non-Line-of-Sight mmWave Mobile Communication", 2012 IEEE *Vehicular Technology Conference (VTC Fall)*. p. 1–6.

Ramasamy, D., S. Venkateswaran, and U. Madhow. 2012. "Compresive tracking with 1000-element arrays: a framework for multi-Gbps mm wave cellular downlinks". *50th Annual Allerton Conference on Communication, Control and Computing Conference*. p. 690-697.

Rangan, S., T. Rappaport, and E. Erkip. 2014. "Millimeter Wave Cellular Wireless Networks: Potentials and Challenges". [Online]. Available: https://arxiv.org/abs/1401.2560v1.

Rappaport, T., E. Ben-Dor, J. Murdock, and Y. Qiao. 2012. "38 GHz and 60 GHz angle-dependent propagation for cellular & peer-to-peer wireless communications". *2012 IEEE International Conference on Communications (ICC)*. p. 4568-4573.

Rappaport, T., Y. Qiao, J. Tamir, J. Murdock, and E. Ben-Dor. 2012. "Cellular broadband millimeter wave propagation and angle of arrival for adaptive beam steering systems (invited paper)". *Radio and Wireless Symposium (RWS)*, *IEEE*. p. 151-154.

Rappaport, T., F. Gutierrez, E. Ben-Dor, J. Murdock, Y. Qiao, and J. Tamir. April 2013. "Broadband Millimeter-Wave Propagation Measurements and Models using Adaptive-Beam Antennas for Outdoor Urban Cellular Communications". *IEEE Trans. on Antennas and Propagation,* vol. 61, nº 4, part: 1, p. 1850-1859.

Rappaport, T., G. MacCartney, M. Samimi, and S. Sun. 2015. "Wideband Millimeter-Wave Propagation Measurements and Channel Models for Future Wireless Communication System Design". *IEEE transactions on Communications*, vol. 63, nº 9, p. 3029-3056.

Remcom. (2016). *Wireless Insite*. [Online]. Available: http://www.remcom.com/wireless-insite

Roh, W., J. Seol, J. Park, B. Lee, J. Lee, Y. Kim, J. Cho, K. Cheun, and F. Aryanfar. 2014. "Millimeter-wave beamforming as an enabling technology for 5G cellular communications: theoretical feasibility and prototype results". *IEEE Communications Magazine,* vol. 52, nº 2, p. 106-113.

Samimi, M., K. Wang, Y. Azar, G.N. Wong, R. Mayzus, H. Zhao, J.K. Schulz, S. Sun, F. Gutierrez, and T.S. Rappaport. 2013. "28 GHz Angle of Arrival and Angle of

Departure Analysis for Outdoor Cellular Communications using Steerable Beam Antennas in New York City". *IEEE 77th Vehicular Technology Conference (VTC)*. p. 1-6.

Sand, S., R. Tanbourgi, C. Mensing, and R. Raulefs. 2009. "Position aware adaptive communication systems". *Proceedings of the 43rd Asilomar conference on Signals, systems and computers*. p. 73–77.

Slock, Dirk, "Location aided wireless communications". 2012. *Proceedings of the 5th International Symposium on Communications, Control and Signal Processing (ISCCSP)*. p. 1-6.

Sun, Shu and Theodore Rappaport. 2013. "Multi-beam antenna combining for 28 GHz cellular link improvement in urban environment". *Global Communications Conference (GLOBECOM)*, *IEEE*. p. 3754-3759.

Taranto, R., S. Muppirisettyn, R. Raulefs, D. Slock, T. Svensson, and H. Wymeersch. 2014. "Location-Aware Communications for 5G Networks: How location information can improve scalability, latency, and robustness of 5G". *IEEE Signal Processing Magazine*, vol. 31, nº 6, p. 102-112.

Tropp, Joel and Anna Gilbert., "Gilbert A. December 2007. Signal Recovery From Random Measurements Via Orthogonal Matching Pursuit", *IEEE Transactions on Information Theory*, vol. 53, p. 4655-4666.

Tsang, Y. Ming and Ada S.Y. Poon. 2011. "Successive AoA Estimation: Revealing the second path for 60 GHz communication system". *49th Annual Allerton Conference on Communication, Control, and Computing (Allerton)*. p. 508–515.

Tsang, Y. Ming and Ada S.Y. Poon. 2012. "Coding the Beams: Improving Beamforming Training in mmWave Communication System". [Online]. Available: https://arxiv.org/abs/1104.1007v4.

Van Trees, Harry L. 2012. *Optimum Array Processing, Part IV: Detection, Estimation and Modulation theory*. New York: John Wiley & Sons, Inc., 1470 p.

Wang, J., Z. Lan, C. Pyo, T. Baykas, C. Sum, M. Rahman, R. Funada, F. Kojima, I. Lakkis, H. Harada, and S. Kato. 2009. "Beam codebook based beamforming protocol for multi-Gbps millimeter-wave WPAN systems". *IEEE J. Sel. Areas in Communications*. vol. 27, nº 8, p. 1390–1399.

Yu, Chia-Hao, Ming-Po Chang, and Jiann-Ching Guey. 2015. "Beam Space Selection for High Rank Millimeter Wave Communication", *2015 IEEE 81st Vehicular Technology Conference (VTC Spring)*. p. 1-5.

Zalzala, A. and P. Flemming. 1997. *Genetic Algorithm in Engineering Systems*. Stevenage, Herts, United Kingdom: Institution of Electrical Engineering in London, 267 p.

Zandbergen, Paul. 2009. "Accuracy of iPhone Locations: A comparison of Assisted GPS, WiFi, and Cellular Positioning". *Transactions in GIS*, vol. 13, s1, p. 5-26.

Zhang, Z., J. Ryu, S. Subramanian, and A. Sampath. 2015. "Coverage and channel characteristics of millimeter wave band using ray tracing". *International Conference on Communications (ICC)*. p. 1380-1385.

Zhao, H., R. Mayzus, S. Sun, M. Samimi, J. K. Schulz, Y. Azar, K. Wang, G. N. Wong, F. Gutierrez, and T. Rappaport. 2013. "28 GHz millimeter wave cellular communication measurements for reflection and penetration loss in and around buildings in New York city*". International Conference on Communnications (ICC)*. p. 5163-5167.

Zhao, Quinling and Jin Li. October 2006. "Rain Attenuation in Millimeter Wave Ranges". 7th *Intl. Simp. on Antennas, Propagation & EM Theory*. p. 1-4.